

https://dspace.org/

Fracture of plain concrete: a comparative study of notched beams of varying depth

Alexander, Mark Gavin

2014-09-12
http://hdl.handle.net/10539/15527

Downloaded from a DSpace repository. https://dspace.org/

assumptions, provided a volume is being considered of size sufficient that reasonable average values of material parameters can be assigned. The problem is therefore one of scale.

Hardened cement paste, mortar and concrete progressively range from a relatively homogeneous to a highly heterogeneous material. However, homogeneity is a function of scale, and even hardened cement paste is heterogeneous at a microscopic level. Concrete is full of inherent flaws and microcracks before any load is applied, and contains severe planes of weakness in the interfaces between paste and aggregate. Under flexural tensile loading, the stress field ahead of the crack will be highly distorted by the presence of these interfaces across which stress will often not be transferred, and also by the fact that the various phases have different stiffnesses. Consequently, when speaking of a parameter such as K_I which characterises the stress field in the region of the notch, this characterisation can only be thought of in broad global terms, and the stress field at any particular point may vary significantly from that assumed. Consequently, notching in small concrete specimens will tend not to influence the stress distribution markedly. Failure will be governed by the inherent flaws in the material, with the net failure stress varying little from that in an unnotched section. In fact for small specimens the aggregate size actually represents the typical flaw size and notching will have very little effect. This would be true of the 100mm deep beams in the present tests, where the nominal ratio between maximum aggregate size and specimen depth was 0,2, but could frequently have been as high as 0,25 or 0,3 due to elongated and larger aggregate particles. While the concept of K can still be applied in broad terms, the concept of a critical value K_c is not valid. However, K can still be viewed as the driving force behind crack propagation. In larger specimens with correspondingly larger crack depths for a given c/d, the influence of c becomes more important. Hence the net stress at failure reduces markedly leading to a condition of notch-sensitivity. In more homogeneous materials such as mortar and hcp, the inherent flaw sizes are far smaller and therefore the notch controls the failure more readily.

assumptions, provided a volume is being considered of size sufficient that reasonable average values of material parameters can be assigned. The problem is therefore one of scale.

Hardened cement paste, mortar and concrete progressively range from a relatively homogeneous to a highly heterogeneous material. However, homogeneity is a function of scale, and even hardened cement paste is heterogeneous at a microscopic level. Concrete is full of inherent flaws and microcracks before any load is applied, and contains severe planes of weakness in the interfaces between paste and aggregate. Under flexural tensile loading, the stress field ahead of the crack will be highly distorted by the presence of these interfaces across which stress will often not be transferred, and also by the fact that the various phases have different stiffnesses. Consequently, when speaking of a parameter such as K_I which characterises the stress field in the region of the notch, this characterisation can only be thought of in broad global terms, and the stress field at any particular point may vary significantly from that assumed. Consequently, notching in small concrete specimens will tend not to influence the stress distribution markedly. Failure will be governed by the inherent flaws in the material, with the net failure stress varying little from that in an unnotched section. In fact for small specimens the aggregate size actually represents the typical flaw size and notching will have very little effect. This would be true of the 100mm deep beams in the present tests, where the nominal ratio between maximum aggregate size and specimen depth was 0,2, but could frequently have been as high as 0,25 or 0,3 due to elongated and larger aggregate particles. While the concept of K can still be applied in broad terms, the concept of a critical value K_c is not valid. However, K can still be viewed as the driving force behind crack propagation. In larger specimens with correspondingly larger crack depths for a given c/d, the influence of c becomes more important. Hence the net stress at failure reduces markedly leading to a condition of notch-sensitivity. In more homogeneous materials such as mortar and hcp, the inherent flaw sizes are far smaller and therefore the notch controls the failure more readily.

One final point concerning the fracture behaviour of unnotched beams is appropriate. For such beams, the inherent flaws associated with the aggregate-paste interfaces control the failure. There is also a very large number of cross sections available for potential fracture, leading to a different practical situation from that of notched beams. Therefore, higher values of fracture parameters are measured, which was noted in ref. 23. This is due to damage occurring in a highly stressed zone which is larger than in a notched beam. A marked instability condition also occurs at maximum load, usually resulting in catastrophic final fracture. Therefore in practical terms we must differentiate between fracture in notched specimens where the failure section is predetermined, and in unnotched specimens where the fracture zone is larger and fracture phenomena are more catastrophic.

9.3 ESTIMATION OF CRACK GROWTH FOR CALCULATING FRACTURE PARAMETERS

It was demonstrated in chapter 6 that actual crack advance generally occurred before maximum load in fracture beams. To ignore this crack growth means that fracture parameters will be underestimated. For series F3 it was possible to obtain reasonable experimental relationships between beam compliance and visible crack depth (see figures 6.3 and 6.8), although the scatter involved in testing of this type of material is always a problem. The advantage of the experimental relationships was that a mean curve could be plotted through the experimental points; this curve essentially "smoothed out" the experimental scatter and allowed better estimates of crack growth to be obtained using measured compliances. Thus the results of all beams of a given size were combined to produce an experimental relationship that, in turn, gave greater confidence in determining crack growth for individual beams. Therefore, for series F3, the approach to estimating crack growth during a test is to use measured compliances and the mean experimental compliance-crack depth curve for the particular beam size. In this case, the crack

depths are referred to as *experimental* crack depths. The reloading compliance curves were used since they were considered more reliable than the conventional compliance curves. These curves are given in figure 6.8.

For series F1 and F2, no direct measurements of crack depth were made, and an experimental compliance-crack depth relationship was not obtained. The problem of estimating crack growth before maximum load can partially be solved by noting from figure 6.9 that observed crack growth at maximum load was similar to crack growth predicted using the conventional compliance relationship (i.e. apparent crack growth, according to 6.7.2). Unfortunately this procedure is not entirely satisfactory, particularly for smaller beams. Figure 6.9 shows that for beams 300mm and deeper, visible crack growth and apparent crack growth at maximum load had similar values. Subject to the limited results, this did not appear to be the case for 100mm and 200mm beams, where observed crack growth was less than apparent crack growth. Therefore it might be expected that for these smaller beams, use of apparent crack growth would cause overestimation of fracture parameters.

To further investigate this problem, the experimental crack depths at maximum load (c_c) for series F3 were plotted against apparent crack depths. Results are shown in figure 9.2, and confirm that a serious overestimation of apparent c_c occurs for the small 100mm beams (+32 per cent on average compared with experimental c_c). Apparent c_c values for deeper beams may also be overestimated, but on average by only about 10 per cent. Nevertheless it will be shown later that even a 10 per cent overestimate of c_c has a marked influence on fracture parameters. Note that use of experimental crack depths (which essentially are an improvement on visible crack depths) in figure 9.2 has shown that c_c for 200mm beams can be adequately estimated.

Apparent crack growth prior to maximum load for series F1 and F2 beams is obtained from the theoretical compliance curves in figure 6.2 using measured conventional compliances. Irrecoverable deformations δ_p prior to maximum load are small (see figure 6.6), thus

substantiating this approach. However, the tendency to overestimate c_c using apparent crack depths must not be forgotten, particularly for the 100mm beams. This will also influence results shown previously in figure 6.10, causing the 100mm beams to be out of phase with the deeper beams.

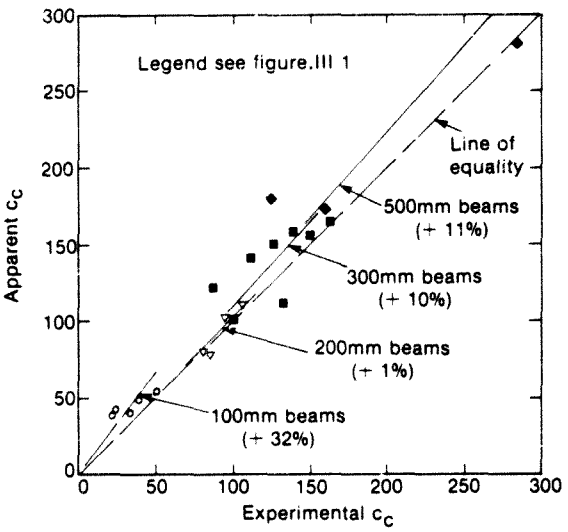


Figure 9.2 Comparison of apparent and experimental c_c values for beams of series F3

9.4 SUMMARY (PRELIMINARY CONSIDERATIONS)

1. The application of fracture mechanics principles to concrete is not simple. This is due to its non-linear behaviour and heterogeneity. LEFM leads to a relation for minimum beam depth to ensure notch-sensitivity, which is a necessary condition for application of fracture mechanics. The question that arises

is which value of critical stress-intensity factor K'_c should be used in the LEFM relation. The most common value of K'_c is that calculated at the point of maximum load instability, K_c. However, this point is not unique relative to the fracture process. The LEFM relation indicates that a K'_c value of approximately 1,0MPa$\sqrt{m}$ fits the notch-sensitivity results for the present beams.

2. An important point for application of fracture mechanics is that a valid condition of crack instability should occur. Failure to achieve this will result in fracture parameters differing from those measured at instability.

3. Crack growth can be estimated from specimen compliance. However, using theoretical (conventional) compliance relations can lead to an overestimate of crack depths. The effect is most serious for 100mm beams, when crack depths at maximum load can be overestimated by about 30 per cent relative to experimentally derived compliance-crack depth relationships.

DIVISION 2 LINEAR ELASTIC FRACTURE MECHANICS PARAMETERS

9.5 INTRODUCTION

The LEFM approach to concrete fracture has been criticised in recent years due to conflicting results being obtained. A full discussion of the issues involved has been given previously in 2.5 and 3.3. Nevertheless there would be considerable advantages in retaining this approach if possible, even though in the end it may prove to be lacking in complete accuracy or general applicability. Its major advantage is its simplicity, since it provides a single parameter measure of concrete toughness. Thus, resistance to fracture may be characterised by a parameter such as K_c, where the subscript c refers t some clearly defined condition of fracture instability. It is precisely the simplicity of the method that has led to its rapid acceptance and development for other materials such as metals and ceramics. Use of LEFM also provides a unified basis for analytical procedures, and allows results of different materials to be compared immediately. There is still no universally accepted test for obtaining an LEFM parameter for concrete, simply because there is not agreement on LEFM validity for concrete. The contentious issue of how to account for slow crack growth prior to instability has also not been resolved. In a fairly recent paper Saouma et al[168] tacitly made a plea for more serious consideration of LEFM parameters. They attempted to show that certain previous analyses were incorrect in deducing that LEFM was not applicable to concrete. It therefore seems that the LEFM approach cannot simply be dismissed. However, there are a number of thorny issues that continually occur which prevent the ready acceptance of LEFM. For instance, the size effect is very critical in relation to concrete fracture testing, and this will be demonstrated in the experimental results that follow. The presence of extensive non-linear fracture zones in notched beams must also influence pa-

DIVISION 2 LINEAR ELASTIC FRACTURE MECHANICS PARAMETERS

9.5 INTRODUCTION

The LEFM approach to concrete fracture has been criticised in recent years due to conflicting results being obtained. A full discussion of the issues involved has been given previously in 2.5 and 3.3. Nevertheless there would be considerable advantages in retaining this approach if possible, even though in the end it may prove to be lacking in complete accuracy or general applicability. Its major advantage is its simplicity, since it provides a single parameter measure of concrete toughness. Thus, resistance to fracture may be characterised by a parameter such as K_c, where the subscript c refers to some clearly defined condition of fracture instability. It is precisely the simplicity of the method that has led to its rapid acceptance and development for other materials such as metals and ceramics. Use of LEFM also provides a unified basis for analytical procedures, and allows results of different materials to be compared immediately. There is still no universally accepted test for obtaining an LEFM parameter for concrete, simply because there is not agreement on LEFM validity for concrete. The contentious issue of how to account for slow crack growth prior to instability has also not been resolved. In a fairly recent paper Saouma et al[188] tacitly made a plea for more serious consideration of LEFM parameters. They attempted to show that certain previous analyses were incorrect in deducing that LEFM was not applicable to concrete. It therefore seems that the LEFM approach cannot simply be dismissed. However, there are a number of thorny issues that continually occur which prevent the ready acceptance of LEFM. For instance, the size effect is very critical in relation to concrete fracture testing, and this will be demonstrated in the experimental results that follow. The presence of extensive non-linear fracture zones in notched beams must also influence

rameters based on assumptions of ideal linear behaviour, and this will be the major barrier to the adoption of LEFM.

9.5.1 LEFM PARAMETERS AND VARIABLES CONSIDERED

Three possible conditions of fracture instability were referred to previously in 9.2.2. Of these, two are appropriate for the consideration of LEFM parameters:- the condition of fracture initiation, and the point of maximum load. For each of these conditions, the parameters of stress-intensity factor (K_0 or K_c respectively) and strain energy release rate (G_0 or G_c respectively) were calculated. These conditions have been defined as valid points of "instability" (although the actual fracture process represented by each will be very different), and hence the measured parameters may be regarded as "critical", i.e. they may be investigated as potential criteria for fracture. The relevant formulae for calculation of the parameters are given in chapter 3 (equations (3.2) and (3.19)). (Since the main analytical emphasis for LEFM was on the stress-intensity factor K, values of G were only calculated for series F1 and F2 beams).

Three primary variables were examined for their influence on measured parameters. These were:-

1. Concrete compressive strength. Since cube strengths ranged from 28,5MPa to 43,5MPa taking all three series together, the results were examined for influence of compressive strength.

2. Initial notch depth ratio c_0/d. For a parameter to be valid as a fracture criterion, initial notch depth ratio should essentially have no influence on results. However, it should be borne in mind that notch depth fundamentally influences fracture instability (in the sense of spontaneous crack growth), and consequently also the fracture process. Unnotched beams have a different fracture instability condition from notched

meters based on assumptions of ideal linear behaviour, and this will be the major barrier to the adoption of LEFM.

9.5.1 LEFM PARAMETERS AND VARIABLES CONSIDERED

Three possible conditions of fracture instability were referred to previously in 9.2.2. Of these, two are appropriate for the consideration of LEFM parameters:- the condition of fracture initiation, and the point of maximum load. For each of these conditions, the parameters of stress-intensity factor (K_0 or K_c respectively) and strain energy release rate (G_0 or G_c respectively) were calculated. These conditions have been defined as valid points of "instability" (although the actual fracture process represented by each will be very different), and hence the measured parameters may be regarded as "critical", i.e. they may be investigated as potential criteria for fracture. The relevant formulae for calculation of the parameters are given in chapter 3 (equations (3.2) and (3.19)). (Since the main analytical emphasis for LEFM was on the stress-intensity factor K, values of G were only calculated for series F1 and F2 beams).

Three primary variables were examined for their influence on measured parameters. These were:-

1. Concrete compressive strength. Since cube strengths ranged from 28,5MPa to 43,5MPa taking all three series together, the results were examined for influence of compressive strength.

2. Initial notch depth ratio c_0/d. For a parameter to be valid as a fracture criterion, initial notch depth ratio should essentially have no influence on results. However, it should be borne in mind that notch depth fundamentally influences fracture instability (in the sense of spontaneous crack growth), and consequently also the fracture process. Unnotched beams have a different fracture instability condition from notched

beams, implying that fracture processes are different. Deeply notched beams (i.e. $c_0/d \geq 0,5$) experience no true fracture instability, implying again that fracture processes are different. Therefore the influence of notch depth ratio should be considered over that range of notch depths where fracture processes are reasonably similar. It is suggested that three different fracture processes can be identified for notched beams. These are:-

a. the unnotched beam condition, for which spontaneous crack growth generally occurs,

b. a notched beam condition where a degree of spontaneous crack growth occurs (i.e. shallow to medium notch depths),

c. a notched beam condition where no unstable crack growth occurs (i.e. deep notching). For the tests, it was found that over the range of notch depths used (c_0/d = 0,2 to 0,5), a degree of spontaneous crack growth occurred for c_0/d = 0,2 to 0,4, but not for c_0/d = 0,5. Therefore the influence of notch depth ratio is considered only for c_0/d = 0,2 to 0,4. The deeply notched beams will be considered later in 9.14.1 under the subject of fracture energy.

3. Absolute beam depth. Results from all three series over the full range of beam depths, i.e. 100mm to 800mm, will be considered.

The LEFM parameters K and G for the two conditions of fracture initiation and instability are shown in tables 9.1(a) and (b). Also shown are the crack depths c_c at maximum load, calculated according to the methods given in 9.3, and ratios of $K^2(1-\nu)^2/EG$ for series F1 and F2 beams.

Before considering stress-intensity factors in greater detail, it is instructive briefly to compare the K and G results in table 9.1(a) on the basis of equation (3.20). For a perfectly elastic-brittle material obeying the laws of LEFM, equation (3.

Table 9.1 (a) LEFM parameters for fracture beams of Series F1 and F2

Specimen identification	K_o (MPa$\sqrt{m}$)	G_o (N/m)	$\frac{K_o^2(1-\nu^2)}{EG_o}$	c_c (m)	K_c (MPa$\sqrt{m}$)	G_c (N/m)	$\frac{K_c^2(1-\nu^2)}{EG_c}$
F2/1 (800/0,2)	1,09	40,4	0,86	0,218	1,93	134,8	0,81
F2/2 (800/0,4)	0,68	18,7	0,77	0,373	1,37	76,9	0,7[illegible]
F2/3 (800/0,4)	0,71	18,4	0,77	0,380	1,69	105,9	0,[illegible]
F2/4 (800/0,4)	0,69	17,7	0,77	0,403	1,81	124,2	0,77
F1/1 (500/0,2)	(0,69)	(15,5)	(0,86)	(0,143)	(1,71)	(102,1)	(0,81)
F1/2 (500/0,2)	0,69	15,5	0,86	0,158	1,61	91,9	0,79
F1/3 (500/0,4)	0,91	29,6	0,77	0,259	1,67	101,8	0,77
F1/4 (500/0,4)	0,82	24,3	0,77	0,262	1,96	139,4	0,77
F1/5 (300/0,2)	0,52	9,7	0,86	0,107	1,88	142,3	0,78
F1/6 (300/0,2)	0,82	24,6	0,86	0,104	1,91	145,8	0,78
F1/7 (200/0,4)	0,40	6,7	0,77	0,102	1,10	52,5	0,77
F1/8 (200/0,4)	0,49	10,2	0,77	0,115	1,30	72,5	0,77
F1/9 (100/0,25)	0,40	5,8	0,82	0,040	1,10	46,2	0,78
F1/10(100/0,25)	0,44	7,1	0,83	0,040	1,07	44,5	0,78
F1/11(100/0,25)	0,51	9,3	0,83	0,045	1,63	104,4	0,76
F2/5 (100/0,25)	(0,63)	(14,3)	(0,83)	(0,034)	(1,08)	(43,8)	(0,79)
F2/6 (100/0,25)	0,53	9,9	0,83	0,041	1,30	65,8	0,76
F2/7 (100/0,25)	0,51	9,7	0,83	0,041	1,40	78,9	0,78
F2/8 (100/0,25)	0,57	12,4	0,83	0,045	1,61	107,0	0,75
F1/12(100/0,4)	0,56	12,2	0,77	0,054	1,76	124,3	0,76
F1/13(100/0,4)	0,43	7,3	0,77	0,052	1,06	44,3	0,77
F1/14(100/0,4)	0,68	18,5	0,77	0,052	1,56	96,5	0,77
F2/9 (100/0,4)	0,59	12,7	0,77	0,057	1,53	85,3	0,78
F2/10(100/0,4)	0,62	14,2	0,77	0,053	1,26	59,6	0,75
F2/11(100/0,4)	0,56	11,7	0,77	0,053	1,12	47,8	0,77
F2/12(100/0,4)	0,59	13,1	0,77	0,053	1,61	98,5	0,77
F2/13(100/0,4)	0,40	5,9	0,77	0,058	1,60	96,4	0,77
F2/14(100/0,4)	0,33	4,2	0,77	0,054	1,22	55,3	0,78
F2/15(100/0,4)	0,46	8,0	0,77	0,058	1,42	74,4	0,79

Note. Results in parentheses indicate the measured fracture record was considered unreliable.

Table 9.1 (b) LEFM parameters for fracture beams of Series F3

Specimen identification	K_o (MPa$\sqrt{m}$)	K_c (MPa$\sqrt{m}$)	c_c (m)
F3/1 (500/0,2)	0,60	1,52	0,160
F3/2 (500/0,2)	0,88	1,48	0,125
F3/3 (500/0,4)	0,66	1,70	0,275
F3/4 (500/0,4)	0,62	1,90	0,285
F3/5 (300/0,2)	0,75	1,71	0,132
F3/6 (300/0,2)	0,44	1,25	0,099
F3/7 (300/0,25)	0,60	1,01	0,087
F3/8 (300/0,25)	0,52	1,24	0,111
F3/9 (300/0,25)	0,43	1,65	0,126
F3/10(300/0,4)	0,66	1,22	0,138
F3/11(300/0,4)	0,47	1,34	0,162
F3/12(300/0,4)	0,50	1,15	0,150
F3/13(200/0,2)	0,61	1,79	0,084
F3/14(200/0,2)	0,52	1,65	0,082
F3/15(200/0,4)	0,54	1,32	0,106
F3/16(200/0,4)	0,63	1,24	0,096
F3/17(100/0,2)	0,46	0,91	0,024
F3/18(100/0,2)	0,60	1,14	0,026
F3/19(100/0,2)	0,28	1,08	0,035
F3/20(100/0,2)	0,47	0,75	0,020
F3/21(100/0,2)	0,52	(1,23)	(0,039)
F3/22(100/0,2)	0,60	(1,25)	(0,034)
F3/24(100/0,25)	0,45	0,70	0,025
F3/25(100/0,4)	0,43	1,25	0,052
F3/26(100/0,4)	0,56	0,80	0,040
F3/27(100/0,4)	0,36	(1,78)	(0,061)
F3/28(100/0,4)	0,48	(1,22)	(0,056)
F3/29(100/0,4)	0,57	(1,09)	(0,048)

Results in parentheses indicate unreliable result due to inaccurate estimate of crack depth at max. load (obtained from "apparent" crack depth).

i.e. $K^2 = EG/(1-\nu^2)$, should hold. Table 9.2 shows mean results for the various beam sizes of series F1 and F2, expressed as a ratio $K^2(1-\nu^2)/EG$. Values of the ratio are less than unity, implying that ideal LEFM behaviour is not occurring. This fact is already well established for concrete, and what is perhaps more striking at first glance is that values fairly close to unity are achieved. This is true particularly for the shallow notched beams. Previous work by the author[23] on cement mortar beams showed that values of the ratio were approximately 1,0 for $c_o/d = 0$ (i.e. for unnotched beams), 0,92 for $c_o/d = 0{,}125$, 0,86 for $c_o/d = 0{,}25$, and 0,82 for $c_o/d = 0{,}50$. Hence, the LEFM condition is more truly approached as notch depths and maximum aggregate size are reduced. Table 9.2 also indicates that the ratio is closer to unity for the fracture initiation condition as compared with the maximum load condition. These remarks indicate that application of LEFM to mortar or concrete beams is not simple, and will depend on the material, the type of test, and the degree of notching (i.e. on the fracture process).

Table 9.2 Comparison of experimental relationships between K and G (series F1 and F2)

Beam depth (mm)/c_o/d	Mean values $\frac{K_o^2(1-\nu^2)}{EG_o}$	$\frac{K_c^2(1-\nu^2)}{EG_c}$
800/0,2	0,86	0.81
800/0,4	0,77	0,77
500/0,4	0,77	0,77
500/0,2	0,86	0,79
300/0,2	0,86	0,78
200/0,4	0,77	0,77
100/0,4	0,77	0,77
100/0,25	0,83	0,77

9.6 CONDITION OF FRACTURE INITIATION

K_0 values were calculated using notch depths, since no main crack advance had occurred at fracture initiation. (Note that "fracture initiation" should be taken to mean the condition for which appreciable development of microcracking ahead of the notch tip begins. It therefore represents the first advance of the effective crack, which comprises the stress-free crack and the microcracked zone. It is the first identifiable point at which fracture occurs, and this fracture initiates at points of maximum stress concentration, which will usually be at interfaces between matrix and coarse aggregate).

Before fracture parameters are discussed, an examination of the effect of beam depth on net stress at the root of the notch is in order. Net stresses σ_n (based on the net section depth $b_0 = d-c_0$) were calculated using the load at fracture initiation for all beams, and expressed as ratios of the relevant modulus of rupture f_r. Mean values of σ_n/f_r for all beams of a given depth and initial notch depth ratio were calculated, and plotted against c_0/d. Results are shown in figure 9.3. There is a clear trend of reducing σ_n/f_r with increasing beam depth. Fracture is initiated in larger beams at significantly lower notch root stresses. This is tantamount to re-stating the notch-sensitivity condition, and figure 9.3 can be compared with the conventional notch-sensitivity curves in figure 5.6. The main difference between the two diagrams is that the net failure stress reduces with increasing notch depth ratio in the case of figure 5.6, while the net stress at fracture initiation remains approximately constant and independent of c_0/d in the case of figure 9.3. (The trend for the 800mm beams in figure 9.3 should be viewed with caution since only one result was available for $c_0/d = 0,2$). It is evident from figure 9.3 that a criterion for fracture initiation other than net stress at the notch root is required. For this reason, K_0 is considered below.

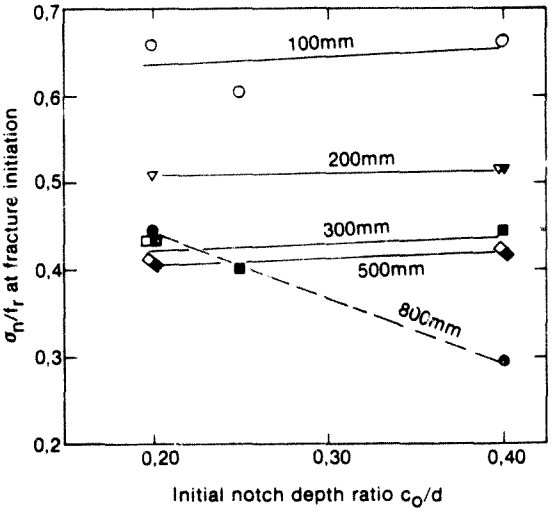


Figure 9.3 Relative net stress at fracture initiation (series F1, F2, F3)

9.6.1 EFFECT OF COMPRESSIVE STRENGTH ON K_0

To consider the effect of compressive strength on K_0, the effect of the other variables (c_0/d and beam depth) have to be eliminated. Nominally identical mixes and materials were used for the present tests, and variations in strength were ascribed to possible variations in cement quality, curing conditions, and effects of bleeding. (See 5.2 and appendix C). Therefore, compressive strength was not considered to be a variable during the design of the tests. For proper investigation of the effect of compressive strength, a full range of strengths would have to be selected and other variables such as beam size and notch depth ratio kept constant. The compressive strengths for only the 100mm beams and the 500mm beams

varied over a reasonable range, and discussion of strength effects must therefore be limited to these beams. (Note that for this section, 100mm beams with c_0/d values of 0,2 and 0,25 have been grouped together, since these two notch depth ratios are sufficiently close to result in virtually identical fracture processes).

Walsh[9] has reported a relationship between K_c and f_{cyl} for notched concrete beams as follows:-

$$K_c = 5\sqrt{f_{cyl}} \quad (Nmm^{-1,5}) \qquad (9.7)$$

where K_c was the critical stress-intensity factor measured at maximum load, and f_{cyl} was the cylinder compressive strength (N/mm^2).

According to equation (9.7), ratios of K_c for concretes of the same materials but different strengths should be equal to $\sqrt{(f_1/f_2)}$ where f_1 and f_2 are different compressive strengths. Assuming cube strengths and cylinder strengths are related by similar constants for the present concretes, and noting from table 5.1 that cube strengths for the present tests could be divided broadly into a 30MPa and a 40MPa group, the relative values of stress-intensity factors for the two groups should be equal to about $\sqrt{(40/30)} = 1,15$. This figure will be compared with results quoted below.

The 100mm and 500mm beams had cube strengths ranging from approximately 29MPa to 44MPa. The variables of c_0/d and beam depth were eliminated from the results as follows:-

1. For any particular c_0/d (i.e. 0,2/0,25 or 0,4) the mean K_0 value for 100mm or 500mm beams for all series was found. This value was denoted $\bar{K}_0(c_0/d,d)$ where c_0/d referred to the particular notch depth ratio, and d to the beam depth.

2. Results for a particular beam size and c_0/d, and for which a mean cube strength was available (i.e. results from a consistent batch of concrete), were averaged, and this average divided by the relevant $\bar{K}_0(c_0/d,d)$ (retaining consistency of c_0/d and

varied over a reasonable range, and discussion of strength effects must therefore be limited to these beams. (Note that for this section, 100mm beams with c_0/d values of 0,2 and 0,25 have been grouped together, since these two notch depth ratios are sufficiently close to result in virtually identical fracture processes).

Walsh[9] has reported a relationship between K_c and f_{cyl} for notched concrete beams as follows:-

$$K_c = 5\sqrt{f_{cyl}} \quad (Nmm^{-1,5}) \tag{9.7}$$

where K_c was the critical stress-intensity factor measured at maximum load, and f_{cyl} was the cylinder compressive strength (N/mm^2).

According to equation (9.7), ratios of K_c for concretes of the same materials but different strengths should be equal to $\sqrt{(f_1/f_2)}$ where f_1 and f_2 are different compressive strengths. Assuming cube strengths and cylinder strengths are related by similar constants for the present concretes, and noting from table 5.1 that cube strengths for the present tests could be divided broadly into a 30MPa and a 40MPa group, the relative values of stress-intensity factors for the two groups should be equal to about $\sqrt{(40/30)} = 1,15$. This figure will be compared with results quoted below.

The 100mm and 500mm beams had cube strengths ranging from approximately 29MPa to 44MPa. The variables of c_0/d and beam depth were eliminated from the results as follows:-

1. For any particular c_0/d (i.e. 0,2/0,25 or 0,4) the mean K_0 value for 100mm or 500mm beams for all series was found. This value was denoted $\bar{K}_0(c_0/d,d)$ where c_0/d referred to the particular notch depth ratio, and d to the beam depth.

2. Results for a particular beam size and c_0/d, and for which a mean cube strength was available (i.e. results from a consistent batch of concrete), were averaged, and this average divided by the relevant $\bar{K}_0(c_0/d,d)$ (retaining consistency of c_0/d and

d). In this way, the particular effect of compressive stength could be isolated.

3. The K_0 ratios (relative K_0) referred to in 2. were plotted against mean cube strength $\bar{f}_{cu}$.

Results are shown in figure 9.4.

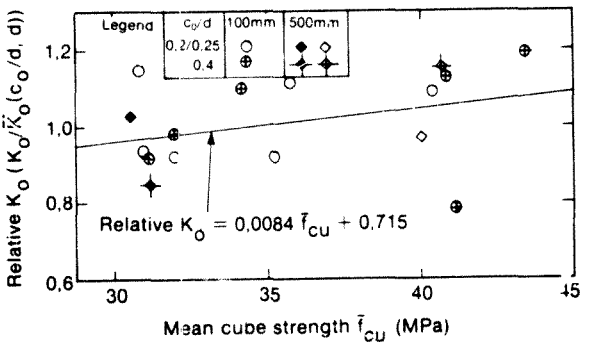


Figure 9.4 Effect of compressive strength on K_0

Note the following from figure 9.4:-

1. The results appear independent of c_0/d and beam depth, as expected.

2. Despite the scatter, particularly for the 100mm beams, a slight trend of increasing K_0 with compressive strength emerges. The linear regression relationship gives that K_0 for 40MPa concrete is approximately 9 per cent greater than K_0 for 30MPa concrete. This value is lower than the 15 per cent quoted previously from Walsh's work. However, following the same reasoning as in appendix C concerning elastic modulus and cube results, it could be expected that fracture parameters would not be as greatly affected by apparent compressive strength variations when such variations are induced by possible bleeding effects.

Although the effect of compressive strength on the present results was small, it was decided initially to divide the concretes into two broad groups:- the first comprising a strength group of approximately 29 to 35MPa, and the second a strength group of approximately 40 to 44MPa.

9.6.2 EFFECT OF INITIAL NOTCH DEPTH ON K_0

The procedure for eliminating effects of compressive strength and beam depth from the K_0 results was as follows:-

1 For any particular beam depth and strength group, a mean value of K_0 for $c_0/d = 0,4$ was found, i.e. $\overline{K}_0(0,4,d,\overline{f}_{cu})$.

2. Retaining consistency of beam depth and stength group, individual K_0 results for all c_0/d ratios were divided by $\overline{K}_0(0,4,d,\overline{f}_{cu})$, to give a relative K_0 value.

3. These relative K_0 values were plotted against c_0/d.

Since figures 5.6 and 9.3 had shown that the 100mm beams were notch-insensitive, it was decided to plot these results separately from results for beams of depth 200mm or greater. Results are shown in figure 9.5, with the 100mm beam results shown in an inset in the figure.

Note the following from figure 9.5:-

1. For beams of depth greater than 100mm, there is no clear trend of increased K_0 for $c_0/d = 0,2$ or 0,25 when compared with K_0 at $c_0/d = 0,4$, if results for $c_0/d = 0,2$ and 0,25 are taken together. There are insufficient results for $c_0/d = 0,25$ to state definitely that lower K_0 values occur in comparison with results for $c_0/d = 0,2$, and it would appear to be better practice to take results for these two notch depth ratios together.

(Later results for K_c will confirm this). In this case, the shallower notched beams have K_0 values about 8 per cent higher than the deeper notched beams.

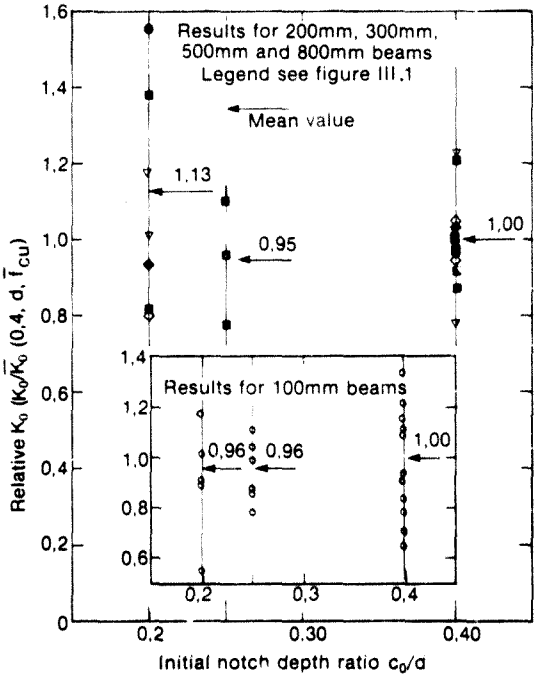


Figure 9.5 Effect of initial notch depth ratio on K_0

2. It should be remembered that it was usually not easy to determine with complete accuracy the precise point of departure from linearity on the load-deflection record. For example, there is one very high result of relative K_0 = 1,56 at c_0/d = 0,2 (800mm deep beam). This result corresponds with the point in figure 9.3 for 800mm beams, c_0/d = 0,2, which appeared out of phase, and should therefore be treated with caution. This single result raises the mean relative K_0 value for c_0/d = 0,2

from 1,07 to 1,13, and for c_0/d = 0,2 and 0,25 taken together from 1,03 to 1,08.

3. Although the shallower notched 100mm beams (c_0/d = 0,2 and 0,25) have slightly lower K_0 values than the deeper notched beams (c_0/d = 0,4) the differences are considered small enough to be inconsequential for practical purposes.

In view of the above (and later K_c results) it was decided to consider the influence of c_0/d on K_0 as being very small if not negligible. This allowed all results for a given beam depth and strength group to be taken together, irrespective of c_0/d.

Before considering the effect of beam depth on K_0, it will be helpful to consider certain K_c results. K_0 and K_c results can then be compared and contrasted where necessary.

9.7 CONDITION OF MAXIMUM LOAD INSTABILITY

K_c values were calculated for all three series, using crack depths c_c at maximum load given in tables 9.1(a) and (b). As explained in 9.3, these c_c values were obtained from theoretical compliance relationships for series F1 and F2, and from experimental compliance relationships for series F3 Due to slow crack growth before maximum load, the point of maximum load does not assume the same relevance or importance for concrete as it does for metallic materials under plane strain conditions. This will be further demonstrated in 9.13 where it will be seen that the point of maximum load does not represent a unique fracture condition, but is merely a point during the fracture process that can be conveniently defined on the load-deflection record. In general, this condition does not represent the maximum fracture toughness that can be developed by concrete. There is no doubt that part of the reason why differing results for K_c have been obtained by different investigators is

because the point of maximum load will be significantly influenced by loading rates and machine-specimen interaction, which in turn will influence slow crack growth.

9.7.1 EFFECT OF COMPRESSIVE STRENGTH ON K_c

This effect was checked for 100mm and 500mm beams by following the same procedure as outlined previously for K_0. Relative K_c values were obtained which were plotted against mean cube strength, and results are shown in figure 9.6. Clearly this figure shows a very similar trend to that of figure 9.4, with the following differences:-

1. There is a significantly lower scatter of results. It appears therefore that determination of K_c values are less liable to experimental scatter than K_0 values. This is true for both the 100mm and 500mm beams.

2. There is on average only a 2,7 per cent increase in K_c values when comparing 40MPa concrete with 30MPa concrete. This difference is so small as to be virtually negligible, and is consistent with remarks made earlier that only small variations of fracture toughness might be expected when compressive strength variations are partially induced by bleeding effects.

It should be noted that K_c values for 100mm beams in figure 9.6 were based on apparent crack depths at maximum load, i.e. crack depths inferred from the theoretical compliance relationship. Therefore, 100mm beams of series F3 where crack depths were obtained from the experimental compliance relationship were not included. This ensured that results for use in figure 9.6 were obtained consistently.

Figure 9.6 confirms the fact that fracture strengths for the present concretes were essentially unaffected by variations in compressive strength. The two strength groupings were retained for checking

the effect of c_0/d on K_c below, but thereafter all results were taken together when considering fracture toughness.

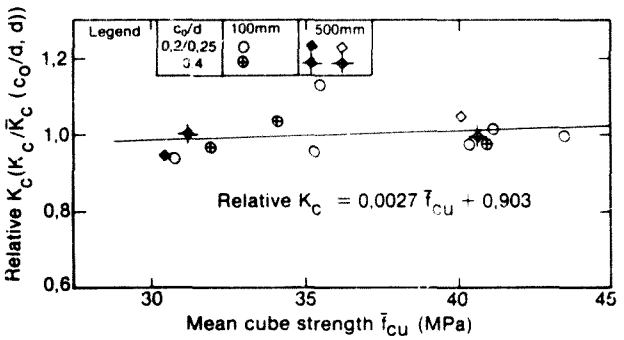


Figure 9.6 Effect of compressive strength on K_c

9.7.2 EFFECT OF INITIAL NOTCH DEPTH ON K_c

The same procedure as outlined for K_0 was followed for eliminating beam depth effects and any small influence of compressive strength on K_c. Results for 100mm beams were plotted separately from results for the deeper beams. Results for the 100mm beams were also grouped into K_c values obtained using the apparent crack depths (i.e. series F1 and F2 mainly) and those obtained using experimental crack depths (i.e. series F3 mainly) since it will be shown later that a basic difference existed between these two sets of results. Results are shown in figure 9.7, with the 100mm results shown in an inset in the figure. A slight trend of decreasing K_c with deeper notching may be evident from the figure, for beams of depth 200mm or greater. Following the same approach as K_0 of taking results for c_0/d = 0,2 and 0,25 together, the shallow notched beams have approximately 8 per cent higher K_c values than the deeper notched beams. An oppo-

site trend is shown for the 100mm beams, where slightly lower K_c values occur for shallow notching.

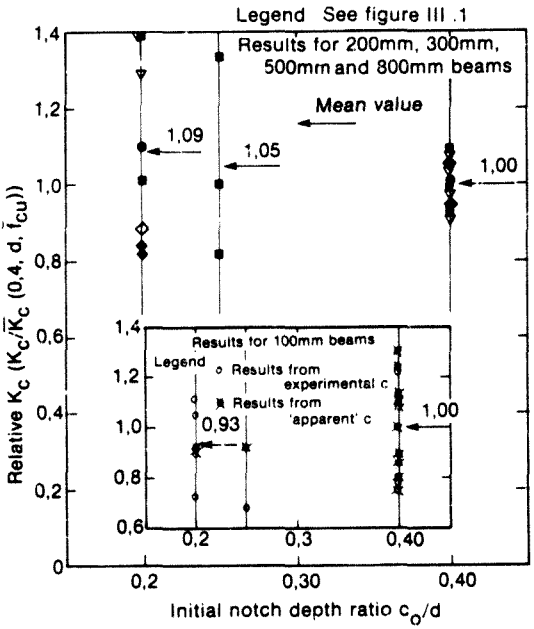


Figure 9.7 Effect of initial notch depth ratio on K_c

Comparison of figures 9.5 and 9.7 will show that overall trends for the two different beam size groupings are consistent. For beams of depth 200mm or greater, there is a slight tendency for fracture toughnesses to increase as notch depth ratio is reduced from 0,4 to 0,2. Note also that for these beams a lower scatter of results occurs for c_0/d = 0,4 as compared with c_0/d = 0,2/0,25, while the opposite trend occurs for 100mm deep beams. The tendency for increasing K values with decreasing c_0/d is consistent with earlier remarks concerning the fundamental difference between fracture of notched and unnotched beams. As notching becomes shallower, the stress intensity effect in the fracture zone increases, leading to a greater intensity of microcracking. This in turn activates ad-

ditional energy absorbing mechanisms. The entire fracture process also becomes more unstable (in the sense that the tendency for spontaneous crack growth increases) as notching becomes shallower. Hence, the minor trends for the deeper beams shown in figures 9.5 and 9.7 are consistent with our understanding of fracture processes in concrete beams. The fact that the influence of notch depth in the range c_0/d = 0,2 to 0,4 is small implies that the fracture processes in concrete beams with c_0/d values within these limits are very similar. This is also borne out by measurements of fracture zone size reported in chapters 7 and 8. It was noted there that initial notch depth had no influence on fracture zone size for the same depth of visible crack. As will be shown later in 9.14.1, there does appear to be a fundamental difference between fracture behaviour of beams with $c_0/d \leq 0,4$ and $c_0/d \geq 0,5$. Within the range $0,2 \leq c_0/d \leq 0,4$ there is only a minor influence of c_0/d on fracture toughness which can probably be ignored for practical purposes.

Finally, note from figures 9.5 and 9.7 that 100mm beams do not follow the same trends as the deeper beams, and if anything there is no influence of c_0/d on K values. This ought not to be interpreted as indicating that K values measured for these beams represent a valid fracture criterion. Rather these results confirm the notch-insensitivity of these beams, and the fact that failure is governed by net stresses at the notch root. The different trends between the 100mm beams and the deeper beams indicates that LEFM concepts are strictly not applicable to notch-insensitive specimens.

9.8 EFFECT OF BEAM DEPTH ON K VALUES

It has been shown that inital notch depth ratio within the range 0,2 to 0,4 has a minor influence on K values. For the present tests, compressive strength variations also had a very minor influence on K. It was therefore considered unnecessary to adjust

results so as to eliminate these effects when investigating the influence of beam depth on K. Therefore results for all the concretes and all the initial notch depth ratios were taken together.

In order to show the spread of results and compare K values for different beam depths, the following procedure was followed:-

1. All results for the three series were taken together irrespective of c_0/d or $\overline{f}_{cu}$. The mean value for K_c ($\overline{K}_c$) or K_0 ($\overline{K}_0$) was thus obtained.

2. Individual beam results for K_c or K_0 were expressed as ratios of $\overline{K}_c$ or $\overline{K}_0$ respectively, and grouped together according to beam depth.

3. The K ratios, or relative K values, were expressed in bar diagram form as a function of beam depth.

   See figures 9.8, 9.9 and 9.10.

FIGURE 9.8. EFFECT OF BEAM DEPTH ON K_c VALUES FOR VARIOUS TEST SERIES

Results have been grouped according to series and beam size. A large spread of results is apparent. K_c values were obtained using c_c values from apparent crack depths for series F1, F2 and five of the 100mm F3 beams, and from experimental crack depths for the balance of the series F3 beams. The consequences of this procedure are briefly analysed below, using figure 9.2 as a basis.

500mm AND 300mm BEAMS (SERIES F1)

Five beams are represented in figure 9.8, with a mean relative K_c value of 1,29. Figure 9.2 indicates that, for 500mm and 300mm beams, the average overestimate of c_c using apparent crack depths rather than experimental crack depths is about 10 per cent. Assuming that this overestimate also applies to the 500mm and 300mm

F1 beams, a more true value of relative K_c can be estimated using the following ratio, obtained from equation (3.2):-

$$\frac{Y_{exp}}{Y_{app}} \left(\frac{c_{exp}}{c_{app}}\right)^{\frac{1}{2}} \qquad (9.8)$$

where c_{exp}, c_{app} are the experimental and apparent values of c_c respectively, and Y_{exp}, Y_{app} are Y values from figure 3.4, using c_{exp} and c_{app} respectively. Taking the 500mm and 300mm F1 beams together by way of simplification, the mean c_c/d ratio based on apparent c_c is 0,41 (from table 9.1(a)) for which Y_{app} = 2,1. An estimate of the experimental c_c/d is 0,41/1,1 = 0,37 for which Y_{exp} = 1,99. Therefore, the ratio (9.8) becomes:-

$$\frac{1,99}{2,1} \left(\frac{0,37}{0,41}\right)^{\frac{1}{2}} = 0,90$$

Hence, it is feasible that K_c values for 500mm and 300mm beams of series F1 may have been overestimated by about 10 per cent, due to use of apparent c_c values. This also helps to explain partially why K_c values for series F3 beams (500mm and 300mm) are lower than those for the corresponding F1 beams.

100mm BEAMS (SERIES F1 AND F2)

Sixteen beams are represented in figure 9.8, with a mean relative K_c value of 1,00. Figure 9.2 shows that for 100mm F3 beams, the average overestimate of c_c using apparent rather than experimental crack depths was 32 per cent. Assuming that this also applies to the 100mm F1 and F2 beams, a more true value of relative K_c can be estimated using the procedure outlined above. In this case, the value of the ratio (9.8) becomes:-

$$\frac{2,0}{2,5} \left(\frac{1}{1,32}\right)^{\frac{1}{2}} = 0,70$$

Applying this to the mean relative K_c value of 1,00 given above, a revised value of 1,00x0,70 = 0,70 is obtained. This value accords

very closely with the value of 0,68 for the 100mm F3 beams obtained using experimental crack depths.

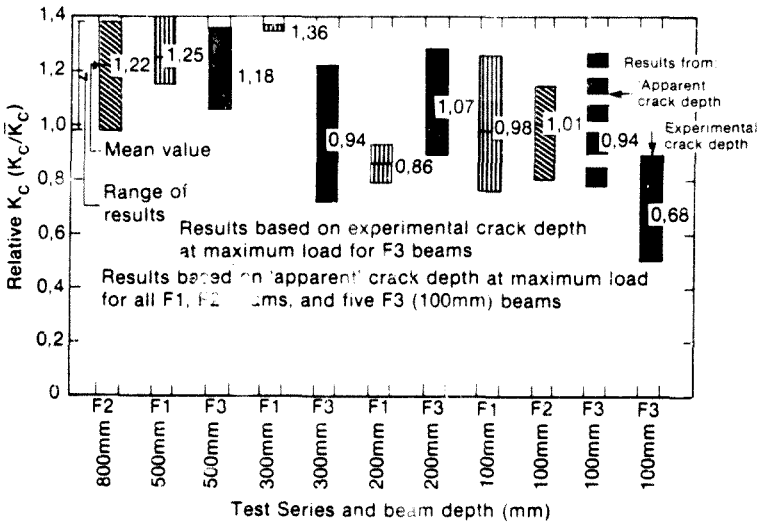


Figure 9.8 Effect of beam depth on K_c for various series

The above analyses indicate the critical importance of accurate estimates of c_c for obtaining proper K_c values. The theoretical compliance relationships may provide a first estimate of c_c. For greater accuracy, experimental relationships based on actual crack extension in the material should be derived; these relationships will incorporate crack-closing stresses and microcracking effects. The small 100mm beams have suffered severely in this regard since the experimental compliance relationship is considerably removed from the theoretical relationship (see figure 6.5(a)). This leads to a serious overestimate of c_c if the theoretical relationship is used. The problem is compounded for deeper notch depths, since Y values begin to increase very rapidly for c/d values exceeding 0,4 (see figure 3.4).

FIGURE 9.9 EFFECT OF BEAM DEPTH ON K_c, COMBINED RESULTS

Results from figure 9.8 have been combined on the basis of beam depth to produce figure 9.9. Note the following:-

1. There is a general trend of K_c reducing with beam depth. However, the use of apparent c_c values for F1 and F2 has affected the results. For instance, 500mm and 300mm beam results for F1 and F2 could be expected to reduce by about 10 per cent with use of lower c_c values according to previous discussion. It is probable that the 800mm results for F2 would also reduce by a similar amount.

2. The 300mm beam results have been affected by some rather low K_c values measured for the F3 beams (see table 9.1(b) and figure 9.8). There is no obvious explanation for these lower values, except possibly that the load-cycling technique has influenced maximum load. The 500mm and 200mm results for series F3 do not seem to have suffered in the same way. Further testing may in fact show that there is very little difference between 300mm and 500mm beam results, and a hint of this is given by the 300mm results for series F1 (figure 9.8). Results for 200mm beams, according to figures 9.8 and 9.9, are not very much different from those for 300mm beams.

3. The remarks in 1. and 2. above imply that there is a measurable influence of beam depth on K_c, but that within the range of beam depths from 200mm to 800mm, the difference between average K_c values might amount to about 10 or 15 per cent.

4. It must be re-iterated that results for 100mm beams using apparent crack depths are invalid, and better K_c values are given by results using experimental crack depths. On this basis, there is a very marked reduction of K_c for the 100mm beams, and they do not conform to the general trend of figure 9.9.

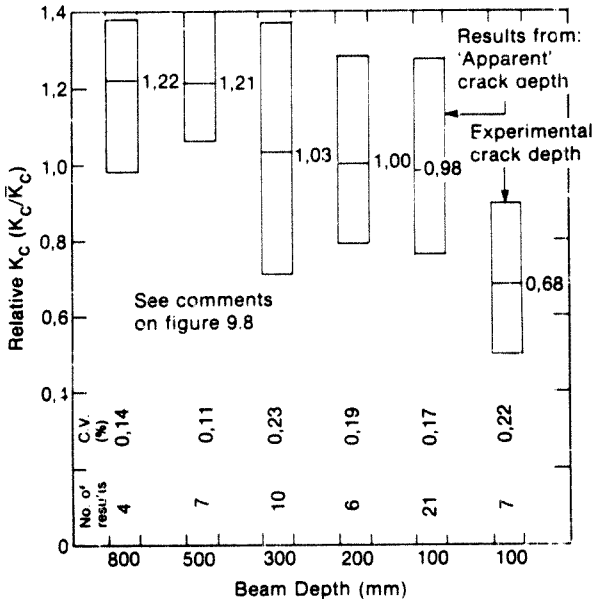


Figure 9.9 Effect of beam depth on K_c, combined results

FIGURE 9.10 EFFECT OF BEAM DEPTH ON K_0, COMBINED RESULTS

The K_0 results for the different series were combined on the basis of beam depth to produce figure 9.10. K_0 values are calculated using initial notch depths which removes much of the uncertainty concerning crack depth that has been discussed relative to figures 9.8 and 9.9. The relative K_0 values shown on figure 9.10 can therefore be regarded as representing the fracture initiation condition. There is a clear trend of K_0 decreasing with beam depth, such that the average K_0 for the 800mm beams is approximately 50 per cent higher than that for the 200mm beams, and 60 per cent higher than that for the 100mm beams.

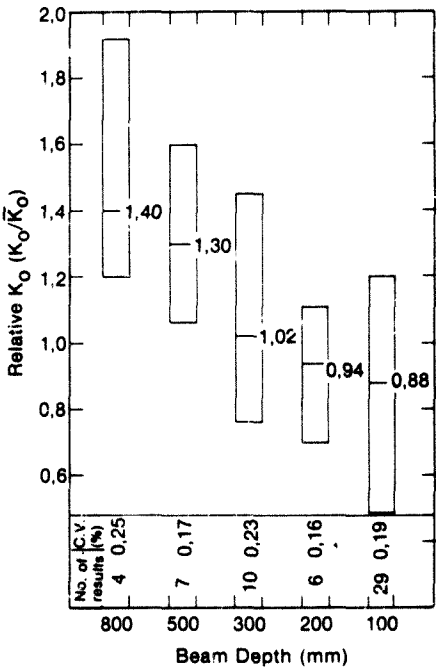


Figure 9.10 Effect of beam depth on K_0, combined results

It is interesting to note that figure 9.10 is in contrast with results obtained by Mai et al[*3] using notched asbestos cement beams of varying depth . Mai et al found that, above a minimum beam depth of 50mm, the fracture initiation condition was characterised by a constant value of K_0. An examination of their results, however, shows that the point of departure from linearity was very much closer to the maximum load point than in the present tests. This point was generally between 55 to 60 per cent of maximum load for the concrete beams, and about 85 per cent for the asbestos cement beams. Hence the reinforced matrix of the asbestos cement beams comformed more closely to a linear brittle material than concrete.

It therefore appears that for a material like concrete which exhibits extensive non-linearity before max m load, the fracture initiation toughnesses are dependent on beam depth. There is a possibility that plane stress/strain effects are influencing the fracture initiation results considerably more than the K_c results, but this is an aspect that will require further investigation. The basic conclusion from figure 9.10 is that K_0 does not appear to be a suitable fracture criterion for notched concrete beams.

A final plot is presented in figure 9.11, where corrected beam stresses at maximum load based on the gross section (i.e. $\sigma_g Y$) are plotted against critical crack depths at maximum load.

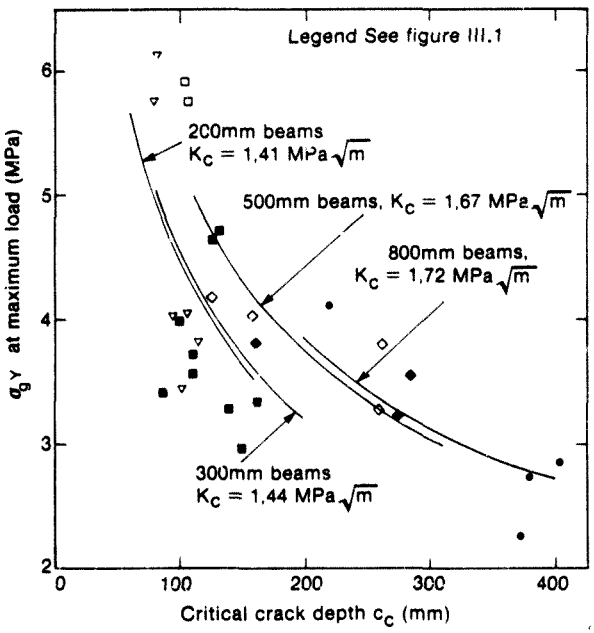


Figure 9.11 Mean K_c values for beams of all three series taken together (unmodified)

According to equation (3.2), the curves in figure 9.11 should give the experimental value of K_c. Results are plotted without any modification for overestimate of c_c and K_c. Results from all beams of a given depth are taken together to determine a mean K_c for that beam size, and the values are shown on the figure. Results for 100mm beams are excluded, since K_c has no true fracture significance for these beams. It can be seen that, despite experimental scatter, results conform to the theoretical trend suggested by equation (3.2). The size effect can also be seen, although this is magnified due to overestimation of c_c as explained above.

The discussion in this section has centred on experimental measurements of LEFM parameters, and the various influencing factors. However, it is necessary to critically examine the results with a view to determining the applicability of LEFM to notched concrete beams. While some of the results may appear encouraging, the influence of the microcracked zone must be considered. The following section will attempt a critical review of the results relative to LEFM principles.

9.9 CRITICAL DISCUSSION AND SUMMARY OF LEFM (K) RESULTS

The results presented above have hopefully shed some light on the applicability of LEFM to a material such as concrete in the form of notched beams. Results at first glance may appear encouraging and yet they show up certain limitations. On the positive side, there are two aspects which might be considered. They are:-

1. The broad concepts of fracture mechanics can be applied to concrete. This is shown by the fact that the material is notch-sensitive, provided a minimum size of specimen is used. The present K_0 and K_c results can be interpreted in the light

of figure 9.1. It was stated that a critical K value of 1,08MPa√m appeared to suit the experimental notch-sensitivity results. A mean value of K_c for the 100mm beams of series F3 using experimental crack depths was [illegible] MPa√m, whereas a mean value for the deeper beams was 1,53MPA√m. Therefore the measured K_c values conform well with the predictions of figure 9.1 based on notch-sensitivity results.

The critical K value of 1,08MPa√m falls between measured K_0 and K_c values for the deeper beams. Obviously K_0 does not represent a condition of "true" fracture instability (in the sense of unstable crack growth), while K_c probably lies beyond the first occurrence of crack instability. This implies that somewhere between K_0 and K_c lies a point where true crack instability commences. If this is true, then the predictions of figure 9.1, based on LEFM, hold up well relative to measured K values.

2. It appears that initial notch depth ratio has a minor effect on K values, for shallow to intermediate notching (i.e. $0,2 \leq c_0/d \leq 0,4$). This is not necessarily true for unnotched beams or for deeply notched beams. The effect of notch depth is related to the fracture process, which changes as notch depths become progressively deeper. In essence, this question of fracture process is what distinguishes cemented materials from, say, metallic or ceramic materials. The extent and intensity of microcracking in the fracture zone will profoundly influence what is measured by way of load, deflection, etc. in the test. This in turn will influence the parameters that are calculated from the fracture record. Concrete fracture is complex, and what is immediately apparent is that fracture parameters must be closely related to the fracture process in hand.

It is obvious that the effect of beam depth is significant. For instance, the 100mm deep beams were notch-insensitive, and very much lower K_c values were measured. There was a clear division between K_c results for the 100mm beams, and those for the deeper beams. K_c values for 100mm beams do not represent a valid fracture criterion. For such beams K_c only has the significance that it

provides a measure of the stress field ahead of the notch, but cannot be regarded as a material parameter. For the deeper beams, there is a trend of K_c increasing with beam depth. However, provided the effect of using experimental rather than inaccurate apparent crack depths at maximum load is accounted for, the differences are not large, amounting to about 10 per cent between 200mm deep beams and 800mm deep beams. There are many tests on concrete where such a variation is accepted as being characteristic of material behaviour. For instance, it has been shown by the author that elastic modulus values can vary by up to 12 per cent depending on whether tests are done on larger concrete cylinders or on smaller concrete beams[66]. Diferences in compressive strengths between cubes of different size are accepted. Up to 100 per cent difference can occur for tensile strengths depending on the type of test[67].

A serious limitation of LEFM for concrete beams is that the fairly small variation in K_c with beam depth is probably fortuitous due to the nature of the beam test itself. It has been shown in chapter 7 that the relationship between microcracked zone size and residual ligament depth does not differ greatly for beam depths between 200mm and 500mm. Therefore, the influence of the relative microcracked zone size will be very similar in all beams where the depth is sufficient for valid fracture phenomena to occur. The very presence of a non-linear zone which is large relative to beam or crack depth must of necessity render the pure LEFM approach questionable, if not invalid for concrete beams. The implication of this is that the measured fracture parameters will depend largely on the nature and size of the non-linear zone; for the present fracture beams the non-linear zone had a similar effect on all beams greater than 200mm in depth, and therefore K_c values were similar. For other specimen types where the nature and size of the non-linear zone differs from that in notched beams, the probability is that very different values of fracture parameters will be measured. Hence, any variable that will affect the microcracked zone, such as specimen type or nature of the material, will influence the measured fracture parameters.

Returning again to the notched beams, fracture toughnesses (K_c) are somewhat higher for deeper beams, despite the net stress at the notch root being lower for these beams. The effect of the greater crack depth (i.e. $\sqrt{c}$ in equation (3.2)) more than outweighs the lower net stress. Interpreting this in terms of the effect of the microcracked zone on fracture, the higher K_c values may be thought of as resulting from higher average stresses in the microcracked zone during fracture which impart a greater fracture resistance to these beams. This point will be discussed in further detail in 9.11 below.

The overall assessment must be that LEFM is limited in its applicability to notched concrete beams, due primarily to the presence and appreciable influence of a relatively large non-linear microcracked zone. For any particular specimen type, it might appear that K_c values are reasonably independent of notch depth and scale effects, but this is true only if the relation between the non-linear zone size and specimen size is more or less constant. (It is also true only for specimens of size large enough to be notch-sensitive). A change in the nature or size of this non-linear zone will influence LEFM parameters, which can therefore not be regarded as fundamentally valid. Unfortunately, only notched beams were tested in the present work, which prevented this contention from being investigated. The LEFM approach, due to its simplicity, may prove valuable in a practical way, provided the type and size of specimen, and nature of the fracture process is accounted for. General applicability would, however, be limited.

To briefly summarise, note the following:-

1. Compressive strength variations were found to have a very minor influence on K_0 and virtually no influence on K_c. This was attributed to these variations being due primarily to bleeding, which will adversely affect compressive strength obtained from cube tests.

2. Initial notch depth ratio has a very minor influence on K_0 and K_c within the range $0,2 \leq c_0/d \leq 0,4$. Differences between pa-

Returning again to the notched beams, fracture toughnesses (K_c) are somewhat higher for deeper beams, despite the net stress at the notch root being lower for these beams. The effect of the greater crack depth (i.e. $\sqrt{c}$ in equation (3.2)) more than outweighs the lower net stress. Interpreting this in terms of the effect of the microcracked zone on fracture, the higher K_c values may be thought of as resulting from higher average stresses in the microcracked zone during fracture which impart a greater fracture resistance to these beams. This point will be discussed in further detail in 9.11 below.

The overall assessment must be that LEFM is limited in its applicability to notched concrete beams, due primarily to the presence and appreciable influence of a relatively large non-linear microcracked zone. For any particular specimen type, it might appear that K_c values are reasonably independent of notch depth and scale effects, but this is true only if the relation between the non-linear zone size and specimen size is more or less constant. (It is also true only for specimens of size large enough to be notch-sensitive). A change in the nature or size of this non-linear zone will influence LEFM parameters, which can therefore not be regarded as fundamentally valid. Unfortunately, only notched beams were tested in the present work, which prevented this contention from being investigated. The LEFM approach, due to its simplicity, may prove valuable in a practical way, provided the type and size of specimen, and nature of the fracture process is accounted for. General applicability would, however, be limited.

To briefly summarise, note the following:-

1. Compressive strength variations were found to have a very minor influence on K_0 and virtually no influence on K_c. This was attributed to these variations being due primarily to bleeding, which will adversely affect compressive strength obtained from cube tests.

2. Initial notch depth ratio has a very minor influence on K_0 and K_c within the range $0,2 \leq c_0/d \leq 0,4$. Differences between pa-

rameters measured at the extremes of this range were generally less than 10 per cent on average, with shallower notches giving higher values. However, 100mm beams show slightly opposite trends.

3. K_0 does not appear suitable as a fracture criterion for notched concrete beams. Differences of up to 50 per cent on average occurred between 800mm and 200mm beams. The reason for this is not clear at this stage, but possibly a plane stress/plane strain effect for the condition of fracture initiation is occurring.

4. Values of K_c differed by 10 to 15 per cent between 800mm and 200mm beams, provided experimental crack depths were used at the point of maximum load. 100mm beams gave K_c values roughly 40 per cent lower than the larger beams, thus confirming their unsuitability for fracture testing of this type. These results may appear encouraging for applicability of LEFM. However, it is considered that the more or less constant relation that the size of the microcracked zone bears to beam depth has resulted in results being consistent between different beam depths. For other specimen geometries where relative microcracked zone sizes may be substantially different from those in notched beams, different K_c values may be measured. This requires further substantiation. The presence of the microcracked zone cannot be ignored.

5. The somewhat higher K_c values measured in the larger beams relative to smaller beams may be interpreted as the influence of higher crack-closing stresses in the microcracked zone which impart a greater fracture toughness. This aspect will receive further attention in the following sections.

6. With regard to the beam test in particular, this test suffers from the critical dependence of K on crack depth, and hence on beam compliance. This fact, coupled with the basic heterogeneity of the concrete being tested, causes an unfortu-

nately large scatter of results, which is a disadvantage of this method.

In view of the limitations for LEFM discussed above, non-linear effects in fracture beams were also investigated. The following sections deal with this aspect of the fracture problem.

DIVISION 3 NON-LINEAR EFFECTS IN FRACTURE BEAMS

9.10 INTRODUCTION

The presence of extensive zones of microcracking in concrete fracture beams has been demonstrated and discussed in chapters 7 and 8. These zones are not small in relation to specimen size, and must therefore exercise an important influence on concrete fracture. This was evident in, for instance, the measurement of beam compliances (see chapter 6). Experimental compliance relationships differed markedly from theoretical relationships, due primarily to the restraining influence of crack-closing stresses which, it was postulated, depended also on beam depth. In this section, non-linear effects will be dealt with:- firstly by considering stresses in fracture zones using a simplified stress model; secondly by applying an R-curve approach to fracture using a stress-intensity factor K_R; and thirdly by discussing effective fracture surface energies in fracture beams.

9.11 STRESSES IN FRACTURE ZONES

One of the main problems with the application of fracture mechanics principles to cemented materials is that of the existence and size of the non-linear microcracked zone ahead of the main crack tip. The behaviour of the material in this zone is characterised by strain-softening in which the crack-closing pressure or stress decays as the displacement between the crack surfaces increases. By making assumptions about the form of the stress-displacement curve, it is possible to estimate the magnitude of the stresses in the non-linear zone and incorporate these into fracture calculations. However, this also requires knowledge of the extent of the micro-

cracked zone ahead of the crack tip. A number of authors (for example Wecharatana and Shah[48], and Reinhardt[49]) have used assumed forms of displacement fields and stress distributions to arrive at theoretical estimates of the size of the non-linear zone. Reinhardt was able to verify his theoretical approach from experiment. In the present work, the approach is somewhat different in that non-linear zone sizes have been measured, and characteristic relationships between zone sizes and a geometrical beam parameter (h) have been derived experimentally. Knowing non-linear zone sizes allows reasonable estimates of stress states in fracture beams to be made. This in turn permits calculations of external beam loads as a function of crack depth. As will be shown later, the crack-closing stresses can also be considered to contribute a component to the stress-intensity factor at the crack tip.

9.11.1 BASIC ASSUMPTIONS

The basis for estimation of stress states has been discussed previously in 3.5.1 and 7.1. To briefly summarise, four distinct stress zones may be identified in fracture beams, and these are shown in figure 7.1. The zones are a destressed zone around the main stress-free crack, a microcracked zone extending ahead of the main crack, an intact tension zone immediately below the neutral axis, and a compression zone above the neutral axis. Stress transfer is possible within the residual ligament depth of the beam, which comprises the sum of the depths of the compression zone, intact tension zone, and microcracked zone.

In order to analyse beam stresses the following assumptions are made:-

1. The beam is considered to contain a crack of effective depth c_{eff} which is the sum of the stress-free crack depth c and depth of the non-linear zone z_{nl}[49]. The stress-free crack might be the initial notch depth or it might be the visible crack depth

measured during a test. Figure 9.12 shows an effective crack in a beam.

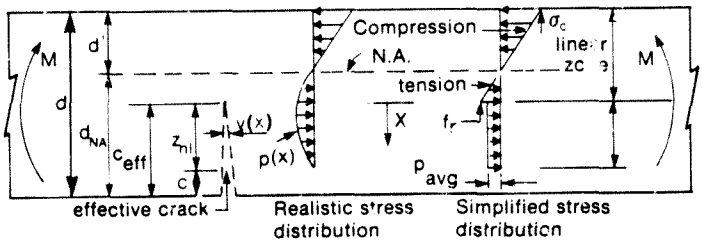


Figure 9.12 Effective crack and assumed stress distributions in concrete fracture beams

2. The beam is acted on by external loads such that a bending moment M exists at the cracked section. The influence of shear on the cracked section as well as on the deformations of the beam as a whole is ignored, since the presence of a notch or crack dominates the localised stress distribution and the overall deflection of the beam.

3. Within the non-linear zone there is a closing stress distribution p(x) such that p(x) = 0 at $x = z_{nl}$, at which point a critical crack opening displacement (COD) occurs. The stress p(x) is a function of the displacement between crack faces v(x) and hence of x. The crack extends when $v(x=z_{nl})$ equals or just exceeds the critical COD, which itself will be a function of specimen type and size of aggregate.

The closing stress distribution p(x) can be obtained from measurements of the strain distribution coupled with an assumed form for p(x), the requirement being that internal force and moment equilibrium is maintained. Various researchers have tackled this problem[101], on the assumption that inelastic deformations in this zone are concentrated in a narrow band around a single major crack. This allows the width of the crack to be equated to the inelastic deformation. On this basis, the relation between the tensile stress

and the width of the crack is assumed to be identical to the closing pressure versus crack opening displacement (COD) relationship. In the work done by Shah et al[6] on double torsion and double cantilever specimens, it was also assumed that this relationship could be obtained from results of uniaxial tests in which the full stress-deformation curve is obtained. For notched beam specimens, it would probably be better to obtain this relationship from flexural tests since Hsu et al[8] have shown that strain gradients can markedly affect the stress-deformation relation. However, the work of Shah et al has also shown that the estimation of non-linear zone size is very little affected by the assumed form of this relationship. For instance, they compared results using a quadratic form for the stress-displacement curve suggested by Evans and Marathe[101] with results using a uniform average stress, and found the results were virtually identical for both relations. Since the entire analysis is based on the simplifying assumptions under discussion, it would seem that refinements at this stage are unjustified. The simplest form for this relationship is an average uniform stress independent of x, i.e. p_{avg}, and this is shown in figure 9.12.

4. The stress distribution across the notched section is assumed to be a combination of a linearly varying and uniform stress, as shown in figure 9.12. The assumption of a linearly varying stress across the elastic portion of the beam is not strictly true, as shown in ref. 86. However, in the compression zone, the stresses are a fairly small proportion of the compressive strength, and therefore a linear stress distribution is reasonable, while in the tension zone the overall compliance of the specimen will be very little affected by a somewhat curvilinear stress distribution as opposed to a purely linear distribution.

5. During fracture or extension of the crack, the value of the maximum tensile stress at the boundary between linear and non-linear zones is assumed to equal the characteristic tensile strength of the material, in this case the modulus of rupture

f_r. This has also been adopted by other investigators, for example Reinhardt[9.8].

9.11.2 CALCULATION OF AVERAGE STRESSES

Using the above assumptions, the fracture zone stresses were calculated by calibrating the neutral axis position derived from theoretical considerations against the experimental neutral axis relationship. The theoretical neutral axis position can be found from applying conditions of internal force equilibrium, i.e. by equating the total compression force to the total tension force at the notched cross-section. The simplified stress distribution shown in figure 9.12 is used. The resulting expression is:-

$$d' = \frac{d^2+c_{eff}\left[c_{eff}+2z_{nl}\left(\frac{p_{avg}}{f_r}\right)\left(\frac{d}{c_{eff}}-1\right)-2d\right]}{2\left[d-c_{eff}+z_{nl}\left(\frac{p_{avg}}{f_r}\right)\right]} \qquad (9.9)$$

where $d' = d-d_{NA}$ (see figure 9.12).

Equation (9.9) can be re-arranged to provide an expression for p_{avg}/f_r:-

$$\frac{p_{avg}}{f_r} = \frac{(c_{eff}-d)(c_{eff}-d+2d')}{2z_{nl}(c_{eff}-d+d')} \qquad (9.10)$$

From the geometry of the stress distribution, an expression for σ_c/f_r can also be found:-

$$\frac{\sigma_c}{f_r} = \frac{d'}{(d-d'-c_{eff})} \qquad (9.11)$$

where σ_c is the extreme fibre compressive stress. If we define $z_{nl} = k_0(d-c)$, and $d' = k_1(d-c)$, then equations (9.10) and (9.11) become:-

$$\frac{p_{avg}}{f_r} = \frac{(k_0-1)(k_0-1+2k_1)}{2k_0(k_0-1+k_1)} \qquad (9.12)$$

and

$$\frac{\sigma_c}{f_r} = \frac{k_1}{1-k_1-k_0} \qquad (9.13)$$

Therefore the average stress in the microcracked zone and the extreme fibre compressive stress are functions only of the relationships between zone size, neutral axis depth and residual ligament depth, and are directly proportional to the modulus of rupture of the material. The relevant k values from figure 7.14 are:-

500mm and 300mm beams,	$k_0 = 0,470$
200mm beams,	$k_0 = 0,446$
100mm beams,	$k_0 = 0,401$
All beams,	$k_1 = 0,316$

(k_0 and k_1 are termed the fracture zone size coefficient and neutral axis position coefficient respectively). Values of p_{avg}/f_r and σ_c/f_r are calculated from equations (9.12) and (9.13) and are shown in table 9.3.

Table 9.3 Relative values of stresses in fracture beams

Beam depth (mm)	500 and 300	200	100
p_{avg}/f_r	0,269	0,264	0,087
σ_c/f_r	1,477	1,328	1,117

The values for p_{avg}/f_r given in table 9.3 are highly significant in the light of previous qualitative conclusions concerning stress states in fracture beams. In chapter 6 (6.6.3), a tentative conclusion was made that average stresses in 100mm beams would be lower than in larger beams, on the basis of rotations of crack faces. For the same c/d, 100mm beams experienced considerably greater crack face rotations than larger beams, leading to greater aggregate pull-out and disruption of stress-carrying ligaments. In chapter 7 (7.5.3), limits to the size of microcracked zones were inferred from the characteristic relationship between compression and tension zone depths in a beam during fracture. It was shown that the upper limit was based on a condition in which the microcracked zone provides all the tension component, while the lower limit gave the condition in which the microcracked zone provides zero stress transfer. Consequently, the positions that measurements of microcracked zone size occupy relative to these limits indicate the degree of stress transfer in this zone. The fact that results for 100mm beams lay very much closer to the lower limit than results for larger beams indicated that lower average stresses occurred in the microcracked zone of these beams. The values in table 9.3 bear out these conclusions, and show that average microcracked zone stresses of 100mm beams are only about one-third of those in larger beams.

The limits of validity of the simplified stress distribution shown in figure 9.12 require some examination. Equation (9.12) indicates that p_{avg}/f_r increases as k_0 increases. The relationship is roughly linear up to $k_0 = 0{,}5$, and thereafter p_{avg}/f_r increases fairly rapidly with increase in k_0 (see figure 9.13). The average stress in the microcracked zone for $k_0 = 0{,}368$ is zero, which accords with the lower limit in figure 7.12.

Figure 9.13 shows that $p_{avg}/f_r = 1$ for $k_0 = 0{,}61$; in this case the uniform stress in the microcracked zone is sustained at a level equal to the modulus of rupture, f_r. Such behaviour is characteristic of a material whose stress-strain relationship is initially linear up to a limiting or "yield" stress, followed by a plateau value of the yield stress with increasing deformation, i.e. an

elastic-plastic material (eg. mild steel). This is essentially the condition described by the Dugdale[45] model for such materials. However, concrete is not an elastic-plastic material, but has a stress-deformation relationship in the post-peak region which can be described as strain-softening, i.e. a reduction in stress with increasing deformation. Therefore, a condition of $p_{avg}/f_r = 1$ ($k_0 = 0,61$) for the assumed stress model of figure 9.12 is impossible for plain concrete (although a fibre-reinforced material may approach this condition).

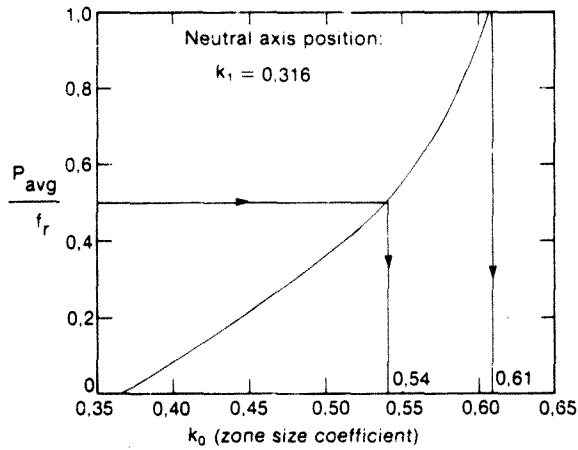


Figure 9.13 Dependence of average stress in microcracked zone on zone size

A more realistic upper limit for plain concrete would be a condition of $p_{avg}/f_r = 0,5$ for which $k_0 = 0,54$. (See also Reinhardt[48]). In this case the stress distribution in the microcracked zone could be considered as triangular, ranging from $p(x) = f_r$ at $x = 0$ to $p(x) = 0$ at $x = z_{n1}$. The upper limit of $k_0 = 0,61$ in figure 9.13 must be considered as applying only to those materials which can develop and sustain very high stresses in the microcracked zone, such as fibre-reinforced materials. Furthermore, the simplified stress model of figure . is no longer valid for $k_0 > 0,61$ and a d_f-

ferent form for the stress distribution would be required for such materials.

Figure 9.13 is valid only for plain concrete beams where the neutral axis position during fracture is given by $k_1 = 0,316$. Other materials will in all likelihood have different relationships for the neutral axis position. Figure 9.13 is nevertheless valuable in indicating the variations of average fracture zone stresses with zone size. Note also that the theoretical upper limit of $k_0 = 0,684$ in figure 7.12 can apply only to strain hardening materials where, with additional strain, stresses higher than an initial yield stress can be developed. This is virtually impossible for cemented materials as we know them at present.

The 300mm and 500mm beams with $k_0 = 0,47$ have results which indicate that average microcracked zone stresses are about one-half of the maximum stresses which could be developed in plain concrete beams. On the other hand, 100mm beams with $K_0 = 0,40$ develop relatively low stresses in the microcracked zone. This is entirely consistent with other observations on 100mm beams, viz.

1. There is very little distortion of strain profiles, indicating a small influence of the microcracked zone.

2. Compliances for 100mm beams are considerably higher for a given c/d than compliances for larger beams, indicating very little restraint on deflections from crack-closing stresses.

3. 100mm beams are notch-insensitive, implying that failure is controlled by the net section stress. If fracture zone stresses are small, they will exercise little influence on beam failure, and the *maximum* tensile stress (i.e. f_r) will govern the failure.

However, the average stresses in fracture zones also appear to be a function of the progress of cracking during a test. This is discussed below.

9.12 RESISTING MOMENTS IN FRACTURE BEAMS

The simplified stress model shown previously in figure 9.12 can be used to calculate the moment of resistance (M_R) developed by a fracture beam. Taking moments of the compression and tension force components about the neutral axis, the expression for M_R is:-

$$\frac{M_R}{bf_r} = \frac{(c_{eff}-d)^2(c_{eff}-d+3d')-1,5z_{nl}(c_{eff}-d)(c_{eff}-d+2d')}{6(d-d'-c_{eff})} \qquad (9.14)$$

Substituting in equation (9.14) using the relationships $z_{nl} = k_0(d-c)$ and $d' = k_1(d-c)$, we have:-

$$\frac{M_R}{bf_r} = (d-c)^2 \frac{(1-k_0)(k_0^2+k_0+6k_1-2)}{12(1-k_0-k_1)} \qquad (9.15)$$

Equation (9.15) expresses a relationship between the moment of resistance, beam dimensions, crack depth, and modulus of rupture. The characteristic relationships for sizes of stress zones (i.e. k_0 and k_1 values) also influence M_R. Equation (9.15) was checked against results for the fracture beams of series F3. For each cycle of load, a crack depth was obtained from the reloading compliance curve (figure 6.8). The applied beam moment at the point of measurement of strain and crack depth could be calculated and the self-weight moment added. Hence experimental relationships between M_R/bf_r and $(d-c)^2$ could be plotted, knowing b (100mm) and f_r (from table 5.1). By drawing straight lines on the graph representing different k_0 values, the curve for any beam could be interpreted in terms of average stress in the fracture zone. (A constant value of $k_1 = 0,316$ was used in equation ((9.15) - see figure 7.11). This procedure was carried out for all the beams of series F3, and results for 300mm beams are shown in figure 9.14. Results for other beam sizes were very similar to those in figure 9.14.

The relationship for any particular beam is shown by the lines (either dashed or solid) joining experimental points, and the arrows indicate the direction followed as the test progressed. Max-

imum load points, and a broad dashed line differentiating between c/d values less than or greater than 0,5, are also shown.

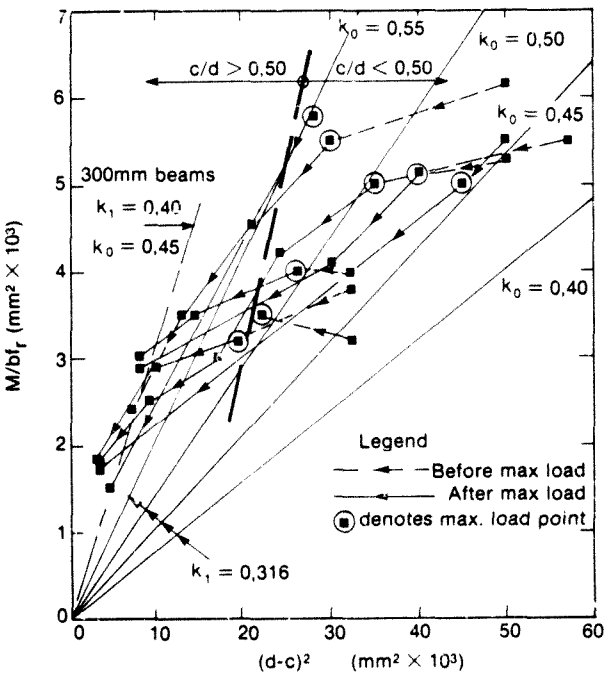


Figure 9.14 Moment of resistance relationships for 300mm fracture beams

Note the following from figure 9.14:-

1. The figure indicates that k_0 values vary during a test, generally increasing as crack depth increases. Thus, for points before maximum load, k_0 values are between about 0,43 and 0,52 for 300mm beams. (Corresponding values for 500mm beams were 0,41 and 0,51). After maximum load, k_0 values up to approximately 0,6 for 300mm beams (and approximately 0,55 for 500mm

beams) occur. These results appear to indicate that non-linear zone sizes increase with the progress of cracking, leading to higher average stresses in these zones.

2. Values of k_0 from the point of maximum load up to c/d = 0,5 vary from about 0,45 to 0,55. These values can be compared with the mean k_0 value of 0,47 indicated in figure 7.14 for 300mm and 500mm beams. Values are similar, despite the difference in methods used to obtain typical values. The moment of resistance method tends to give somewhat higher k_0 values than the strain and ultrasonic methods. However it is important to note that load cycles used in the latter method to obtain measurements of microcracked zone depth invariably had c/d values less than 0,5. Load cycles prior to maximum load were also not used on the grounds that the microcracked zone size was not yet fully developed, a point also illustrated by the dashed lines in figure 9.14. It is strictly correct to compare k_0 values from the various methods only for experimental points at or beyond maximum load, and for c/d less than 0,5. Figure 9.14 helps to explain the scatter of results shown in figure 7.14, since k_0 values appear to vary during a test.

The variation in k_0 values for 200mm and 100mm beams using the moment of resistance method were similar to those quoted above for 500mm and 300mm beams. At first glance, the fact that the 100mm beam results were similar to those for the larger beams might appear contradictory to the trend shown in figure 7.14. However the aspect of roller friction must be considered. This has been discussed previously in 5.5, and receives further attention in 9.14. Suffice to say that results for the 100mm beams of series F3 appear to have been significantly affected by roller friction, which will tend to increase measured beam loads and moments. Using beam loads reduced according to the mean value for the coefficient of friction of 0,5 suggested in 9.14 (see later), the k_0 values for the 100mm beams were reduced by about 10 per cent. This reduction is comparable to the difference in k_0 values between 100mm beams, and beams larger than 100mm (figure 7.14). The difference in k_0 values obtained from the various methods highlights the difficulty of measuring

non-linear zone sizes in concrete. Values given by the strain/ultrasonic methods are considered to be superior to those given by the moment of resistance method, since the latter method is affected by extraneous influences such as roller friction.

3. The k_0 values given in figure 9.14 should be viewed in the light of the suggested limit of $k_0 = 0{,}54$ given in figure 9.13. The fact that some k_0 values exceed 0,54, particularly for the 300mm beams, might again be attributed to effects of roller friction. However, equation (9.15) is very sensitive to changes in the value of k_1, and for deep cracking when the size and influence of the microcracked zone is small, the k_1 value tends to increase to a value above 0,316. This fact was mentioned in 7.5.2 and figure 7.11 shows that for $(d-c) < 50$mm, $k_1 \rightarrow 0{,}5$. Applying this reasoning to figure 9.14, a line with $k_1 = 0{,}40$, and $k_0 = 0{,}45$ has been drawn in. For the 300mm beams, results during the final stages of fracture cluster about this line, and would tend to fall entirely below the line had roller friction been absent. (In the case of the 500mm beams, all results fall well below this line). Therefore, the dual effects of roller friction and an increase in the value of k_1 (i.e. a relative lowering of the neutral axis position) provide the most likely explanation for the experimental points representing final stages of cracking in figure 9.14. Note also that applying $k_1 = 0{,}40$ and $k_0 = 0{,}45$ to equations (9.12) and (9.13) show that $p_{avg}/f_r = 1{,}0$ and $\sigma_c/f_r = 2{,}7$. This indicates that in the final stages of cracking when the microcracked zone size is small in an absolute sense, the entire zone is highly stressed and the condition of an elastic-plastic material is approached. However, considering only 500mm beam results, a line passing through the experimental points during the last stages of fracture would have k_0 and k_1 values which would give values of p_{avg}/f_r less than unity. This would conform more with our understanding of the behaviour of concrete in the fracture zone. Hence, where roller friction has affected results as in the case of 300mm beams, results for conditions approaching the final stages of fracture should be treated with caution.

9.13 R-CURVES USING K_R

The concept of crack growth resistance curves (R-curves) was introduced in chapter 3. An R-curve shows the resistance of a material to crack propagation. This crack growth resistance may be measured in terms of a stress-intensity factor. The R-curve technique was developed to deal with the problems of plasticity and non-linear fracture behaviour, and therefore takes into account those factors influencing such behaviour, such as size of microcracked zone and specimen shape. The technique has also become a very useful tool for characterising fracture of materials, and this is examined in this section. The R-curve can also be used to assess the fracture strength of a specimen, provided the R-curve is related to the particular specimen geometry and fracture process. This section will deal briefly with the calculation of R-curves for the present tests, based on a stress-intensity parameter K_R. A later section (9.14.2) will deal with R-curves based on a fracture energy parameter.

9.13.1 STRESS-INTENSITY PARAMETERS

Limitations in applying LEFM to concrete fracture beams have been discussed earlier in 9.2 and 9.9. The non-linearity introduced by the microcracked zone indicates that a non-linear type of fracture parameter might be more appropriate. It is possible to express a material's resistance to crack growth by means of a stress-intensity factor. The approach adopted here is to accept the non-linearity of the material, and account for this by using the effective crack depth, c_{eff} (see figure 9.12). Wecharatana and Shah[48] were able to show that by using this parameter, specimen-type-independent R-curves from tests on double cantilever beams and double torsion specimens could be drawn. Use of c_{eff} has the advantage of characterising aspects of the fracture process that would not be obvious if only the stress-free crack depth c was

used. Hence, stress-intensity factors are calculated in the normal way, except that c_{eff} is used in place of c. The work on fracture zone sizes presented in chapters 7 and 8 can therefore be used.

Referring to a typical load-deflection record (see figure 4.6(a)), the following stages in the fracture process can be identified. Each stage has a characteristic effective crack depth and stress-intensity factor:-

1. An initial linear portion, which terminates at the point of departure from linearity. This point has been defined earlier in 9.2.2 as the point of fracture initiation, or the point where non-linear behaviour begins. It is taken as the point at which significant onset of microcracking and damage in the zone ahead of the notch begins. The characteristic crack depth and stress intensity factor are c_0 (initial notch depth), and K_0 respectively. K_0 has been given previously in table 9.1.

2. A portion beyond the point of fracture initiation, and generally terminating before the maximum load point. During this stage, there is no visible crack advance, but the microcracked zone develops to its full extent. At the upper limit of this portion, there is initiation of main (stress-free) crack growth. The characteristic crack depth and stress intensity factor are $c_{eff} = c_0 + z_{nl}(max)$ and K_i respectively, where $z_{nl}(max)$ is the maximum depth of the microcracked zone, and K_i represents the maximum ability of the material to resist fracture without main crack extension.

3. The portion beyond that described in 2. above. This portion generally includes the maximum load point and is characterised by main crack advance. During this fracture stage, the stress intensity calculated at the tip of the effective crack rises, and depending on the depth of the beam, achieves a plateau value. The characteristic crack depth is $c_{eff} = c + z_{nl}$, where c is increasing and z_{nl} is decreasing due to decreasing h, and the characteristic stress-intensity factor is K_R, which re-

presents the ability of the material to resist fracture during crack extension. K_R is therefore a function of crack extension.

The fact that stress-intensity factors are calculated at the tip of the effective crack implies that the influence of closing stresses in the microcracked zone are accounted for. These closing stresses essentially contribute an additional component to the stress-intensity factor at the crack tip, as noted by Lenain and Bunsell[42] and Reinhardt[48]. For the present work therefore, K_R will be considered to include the effects of crack-closing stresses.

9.13.2 CALCULATION OF R-CURVES

K_R-curves were calculated for the beams of series F3 only, since a confident assessment of crack growth had been obtained. Results are therefore limited, and conclusions should be regarded as tentative. It was hoped that the feasibility of the K_R-curve method for beams could be investigated, and further work could then be undertaken based on these results. K_R-curves were not calculated for 100mm beams since previous sections have shown that fracture principles cannot be applied to these beams. The method of calculating R-curves was as follows:-

1. K_0 was obtained from the initial notch depth and the load at the point of departure from linearity. K_0 values have been given previously in table 9.1(b). The effective crack depth for K_0 was c_0.

2. K_i was estimated from one of the earlier load cycles immediately before main crack advance was observed. The depth of the microcracked zone was therefore a maximum, i.e. $z_{nl}(max) = k_0 h_0$, where k_0 is the fracture zone size coefficient and h_0 is the initial residual ligament depth. The effective crack depth was therefore $c_0 + z_{nl}(max)$. K_i was calculated from equation

(3.2), using Y values based on c_{eff}, and obtained from figure 3.4.

3. K_R values were calculated using the loads at which strain readings and crack depth readings were taken. These loads were approximately the peak cycle loads. The effective crack depth was calculated using equation (3.25), i.e. $c_{eff} = c + k_0 (d-c)$. K_R values were calculated from equation (3.2), using Y values based on c_{eff}, and obtained from figure 3.4.

4. The R-curve was produced by plotting K values against their respective c_{eff} values. The maximum effective crack depth ratio (i.e. c_{eff}/d) used was 0,8, for reasons outlined in 3.3.1. (Note that beam self-weight was included in the K calculations).

K_R curves are shown in figure 9.15 for the 300mm beams of series F3. (Beam F3/5(300/0,2) was omitted due to a scarcity of experimental points). Note the following:-

1. Curves for beams with various initial c_0/d values are shown, as well as points representing K_0, K_i, and K_R at the point of maximum load.

2. K_0 values are generally consistent for the different c_0 values, with a mean value of 0,52MPa$\sqrt{m}$. Thus the point of fracture initiation is independent of initial notch depth within the range c_0/d = 0,2 to 0,4. K_i values are more erratic than K_0 values, with a mean of 2,31MPa$\sqrt{m}$. This value represents the maximum effective fracture toughness of the material without crack extension. K_R values at maximum load are very erratic, indicating that this point has no real significance relative to the fracture process (except possibly that it represents a condition of crack instability). K_R generally continues to increase beyond K_R at maximum load.

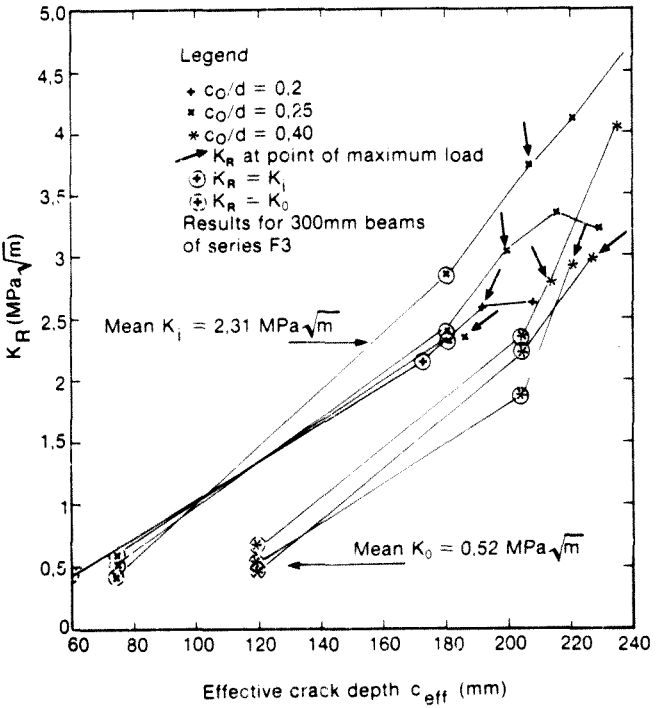


Figure 9.15 K_R-curves for 300mm beams of series F3

3. There is a general trend of the slope of the curves increasing after K_i. The significance of this will be discussed later. The curves for c_0/d = 0,4 are also generally steeper than those for c_0/d = 0,2 or 0,25. Resistance to crack growth therefore increases at a faster rate with effective crack growth for deeper notching. The curves for c_0/d = 0,2 or 0,25 generally continue past the point of maximum load, while those for c_0/d = 0,4 generally terminate at the point of maximum load. This is partially because K_R values were plotted only up to a c_{eff}/d ratio of 0,8. It also indicates that for the deeper

notched beams, there is insufficient beam depth for crack growth resistance to achieve higher values.

4. A plateau value for K_R is not evident in figure 9.15, due to the insufficient beam depth condition discussed above. Figure 9.16 that follows shows that a plateau value may possibly exist.

Figure 9.15 is typical of K_R-curves that were obtained for series F3 beams. It is necessary to show curves for the full range of beam depths (i.e. 200mm to 500mm), since specific features were more noticeable particularly in the larger beams. A preliminary investigation of the K_R-curves showed that the basic shapes of the curves were similar for all beam sizes. However, the average slopes differed, being flatter for the larger beams and steeper for the smaller beams. A roughly size-independent K_R-curve could be obtained by plotting K_R values against the relative crack advance of the effective crack, given by

$$\frac{c_{eff} - c_0}{d - c_0} \qquad (9.16)$$

This procedure was carried out for the 200mm, 300mm, and 500mm beams of series F3, and results are shown in figure 9.16. (Note that preliminary K_R-curves based on visible crack depth c were also plotted; however there was a far greater scatter than that shown in figure 9.16, and less consistent trends). Note the following from figure 9.16:-

1. A rather large scatter of results occurs. This seems to be a consistent feature of fracture testing of heterogeneous materials like concrete.

2. K_0, K_i, and K_R at maximum load are shown. The scatter increases with increase of K values.

3. Results from all beams have been grouped together, and general trends drawn through the points. These trend lines intersect the mean values of K_0 and K_i. It can be seen that the material

develops very significant additional fracture resistance before main crack extension begins (i.e. from K_0 to K_i). This occurs over a relatively small portion of the load-deflection curve. (Intermediate points between K_0 and K_i have not been plotted since it was not possible to assess the extent of the micro-cracked zone as it developed from K_0 to K_i).

4. The relative effective crack depths at which K_i values are plotted reflect the characteristic relationship between the microcracked zone size and h, i.e. the k_0 value. The values shown are 0,47 for 300mm and 500mm beams, and 0,45 for 200mm beams.

5. After K_i, there is an increase in the rate of development of fracture resistance with effective crack growth. This is very significant when interpreted in the light of figure 9.14, which showed that average stresses in the microcracked zone increased with crack growth. In moving from K_0 to K_i, the microcracked zone is developing to its maximum size, and average stresses are fairly low. After initiation of main crack growth (i.e. after K_i), average microcracked zone stresses increase throughout the fracture process. The flatter initial slope in figure 9.16 therefore represents the initial build-up of stresses during the development of the microcracked zone; the steeper slope represents the further increase in fracture zone stresses that has been indicated in figure 9.14. The K_R-curves therefore confirm the findings from analyses of fracture zone stresses performed earlier. (Note that the K_R curves are based on constant values of $k_0 = z_{nl}/h$. Figure 9.14 indicates that k_0 also increases during crack growth. This would tend to slightly flatten the steeper curve in figure 9.16. An analysis was carried out which showed that the maximum reduction in slope would be about 15 per cent, which does not affect the general trend shown in figure 9.16).

6. Figure 9.16 shows that generally K_R values near the termination of the test increased for the deeper beams. This implies that shallower beams, and in particular the 200mm deep beams, have

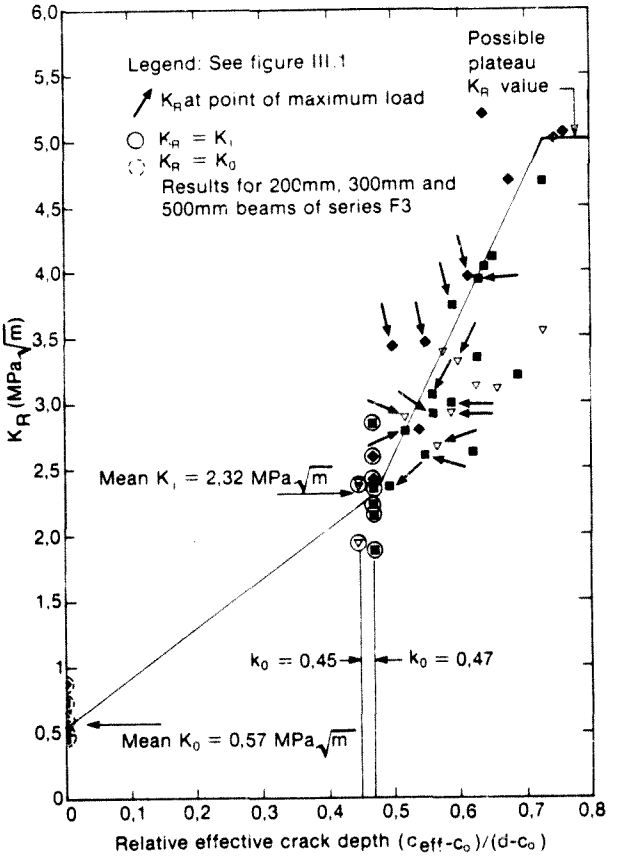


Figure 9.16 K_R-curve for beams of series F3 expressed as a function of relative effective crack depth

insufficient depth to allow the fracture resistance of the material to develop fully. The 500mm beams may possibly have been deep enough to allow full development of fracture resistance, i.e. a plateau value possibly exists for these beams at a K_R value of between 5 to 5,5MPa$\sqrt{m}$. This value is relatively high especially when compared with plateau K_R values of 6 to 7 MPa$\sqrt{m}$ obtained for asbestos cement by Mai et al[43]. There is a possibility that the high K_R values near the termination of the fractura test may be influenced by additional uncharacteristic fracture processes coming into play. These extraneous processes would be associated with the beam test itself; further discussion is given later in 9.14.2.

7. The general conclusion from figure 9.16 is that the existence in a concrete beam of a microcracked zone that can develop significant crack-closing stresses imparts a considerable toughening effect to the material. Where a microcracked zone does not develop, fracture behaviour is less tough. Also, where stresses in the microcracked zone are small, as in the present 100mm beams, the resistance to crack growth is lowered, and a lower fracture toughness results.

It should be stressed that the plotting of R-curves based on c_{eff} and the conclusions drawn therefrom are exploratory rather than definitive at this stage. One of the important questions that still requires resolution is the validity of the assumption that the full depth of the microcracked zone, i.e. $z_{nl} = k_0 h$, should be included in c_{eff}. Wecharatana and Shah[40] suggest that this is true for cement mortar, but Lenain and Bunsell[42] suggest that, for asbestos cement specimens, about one-third of the microcracked zone depth can be included in c_{eff}. Obviously, the answer will depend on the type of material and the type of specimen. Further analytical and experimental studies will be required to resolve this. However, there are advantages in adopting the principle that non-linear zone effects ought to be included in fracture formulations, since aspects of the fracture process are thereby revealed. For instance, estimates can be made of the stress-intensity factor (K_i) required

to develop the microcracked zone; the apparent change in the slope of the K_R-curve after K_i helps to shed light on mechanisms of fracture toughness. To conclude, the intention of this section on R-curves using K_R was to explore the feasibility of the method for characterising fracture and providing a measure of fracture strength, and encouraging results have been obtained. Further work is needed, and the scatter of results remains a major problem.

9.14 EFFECTIVE FRACTURE SURFACE ENERGY

The effective fracture surface energy γ' has been defined in chapter 3 as the *average energy consumed* by the creation of new fracture surfaces over the full fracture process. True free surface energy as well as energy expended due to other mechanisms (for instance damage due to microcracking, aggregate interlock and pull-out, creep, thermal, and acoustic energy) are included in γ'. γ' may therefore be regarded as a "global" measure of fracture toughness, without regard to particular mechanisms of energy dissipation.

The method of determining γ' involves measuring the total work of fracture, usually represented by the area under a load-deflection curve. It is necessary to include work done by specimen self-weight if specimens are large. Since γ' includes non-linear and irrecoverable effects, it may be regarded as a non-linear fracture parameter. However, conceptually it cannot be easily related to other parameters (except possibly J_c). This is because γ' is based on the energy approach to fracture, whereas a parameter such as K is based on a stress-intensity approach. In LEFM, it can be shown that there is a direct equivalence between the energy and stress-intensity approaches (see 2.2). For highly heterogeneous and non-linear materials such as concrete, the concept breaks down. Thus γ' embraces mechanisms of crack initiation as well as propagation, and can be related only to the average condition occurring during crack growth. On the other hand, stress-intensity factors can be related to specific points during the fracture process, and

are normally related to the point of instability. The fact that $\mathcal{G}'$ includes for conditions of instability and later conditions where crack growth is stable and requires external energy for its continued occurrence, makes any fundamental relation between $\mathcal{G}'$ and K a very tenuous one. The two different types of parameter should rather be regarded as describing different fracture phenomena, and use of one or the other will depend on the particular problem in hand.

The use of $\mathcal{G}'$ has been proposed as a fracture criterion (see for instance recommendations of RILEM for a standard fracture test[73]). This is not a new concept, since it has been applied to other materials such as ceramics[6], PMMA[102], and fibre-reinforced cement[71]. However, it should be appreciated from the outset that for cemented materials, the use of $\mathcal{G}'$ as a fracture criterion will depend on the energy-absorbing mechanisms that are mobilised by virtue of the test method. This becomes very obvious when, for instance, the degree of microcracking is limited due to deep notching, as will be shown below. Therefore, $\mathcal{G}'$ is unlikely to become a "universal" criterion for a material like concrete, since the type of fracture occurring will influence the parameter.

This section considers $\mathcal{G}'$ as a possible fracture criterion in two ways:- firstly the use of $\mathcal{G}'$ representing the total work of fracture, i.e. the average value over the full fracture process; and secondly the use of $\mathcal{G}'$ in the form of a crack growth resistance curve (R-curve). For this case, $\mathcal{G}'$ will be referred to as $\mathcal{G}_R$. These two aspects will be dealt with in order.

9.14.1 EFFECTIVE FRACTURE SURFACE ENERGY FROM TOTAL WORK OF FRACTURE

$\mathcal{G}'$ was evaluated from load-deflection records for all three series of fracture beams. Results are shown in table 9.4 in the form of two $\mathcal{G}'$ values as follows:-

Table 9.4 Effective fracture surface energy results

Beam	δ_m (mm)	$\gamma'(\delta_m)$ (N/m)	δ_u (mm)	$\gamma'(\delta_u)$ (N/m)
F1/1 (500/0,2)		Incomplete record		
F1/2 (500/0,2)	1,088	85,2	2,176	101,2
F1/3 (500/0,4)	1,186	91,7	2,372	114,9
F1/4 (500/0,4)	1,509	130,0	3,018	159,6
F1/5 (300/0,2)		Incomplete record		
F1/6 (300/0,2)	1,465	116,4	2,930	129,3
F1/7 (200/0,4)	2,029	101,1	4,058	117,0
F1/8 (200/0,4)	1,934	85,0	3,868	100,2
F1/9 (100/0,25)	2,104	95,3	4,208	102,1
F1/10(100/0,25)	1,991	73,4	3,982	79,9
F1/11(100/0,25)	2,380	126,2	4,760	133,9
F1/12(100/0,4)	1,836	127,8	3,672	135,2
F1/13(100/0,4)	1,722	81,5	3,444	88,4
F1/14(100/0,4)	1,398	81,7	2,796	87,4
F2/5 (100/0,25)		Beam damaged		
F2/6 (100/0,25)	1,241	79,8	2,482	83,8
F2/7 (100/0,25)	1,804	94,2	3,608	100,0
F2/8 (100/0,25)	1,825	104,6	3,650	110,5
F2/9 (100/0,4)	1,213	66,3	2,426	71,2
F2/10(100/0,4)	1,509	82,2	3,018	88,3
F2/11(100/0,4)	1,184	59,2	2,368	64,0
F2/12(100/0,4)	1,747	107,1	3,494	114,1
F2/13(100/0,4)	1,919	100,2	3,838	107,9
F2/14(100/0,4)	2,654	98,3	5,308	109,0
F2/15(100/0,4)	1,719	75,8	3,438	82,7
F2/16(100/0,5)	1,833	67,5	3,666	84,8
F2/17(100/0,5)	1,108	29,2	2,216	35,6
F2/18(100/0,5)	0,963	32,0	1,926	41,0
F2/19(100/0,5)	1,742	65,8	3,484	82,1
F2/20(100/0,5)	0,573	25,9	1,146	31,3
F2/21(100/0,5)	1,079	43,0	2,158	53,2
F2/22(100/0,5)	1,050	48,6	2,100	58,4
F2/23(100/0,5)	0,945	35,8	1,890	44,7
F2/24(100/0,5)	1,957	73,9	3,914	92,3
F2/25(100/0,5)	1,556	55,6	3,112	70,3
F2/26(100/0,5)	1,910	72,9	3,820	90,8

Table 9.4. Effective fracture surface energy results (Continued)

Beam	δ_m (mm)	$\gamma'(\delta_m)$ (N/m)	δ_u (mm)	$\gamma'(\delta_u)$ (N/m)
F3/1 (500/0,2)	1,253	101,3	1,754	106,8
F3/2 (500/0,2)	1,297	104,0	2,506	117,2
F3/3 (500/0,4)	0,902	(60,1)	1,504	(68,9)
F3/4 (500/0,4)	1,403	81,0	2,945	103,4
F3/5 (300/0,2)	↑	108,4	↑	114,6
F3/6 (300/0,2)	↑	102,2	↑	108,4
F3/7 (300/0,25)	2,410*	115,7	3,360*	122,3
F3/8 (300/0,25)	↓	116,6	↓	123,2
F3/9 (300/0,25)	↓	(153,8)	↓	(160,4)
F3/10(300/0,4)	2,017	114,9	2,506	119,2
F3/11(300/0,4)	2,763	89,0	3,759	97,7
F3/12(300/0,4)	2,443	89,5	3,822	101,6
F3/13(200/0,2)	3,252	136,9	4,010	141,4
F3/14(200/0,2)	2,512	122,8	3,759	130,2
F3/15(200/0,4)	2,318	125,7	3,527	135,4
F3/16(200/0,4)	2,851	(157,0)	4,010	(166,3)
F3/17(100/0,2)	↑	(161,4)	↑	(165,9)
F3/18(100/0,2)	↑	(182,0)	↑	(186,5)
F3/19(100/0,2)	2,240*	92,8	3,730*	97,3
F3/20(100/0,2)	↓	106,0	↓	110,4
F3/21(100/0,2)	1,886	99,0	3,884	105,0
F3/22(100/0,2)	3,114	138,7	4,573	143,0
F3/23(100/0,2)	↑	(~420)	↑	(~420)
F3/24(100/0,25)	↑	127,2	↑	131,9
F3/25(100/0,4)	2,240*	118,5	3,730*	124,5
F3/26(100/0,4)	↓	110,0	↓	116,0
F3/27(100/0,4)	2,362	133,9	3,759	139,5
F3/28(100/0,4)	1,604	81,6	3,007	87,2
F3/29(100/0,4)	2,218	119,7	3,446	124,6

1. δ_u for Series F1 and F2 is assumed equal to 2 x δ_m (from ref. 73).
2. Results in brackets indicate "outliers" i.e. regarded as unrepresentative.
3. Result for F3/23 was excessive, due to unusual crack pattern.
4. *These values are mean values from beams of the same size using free rollers. They are used in place of recorded values which were affected by the use of fixed rollers for these beams.

1. γ' (δ_m) based on the total area under the load-deflection curve ($A_{F,\delta}$), plus a component of beam self-weight resulting from the maximum mid-span deflection at zero load, i.e. δ_m. (Values of δ_m are also shown in the table). This value of γ' was adopted for two reasons:- firstly, it allowed direct comparison between results for all three series, since δ_m was measured with reasonable accuracy for all beams; secondly it was found that the incremental γ' value over the last stages of crack growth, and particularly during the stage immediately before ultimate fracture, became very large and appeared to be unrepresentative of the majority of the fracture process (see later discussion). Evaluating γ' up to only δ_m minimised this effect.

2. γ' (δ_u) based on the total area under the load-deflection curve (i.e. $A_{F,\delta}$ up to δ_m) plus the component of beam self-weight resulting from the ultimate mid-span deflection, i.e. δ_u. For reasons discussed later, this value is not considered truly representative of the majority of the fracture process. Nevertheless, it is included specifically to show the increase brought about by the use of δ_u as opposed to δ_m. Note however that δ_u was measured accurately only for beams of series F3. For series F1 and F2, δ_u has been assumed to be equal to twice the value of δ_m, based on a RILEM recommendation[7].

(Note also that:- (a) results for 800mm beams of series F2 are omitted from table 9.4 as δ_m values could not be measured accurately, and (b) beams F3/21-23 and 29 had sawn notches which do not appear to have influenced results in comparison with cast-notch beams).

Table 9.4 contains deflection values based on use of free support rollers under beam ends. Fixed rollers can cause appreciable increase in fracture energies, since additional external load is required during fracture to overcome frictional resistance, and beam deflections also increase accordingly. All beams of series F1 and F2 had free rollers; a number of beams of series F3 had fixed rollers, and for these beams table 9.4 shows that mean deflection values from beams of the same size with free rollers have been used

to calculate fracture energies. The influence of frictional resistance on γ' will be discussed in more detail later.

A number of results from series F3 are placed in parentheses in table 9.4, since they were deemed excessively high or excessively low. These values were tested using the statistical "T"-test to determine whether they were outliers[92]. In all cases they were found to be outliers on the basis of the mean values from the balance of the results. However, these values are very significant in view of this type of testing where a large spread of values occurs. The values should not be regarded as invalid in themselves, but rather as representing extreme types of fracture behaviour induced by different mechanisms of energy absorption. Of the six beams thus deemed unrepresentative relative to surface energy calculations, it is significant that only one had a very low value (F3/3), indicating possibly some prior damage in this beam. The rest had excessively high values. In the case of F3/23 only an estimate of γ' could be obtained due to an incomplete test record. This beam also had excessively high values of F_{max} and δ_m, and the estimate of $\gamma' \approx 420$N/m shows how exceptional this beam was.

High γ' values indicate the occurrence of additional energy mechanisms, such as highly tortuous and irregular cracking, crack branching, and extensive microcracking. This is illustrated in figures 9.17 and 9.18, showing fractured beams F3/17(100/0,2) and F3/26(100/0,4) respectively. In both cases tortuous and multiple cracking is evident. However, F3/17 yielded a very high γ', while γ' for F3/26 seemed reasonable relative to other beams. Therefore, high values of γ' should not necessarily be expected when fracture surfaces such as those in figures 9.17 and 9.18 occur. Where high γ' values do occur, however, this is evidence of unusually large energy absorption in the fracture zone.

The self-weight energy component is calculated by considering the mean distance through which each half of the beam moves. Considering the sketch in figure 5.10 this mean distance is equal to one-half of the mid-span deflection, assuming a straight-line beam



Figure 9.17 Cracking pattern at failure for beam F3/17(100/0,2)

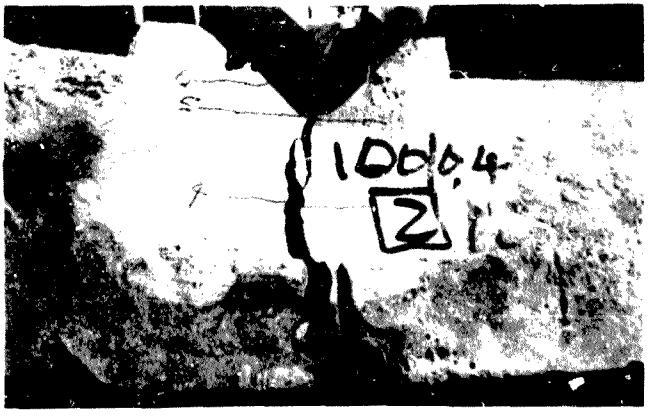


Figure 9.18 Cracking pattern at failure for beam F3/26(100/0,4)

profile between supports and mid-span, which is reasonable when δ_m is being approached. Therefore, the self-weight component is:-

$$\text{Self-weight energy} = 2 \frac{mg}{2} \frac{\delta}{2}$$

$$= \frac{mg\ \delta}{2} \qquad (9.17)$$

where mg is total weight of the beam (between supports) and δ is mid-span deflection. The fact that a self-weight term mgδ is suggested by RILEM[7] implies that the ultimate deflection is twice the value of the maximum deflection at zero load. For variable section beams, the same approach to calculation of self-weight energy is used, except that the beam is considered as a series of rectangles and triangles whose centres of gravity move through distances which are related to the mid-span deflection by beam geometry. Table 9.5 summarises the factors by which mid-span deflection is multiplied in order to obtain the self-weight term, assuming a unit weight of concrete of 23,9kN/m³ (see table 5.1). (Note that the short extensions of the beam beyond the supports have been ignored in table 9.5, as they have a negligible effect on self-weight energy).

Areas under load-deflection curves (external load energies) were obtained by discretizing the experimental curves using approximately ten points, and calculating areas using various forms of the trapezoidal rule. Areas for the load-cycled beams of series F3 were calculated as the slanted areas between successive reloading curves (see figure 6.1). These were used to obtain γ_R values for increments of crack growth. The incremental values were than summed for calculating γ' values. Incremental self-weight energies were also calculated by using the incremental δ_p values for each cycle. Finally, γ' values were obtained by summing external load energies and self-weight energies, and using equation (3.27), i.e. dividing the total energy by twice the nominal cross-sectional area.

Self-weight energies should not be neglected since they can comprise appreciable proportions of total fracture energy. This is shown in table 9.6, where self-weight energy is expressed as a

Table 9.5 Factors for calculating self-weight energies

Beam depth (mm)	Type	Self-weight energy for beam mid-span deflection of δ(mm) (Nm)
500	Constant section	1,19 δ
	Variable section	0,87 δ
300	Constant section	0,43 δ
	Variable section	0,31 δ
200	Constant section	0,19 δ
100 (400mm span)	Constant section	0,05 δ
100 (800mm span)	Constant section	0,10 δ

Table 9.6 Self-weight energies of fracture beams

Beam type	Self-weight energy as percentage of total fracture energy (%) (up to δ_m)	
	Constant Section	Variable Section
500/0,2	20,6	13,5
500/0,4	24,0	21,6
300/0,2/0,25	11,3	13,6
300/0,4	-	21,3
200/0,2	13,2	
200/0,4	15,4	
100/0,2/0,25	6,0	
100/0,4	7,9	
100x100x 800/0,5	26,3	

fraction of total energy, using mean values for any particular beam size, and based on energies up to δ_m. Self-weight energies become more important as beam size (depth and/or length) and notch-depth ratio increase. Thus, the 800mm span 100/0,5 beams have the largest fraction of self-weight energy (26,3 per cent), with the 400mm span 100/0,2 beams having the smallest (6,0 per cent). The effect of a variable section is to reduce mass and therefore the magnitude of self-weight energy. Self-weight energy is significant even for the smallest beams tested, and can rise to as much as 26 per cent of the total fracture energy in large beams or where span and notch depth ratio increase simultaneously.

Analysis of table 9.4 (series F3) shows that ratios of δ_u/δ_m vary from 1,39 to 1,74, with no definite trend relative to beam size. This value is somewhat smaller than the value of 2,0 suggested in the RILEM recommendations[73]. These recommendations also specify use of an 800mm span beam with 100mm square cross-section and $c_0/d = 0,5$. Self-weight energy is very appreciable for these beams, and an overestimate of δ_u will therefore aggravate the situation. It would appear to be better to use smaller span/depth ratio beams where any errors in estimating δ_m will be minimised. (Refer also to 5.5 for problems associated with measuring δ_m and δ_u).

EFFECT OF COMPRESSIVE STRENGTH ON γ'

It was found previously that compressive strength had a very minor influence on the LEFM parameters K_0 and K_c, and this influence was small enough to be neglected when considering the influence of beam depth. It was therefore expected that compressive strength would have a minor or negligible influence on γ' values. This was checked by following the same procedure as outlined in 9.6.1 for eliminating effects of beam depth and notch depth. Only the 500mm beams of series F1 and F3, and the 100mm beams of series F1 and F2, were analysed. These beams had a sufficient range of compressive strength to provide a trend if one existed. The 100mm beams of series F3 were excluded since it was found that the effects of

roller friction had resulted in unrepresentatively high γ' values. This is discussed later in this section.

The plotted results for effect of compressive strength on γ' have not been shown. The correlation coefficient for a linear regression done on the 11 points used in the analysis was -0,213, indicating poor correlation. There was a slight negative trend of γ' with compressive strength, but the scatter was large, and essentially no definite trend could be defined. Hence these results were consistent with those for K_0 and K_c. The influence of compressive strength could therefore be ignored for the balance of the analyses.

EFFECT OF INITIAL NOTCH DEPTH ON γ'

To test whether initial notch depth ratio c_0/d had any appreciable effect on γ', the results in table 9.4 were processed using the same procedure as outlined in 9 6.2 for eliminating effect of beam depth. Briefly, this procedure was:-

1. For any particular beam depth, a mean γ' value for beams with $c_0/d = 0,4$ was obtained ($\overline{\gamma'}(0,4, d)$).

2. For the same beam depth, ratios of individual γ' values to the mean value described above were calculated, for all the initial notch depth ratios.

3. These ratios were plotted against c_0/d. and results are shown in figure 9.19. Results for 100mm beam depths are plotted separately from those for deeper beams, since 9.6.2 and 9.7.2 had shown these small beams exhibited different fracture behaviour. Series F3 100mm beam results were also kept separate from those of series F1 and F2, due to effects of roller friction, to be discussed later. Results for the deeper beams are shown in an inset in figure 9.19.

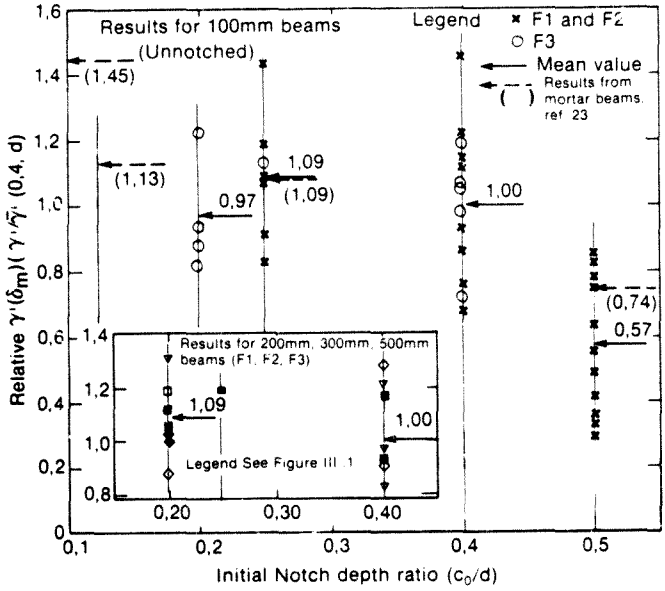


Figure 9.19 Effect of initial notch depth ratio on γ'

Note the following from figure 9.19:-

1. The figure is based on γ' values calculated using δ_m. For any particular c_0/d ratio, a fairly large scatter of results has occurred. Mean values for all results at a given c_0/d are shown on the diagram. Referring to c_0/d values less than 0,4, it appears that γ' values are nominally higher than those at c_c/d = 0,4, but the trend is not very marked. In the case of the 100mm beams of series F3 with c_0/d = 0,2, a nominally lower value of γ' occurs. It is interesting that this follows the same trend as for K_c in figure 9.7. The overall impression is that γ' is very little affected by notch depth ratios between 0,2 and 0,4 and this is consistent with earlier results for K_c and K_0.

2. A very different picture from that above emerges for results from the 100x100x800mm beams with $c_0/d = 0,5$ of series F2. Average γ' values for these beams were considerably lower than those from smaller span/depth and notch depth ratio beams, the reduction being on average about 40 per cent. The scatter of results for these beams, however, is similar to that for other 100mm beams (refer to results at $c_0/d = 0,4$).

The reason for the very marked reduction in γ' values for the longer span 100mm beams of series F2 is not immediately apparent, but is considered to depend primarily on the larger notch depth ratio. Deeper notching results in fracture behaviour that does not exhibit a true instability condition, implying that strain energies are low and the Griffith energy balance for fracture is never achieved. Consequently crack propagation occurs at low overall stress levels, and energy-absorption by damage in the fracture zone is limited. Low γ' values for these beams therefore represent a less intense fracture process when compared with the shallower notched beams. This highlights the importance of linking fracture testing with the mode of failure and likely energy-absorbing mechanisms to be encountered in practice.

It should be noted that previous work by the author[23] had shown that γ' was higher in unnotched beams when compared with notched beams. Results from ref. 23 for mortar beams with support span of 610mm loaded at the third points have been reworked in order to compare them with present results, and are also shown in figure 9.19. Initial notch depth ratios of 0, 0,125, 0,25, and 0,5 were used, and results have been processed such that mean values at $c_0/d = 0,25$ have been matched. A similar trend to the present results is evident, with unnotched beams showing markedly higher γ' values, and deeply notched beams markedly lower values. Within the range of c_0/d from 0,125 to 0,25, γ' is influenced only minimally or not at all by notch-depth. The different results between the unnotched and deeply notched beams is again indicative of different fracture processes.

Values of γ' based on δ_u (i.e. series F3) were also compared for effects of notch depth. It was found that there was a negligible (1 per cent) increase in mean γ' for $c_0/d = 0,2$ compared with $c_0/d = 0,4$. Only three results were available for $c_0/d = 0,25$, and the increase of 14 per cent in the mean γ' value that was obtained for this notch depth should therefore be treated with caution.

To summarise:- for shallow to medium notch depths (i.e. $0,2 \leq c_0/d \leq 0,4$), it appears that γ' is independent of notch depth, for practical purposes. Unnotched beams show markedly higher γ' values, while deep notching ($c_0/d = 0,5$) results in very much lower γ' values. The most likely reason for this is the varying intensities of fracture processes operating at the two extremes of notch depth when compared with intermediate values of notch depth. The different γ' values are simply representative of different fracture conditions, and can be regarded as valid for those particular conditions.

EFFECT OF BEAM SIZE

The problem of the dependence of fracture parameters on specimen size and geometry has been discussed previously in 3.3 and 9.8. Once it had been established that shallow to medium notch depths had a small if not negligible influence on γ', it was possible to combine all γ' values for a beam of given depth in order to compare them with results from other beam depths. The comparison has been made on the basis of γ' calculated using δ_m. Results are given in bar diagram form in figure 9.20. The number and range of results and mean values for each set are also given. (Note that results for the 100mm deep 800mm span beams ($c_0/d = 0,5$) of series F2 are excluded). Comments are as follows:-

1. A total of 46 results are represented in the figure. A limited number of results are available for 200mm and 500mm beams, but they are nevertheless sufficient to establish a general trend.

2. For series F3, there is possibly a slight trend of γ' increasing with decreasing beam depth. This will be discussed later with reference to roller friction. The 200mm beams have shown particularly high γ' values,. However, limited results are available for 300mm and 200mm beams of series F3. Therefore the mean values for these beam sizes must be viewed with caution.

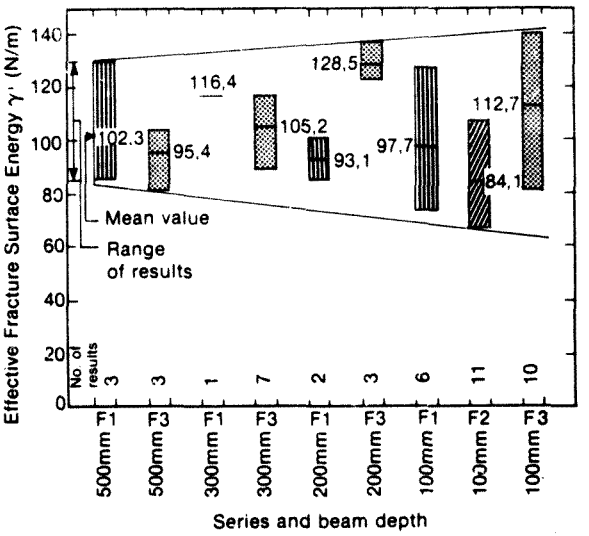


Figure 9.20 Effect of beam depth on effective fracture surface energy

3. For series F1 and F2, a slight reverse trend to that of series F3 occurs. Note that the 200mm beams have a limited number of results and a lower mean value which is in contrast to the 200mm beams of series F3. There is no great significance in the single fairly high result for the 300mm beam, except to note that it is within the range of 300mm beam results for series F3. For 100mm beams, results for series F2 are somewhat lower than series F1, and substantially lower than series F3.

4. The overall impression from figure 9.20 is apparently one of little or no practical dependence of γ' on beam size. However, the spread of results increases with decrease in beam size. This is to be expected in testing of concrete beams of fairly small cross-section in which aggregate size is an appreciable proportion of specimen dimensions.

It has been mentioned above that support roller friction has affected the results of particularly the 100mm beams of series F3. This will influence the apparent trends shown in figure 9.20. This subject is discussed below.

EFFECT OF FRICTION OF SUPPORT ROLLERS ON γ'

The significantly higher γ' results for the 100mm beams of series F3 compared with values for similar beams of series F1 and F2 should be interpreted in the light of support roller friction that was known to act on the F3 beams. The effect of friction was to increase the applied load for any given increment of crack growth, due to a restraining moment applied by the frictional forces. Consequently the area under the load-deflection curve was increased by the action of friction. Note from table 9.4 that there was essentially no difference between γ' values of fixed and free roller 100mm beams of series F3. (Table 5.6 gives details of support roller conditions). This is part'y since δ_m and δ_u values for fixed roller beams were taken from mean values of free roller beams. Despite this adjustment it appears that similar restraint conditions have been operating on all 100mm beams of series F3. In the light of γ' results and results for moments of resistance discussed in 9.11, roller friction was considered to be the most likely cause for the higher γ' results for series F3 100mm beams. An estimate of the mean coefficient of friction $\bar{\mu}$ for the fixed roller 100mm beams of series F3 can be obtained by considering the influence on applied moment of the frictional forces acting at the supports. This has been done in appendix F, and $\bar{\mu}$ was found to be approximately 0,5. The estimate is based on the ratio of mean γ' for 100mm beams of series F1 and F2, where roller friction would have been

very small, to mean γ' for 100mm beams of series F3. From table 9.4:-

$$\text{Ratio of mean } \gamma' \text{ values (100mm beams)} = \frac{88,9 \text{ (Series F1,F2)}}{112,7 \text{ (Series F3)}} = 0,79 \qquad (9.18)$$

Since $\overline{u}$ will vary from zero at the start of a test to a value of approximately one in the final stages of fracture (see 5.5), the average value of 0,5 appears reasonable.

COMBINED γ' RESULTS FOR DIFFERENT BEAM SIZES

Figure 9.20 suggests that γ' results can be combined for any particular beam size. This is shown in figure 9.21, using results directly from figure 9.20. However, results for 100mm beams for series F3 have also been reduced according to equation (9.18) to account for effects of roller friction. The revised results are plotted as dashed lines, with mean values in parentheses.

Results for 300mm beams have also been revised, since beams F3/5-9 had fixed rollers. The revised results are plotted by simply ignoring results for fixed roller beams. Results for 500mm and 300mm beams appear very consistent, with smaller beam generally showing a wider scatter of mean and extreme values. There is a trend of γ' reducing for 100mm beams, but the trend is not as marked as it was for K_c (see figure 9.9). Therefore it appears that γ' is not as seriously effected by the fact that fracture mechanics principles cannot be applied to the 100mm beams as K_c. This again highlights the fundamental difference between the total work of fracture approach (γ') and the stress-intensity approach (K_c). However, the consistent reduction of both K_c and γ' for the 100mm beams is significant:- a lower stress-intensity factor implies that the fracture process is "milder" and that damage will be restricted. Therefore it was to be expected that γ' which measures the amount of energy absorbed in fracture would also be lower.

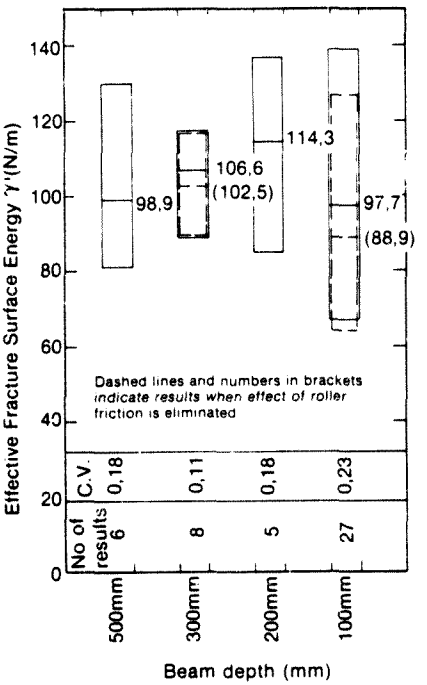


Figure 9.21 Combined results for effective fracture surface energy from all series

It is probable that the effects of roller friction are highly variable, and may differ for different beam sizes. Therefore, conclusions based on effects of roller friction can only be regarded as tentative. For this reason, γ_R values dealt with in 9.14.2 below have not been revised. The effects of roller friction discussed above and elsewhere emphasize again the need for attention to detail in fracture testing.

RELATIONSHIP BETWEEN γ' AND G_c

For LEFM, equation (3.28) indicates that an ideal elastic-brittle material should have $G_c = 2\gamma'$. When applied to concrete, we clearly do not have an ideal Griffith material, and the condition inherent in equation (3.28) that fracture occurs spontaneously at first crack extension does not apply generally to notched concrete beams. Consequently, ratios of G_c/γ' have values very much less than the ideal value of two, as shown below for the present beams:-

500mm beams, mean G_c/γ' = 1,07
300mm beams, mean G_c/γ' = 0,81
200mm beams, mean G_c/γ' = 0,72
100mm beams, mean G_c/γ' = 0,45

(Mean G_c values above were obtained from beams of series F1, F2 and F3 by a combination of results in tables 9.1(a) and (b) and table 9.2; mean γ' values were obtained from figure 9.2 ; for 100mm beams, effects of using apparent c_c values and effects of roller friction were excluded). By way of comparison, G_c/γ' values for 100mm mortar beams from ref. 23 were:-

Mean for unnotched beams:- 2,06
Mean for rectangular notched beams:- 1,16

The fundamental difference between the two types of parameter is highlighted by the ratios given above. It is interesting to note that the more homogeneous and brittle mortar beams from ref.23 gave higher ratios that the present concretes, and for the unnotched condition where fracture was spontaneous gave a virtually ideal ratio. These comments serve to emphasize the difference between fracture processes for different cemented materials and specimen types.

9.14.2 CRACK GROWTH RESISTANCE CURVES USING EFFECTIVE FRACTURE SURFACE ENERGY

The concept of crack growth resistance curves (R-curves) has been discussed previously in 3.5.1 and 9.13. The crack growth resistance parameter may be formulated either in stress-intensity terms, or in energy terms. Considering the energy formulation, crack advance will occur when the rate of strain energy being released by the body equals or exceeds the energy required to create new fracture surfaces. This is basically Griffiths's energy balance criterion. The basic premise of the R-curve is that for a given material and thickness there is a unique relationship between crack growth and resistance to that growth. In terms of figure 3.6, this implies that as stress level rises, additional energy-absorbing mechanisms come into play to resist crack growth, until the energy balance is favourable for crack extension. Whether the material will then fracture catastrophically by means of spontaneous crack propagation or not, will depend on whether further resisting mechanisms can be mobilised to prevent crack growth.

In this section R-curves are expressed in terms of a parameter γ_R defined later, which was obtained from beams of series F3. The method of producing γ_R-curves involved plotting incremental values of γ_R against crack extension values. The incremental energy terms were measured using the area on the load-deflection curve bounded by any two successive reloading compliance lines, the abscissa axis, and the envelope curve of the fracture record. (see figure 6.1). This was done for each cycle of loading, and could be related to cyclic crack growth. Wecharatana and Shah[4] have pointed out that use of cyclic fracture energy is sensitive to the particular material behaviour and the influence of, say, aggregate addition.

For cemented materials where a considerable microcracked zone develops, the problem arises of exactly which terms for effective fracture surface energy and crack growth should be used for constructing the γ_R-curve. The simplest approach would be to use γ_R calculated as incremental cyclic fracture energy (including incre-

mental self-weight energy) divided by incremental stress-free crack growth for the cycle. (This γ_R would therefore be conceptually identical to the definition of γ' in the previous section). This was done for 300mm beams of series F3, and the γ_R values plotted against experimental crack depth c. The resulting plot showed that there was an excessively large scatter in γ_R values, making it very difficult to define any meaningful relationship. Considering the heterogeneous nature of the material, the results were not entirely surprising. Where γ_R is measured for incremental crack growth, it is possible to visualise crack growth resistance varying widely from increment to increment as varying degrees of microcracking, aggregate interlock and crack tortuosity due to the aggregate are encountered. A more homogeneous material such as mortar or hardened cement paste could be expected to have far less cyclical variation.

An alternative approach is to use parameters which account for the influence of the microcracked zone on fracture resistance and crack growth. Parameters selected for the present work are described below.

CRACK GROWTH RESISTANCE PARAMETER γ_R

The influence of the microcracked zone is accounted for by using a parameter γ_R as follows:-

$$\gamma_R \text{ (N/m)} = \frac{\text{Total cyclic fracture energy}}{2b(\Delta c + z_{nl})_{\text{cycle}}} \qquad (9.19)$$

where Total cyclic fracture energy comprises external load energy plus incremental self-weight energy (Nm),
b is the breadth of the beam (m),
Δc is the cyclic increment of main crack growth (m),
and z_{nl} is the depth of the microcracked zone for the particular cycle (m).

(The number 2 in equation (9.19) accounts for the eventual creation of two new fracture surfaces).

The above parameter accounts for the creation of new stress-free crack surfaces and cumulative damage in the microcracked zone. Figure 9.22 shows that, for any cycle of crack growth, energy is required to form new fracture surfaces (Δc) as well as to cause a degree of damage in the microcracked zone. During the subsequent cycle, further fracture surfaces are formed, and material in the microcracked zone which in the previous cycle was damaged, is now further damaged by the latest increment of crack extension. Therefore cumulative damage occurs in the microcracked zone, and it is necessary to account for this in the γ_R term.

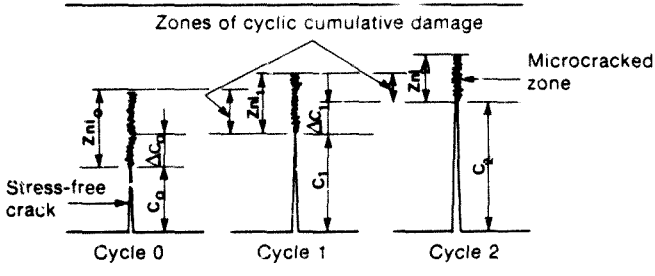


Figure 9.22 Schematic illustration of cyclic crack extension resulting in cumulative damage in the microcracked zone

RELATIVE EFFECTIVE CRACK DEPTH PARAMETER

This parameter is identical to that defined in equation (9.16) for the K_R-curve, i.e.

$$\text{Relative } c_{eff} = \frac{c_{eff} - c_0}{d - c_0}$$

This parameter has been chosen since it was observed when plotting γ_R versus c_{eff} for any beam size that curves for the individual

c_0/d ratios could be made to fall reasonably within a common band by normalising c_{eff} according to equation (9.16).

Results for 500mm, 300mm, and 200mm beams of series F3 were reduced using equations (9.19) and (9.16), and plotted in figure 9.23. Results for 100mm beams were excluded since the fracture behaviour of these beams has been shown to differ from that of deeper beams. Comments are as follows:-

1. A fair scatter of results occurred. However, the scatter was very much less than if the conventional $\mathcal{G}'$ was used instead of $\mathcal{G}_R$. Scatter of results remains a problem in fracture testing of this type of material.

2. A clear trend of $\mathcal{G}_R$ increasing with relative c_{eff} occurred. Results for different beam depths fell uniformly within the scatter band.

3. Values of $\mathcal{G}_R$ were generally very much smaller than $\mathcal{G}'$ values. This reflects the energy consumed in creating damage in the microcracked zone, over and above the energy required for creation of new fracture surfaces. The initial values shown at the k_0 = 0,45 and 0,47 positions represented the energy required to initially develop the microcracked zone, before any main crack extension occurred. Thereafter the energy demand rose at a more or less constant rate as main crack extension occurred. In this respect, the trend of figure 9.23 was similar to that for K_R in figure 9.16.

4. The slope began to increase markedly at a relative c_{eff} of approximately 0,85. Note that a change of vertical scale occurs for $\mathcal{G}_R$ > 80N/m, and very large $\mathcal{G}_R$ values occurred at ultimate fracture. Immediately prior to this condition, $\mathcal{G}_R$ values approached $\mathcal{G}'$ values, showing that as the size and influence of the microcracked zone diminished, fracture energy was consumed almost solely in the creation of new fracture surfaces.

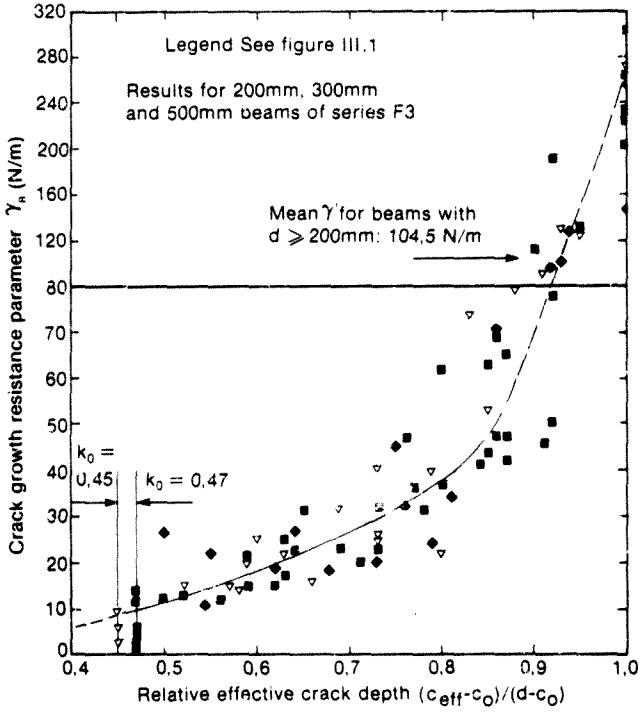


Figure 9.23 γ_R-curve for beams of series F3 expressed as a function of relative effective crack depth

The rapid increase in γ_R values approaching ultimate fracture is considered unrepresentative of true material behaviour, and is related to the beam type of test. Near ultimate fracture, only a small area near the upper face of the beam remains stressed, and the deflection of the beam becomes very large. Frictional effects from support rollers also become very significant. The main type of damage occurring in the fracture zone would therefore be that due to crushing and excessive plastic-type deformation. This would be unrepresentative of earlier damage when significant residual ligament depth was available. Hence, additional extraneous mechanisms occur as final fracture is approached. In view of this, γ' calculated as an average value for the entire fracture test will tend to be somewhat overestimated. A rough analysis using mean values of γ' in the earlier stages of crack growth shows that overestimation may amount to about 20 per cent. This would seem to be a major drawback in the normal γ' test. A load-cycled test resulting in the plotting of γ_R curves could assist in providing better values, but the further complication of crack depth monitoring arises in this type of test.

9.15 SUMMARY (NON-LINEAR EFFECTS)

1. This section has introduced the concept of the existence of various stress zones in fracture beams. An effective crack depth which includes the microcracked zone can be defined. Crack-closing stresses exist in the microcracked zone. These zones can be used to construct a simple stress model with a combination of linearly varying and constant stresses. Using the condition of internal force equilibrium, and the experimental neutral axis position, average stress in the microcracked zone was found to be a function of the relationships between zone size, neutral axis depth and residual ligament depth. Results from the stress model showed that fracture zone stresses tended to be larger in the larger beams, which confirmed earlier qualitative conclusions.

2. Using relationships based on the stress model for the moment of resistance of fracture beams, it was found that stresses in the fracture zone were a function of crack growth, generally increasing as the crack extended.

3. A stress-intensity factor K_R calculated at the tip of the effective crack could be defined, which allowed the influence of crack closing stresses to be accounted for. These K_R values were used to plot K_R-curves (a form of R-curve). A particular value of K_R, called K_i, gave the stress-intensity factor required to just fully develop the microcracked zone. K_R values were plotted against crack extension, from which it could be seen that K_c values were not unique relative to the fracture process, whereas K_i values were. If K_R was plotted against a parameter called the relative effective crack depth for the different beam sizes, a reasonably size-independent K_R-curve resulted. There was an increase in the slope of the K_R curve after K_i, which was consistent with the increase in fracture zone stresses during crack growth predicted earlier by the stress model. For the 500mm beams, a possible plateau K_R value occurred at approximately 5 to 5,5MPa$\sqrt{m}$. The relatively high K_R values should be interpreted in terms of the contribution to the stress-intensity factor at the effective crack tip of the crack-closing stresses in the microcracked zone. Results are tentative, and further work is required.

4. The effective fracture surface energy γ' was evaluated over the entire fracture process for use as a possible fracture criterion. Self-weight energy became relatively more important as beam size or notch depth increased, and amounted to as much as 26 per cent in the case of the 800mm span 100mm deep beams ($c_o/d = 0,5$). It was found that the influence of c_o/d on γ' for shallow to medium notching was small. However, for $c_o/d = 0,5$, approximately a 40 per cent reduction occurred in γ' values relative to shallower notched beams. This was attributed to the different intensities of fracture process operating for the different c_o/d ratios. γ' values for 100mm beams were 10 to

15 per cent lower than those for 300mm and 500mm beams, provided the influence of support roller friction was accounted for.

5. R-curves were plotted using a modified γ_R parameter which accounted for cumulative damage in the microcracked zone. Size-independent γ_R-curves for the different beam sizes were obtained by plotting γ_R against the relative effective crack depth parameter used for the K_R-curves. The γ_R-curves revealed that the fracture processes approaching ultimate failure were different from those of earlier stages due to excessive damage in the fracture zone. This meant that γ' values which are normally evaluated over the entire fracture process were overestimated. A rough analysis showed that the overestimation could amount to approximately 20 per cent.

To conclude this section, there are a number of aspects concerning non-linear effects that are not entirely satisfactory at this stage. Amongst these are the fact that stress models require much further work to corroborate the validity of the basic approach; effects such as friction of support rollers need to be eliminated as far as possible from tests; the ever-present problem of scatter of results requires investigation; and finally the fact that no true size-independent R-curve relationships (in the absolute sense) were obtained implies that even this approach may be questionable. However, the non-linear parameters that were used had the distinct advantage over LEFM parameters of revealing important fracture aspects such as the stress-intensity factor required for development of the microcracked zone, and the characterisation of damage in this zone using an energy parameter

9.16 CONCLUDING REMARKS

A great deal of material has been presented in this chapter, all of which has had relevance to the various parameters and criteria for concrete fracture. The chapter, due to its length, contained

three divisions, and each one was concluded with a summary and critical comment. It is unnecessary to repeat these summaries here and 9.4, 9.9 and 9.15 should be consulted. A few salient conclusions and observations are given below:-

1. Regarding criteria for fracture of concrete, it is becoming obvious that a single parameter is unlikely to be able to cover all the various fracture processes that occur. Thus, there are fundamental differences between fracture in notched and unnotched beams, and between the energy and stress-intensity approaches. The fracture processes in notched beams also differ in damage intensity as notching is reduced or increased. Parameters must be linked to fracture processes, which implies that a number of different parameters will be required. Results presented in this chapter have shown that the presence of an extensive microcracked zone profoundly influences measured fracture parameters. This implies that, ultimately, some form of non-linear parameter will probably suit the concrete fracture problem best.

2. LEFM parameters calculated without regard to the non-linear microcracked zone in concrete beams are reasonably independent of initial notch depth (for shallow to medium notching) and beam depth, provided a minimum beam size is used. The present 100mm beams were unsuitable for fracture testing, being basically notch-insensitive. However, it is postulated that the influence of the microcracked zone was similar for all beam sizes (except the 100mm beams), and this led to the consistency of LEFM results. Specimen types other than notched beams, and with different microcracked zone size relationships, may therefore exhibit different values of LEFM parameters. Despite this drawback, LEFM fracture criteria may yet prove to be practically valuable if specimen type is taken into account.

3. The work on non-linear effects presented earlier is still very much in preliminary form, and much additional work is needed. Nevertheless, an analysis of stresses in fracture zones has shown that experimental observations (for example compliances,

crack face rotations, and microcracked zone sizes) may be explained by the average stresses developed in fracture zones. R-curves using a K_R or $\mathcal{G}_R$ parameter help to reveal fracture processes in the microcracked zone, and are reasonably size-independent, if a relative effective crack depth is used. There is much scope for development of the ideas presented in the text, and for corroboration of preliminary trends.

4. Other parameters such as J_c exist for the study of fracture. It was mentioned earlier that J_c and $\mathcal{G}$ are connected in that they are both energy-related parameters. However, study of J_c and other parameters was outside the scope of this thesis. In any event, Swamy[54] and others have pointed out that there are fundamental objections to the use of J_c for concrete, due to the strain-softening behaviour of concrete in the fracture zone as opposed to the more truly plastic behaviour of metals. This also means that fracture parameters developed for use with metals are not always fundamentally valid for or directly applicable to cemented materials.

5. Finally, it must be acknowledged that no single fracture criterion can be put forward from the present work as the final solution for the concrete fracture problem! However, the development of the various parameters has assisted, it is felt, in a better understanding of the fracture processes in concrete beams. If this is true, then one of the important functions of fracture parameters has been fulfilled.

10 CONCLUSION

This chapter is kept as brief as possible. Its purpose is to draw together the main threads of the work described in earlier chapters. Summaries of aspects such as the experimental work and major results, as well as implications of the results for concrete fracture testing and recommendations for further work will be attempted. The preceding chapters contain concluding summaries which can be followed through for the development of the work and the major conclusions. Critical comments and assessments are also given in most chapters. These will only be re-iterated briefly, in order to set the individual parts in their relation to the work as a whole. Final conclusions will then be drawn, before ending with some personal reflections.

10.1 THESIS OBJECTIVES

The fracture testing of concrete had been investigated previously by the author for an MSc(Eng) dissertation[23]. This aroused a continuing interest in the subject. Clearly, the fracture phenomenon in concrete is one of its most important behavioural features, due to the relatively brittle nature of its components, its low tensile strength, and the ever-present problem of cracking. Also, it seemed that a better understanding of fracture would shed light on other properties such as the relation between load and deformation, the interaction between paste and aggregate which in turn governs the basic strength mechanisms, and long-term strength and deformations which are affected to some degree by crack growth. A study of the literature had revealed that conflicts, inconsistencies, and discrepancies occurred in experimental results. Lack of a uniform

approach to solving the concrete fractu. problem was very evident. It therefore seemed obvious that greater clarity was required on basic fracture processes, on how to test concrete for its fracture properties, and on how to evaluate the parameters describing fracture behaviour that were derived from the tests.

Therefore the major purpose of the thesis was to study the fracture behaviour of plain concrete in the form of notched beams, by means of carefu. experiment and analysis. This would specifically involve study of the nature and development of microcracking during fracture, the influence of macro-and microcracking on deformations (i.e. compliance), material characterisation with reference to the development and nature of fracture zones, and the examination of fracture parameters for their ability to describe fracture behaviour and fracture strength.

Further specific objectives were to carefully analyse and characterise load-deflection curves from fracture tests; to assess the influence of testing conditions (eg. support roller condition); and to investigate the use of strain and ultrasonic velocity measurement techniques for studying fracture processes. An overriding objective was to assess the effect of beam size on fracture processes and parameters, since the general consensus of the literature was that large concrete beams would be required for valid fracture testing.

The experimental work was restricted to notched beams; however, within this limitation, the scope of the work was kept as wide as possible, to try and get a broad picture of fracture in these specimens. During the progress of the work it was realised that due to the complex nature of concrete, and the fact that its fracture behaviour was critically dependent on the presence of a microcracked zone, results and conclusions would have to be limited at this stage to the notched beam type of specimen.

The overall framework within which the experimental work was conducted is the need to develop practical design methods for use by engineers in solving daily problems of concrete design and con-

struction. Equally as important is the need to establish criteria and procedures for valid fracture testing.

10.2 SUMMARY OF INVESTIGATIONS AND RESULTS

10.2.1 EXPERIMENTAL WORK

A total of 49 notched beams of width 100mm and with depths ranging from 100mm to 800mm were tested. Notch depth ratios used were 0,2, 0,25, 0,4, 0,5. The beams were loaded at mid-span and simply supported with a span/depth ratio of four. Most beams were prismatic with constant cross-section along the beam length; a number of the large beams were triangular in elevation with variable sections to reduce mass and to accommodate ultrasonic probes. Three series of tests were done, all with nominally the same aggregates; the final series employed a different batch of cement. Mix ratios were kept constant.

The fracture tests involved measurements of mid-span load and deflection. Strains across the fracturing section were also measured and used to assess compression and tension zone relationships and crack widths. Longitudinal ultrasonic pulse velocity measurements at various heights above the lower face were also made. The strain and ultrasonic measurements were used primarily to study the presence, extent, and intensity of the microcracked zone ahead of the main crack. The main crack itself was visually observed. A load-cycling technique was used to create stable crack growth through the beams.

Materials control tests were performed as checks on material quality and to provide basic material parameters for use in the fracture calculations. These tests involved cube compressive strength, modulus of rupture, and elastic modulus. Compressive strength

ranged from 28,7MPa to 43,5MPa, the variation being attributed to differences in curing, use of different batches, and effects of bleeding. Relationships between compressive strength and modulus of rupture, and compressive strength and elastic modulus were consistent with other quoted work. Elastic modulus values for series F3 were considered unrepresentatively low due to the influence of bleeding; consequently E values were inferred directly from the fracture records. For all three series, elastic modulus results were reasonably consistent, and values used for the fracture calculations ranged from 29GPa to 35GPa.

10.2.2 CRACK GROWTH AND FRACTURE ZONE STUDIES

A large portion of the experimental work was devoted to studies of crack growth during fracture tests, the influence of crack growth on beam compliances, and the presence and extent of non-linear microcracked zones. These zones also influence beam compliances. Experimental relationships between compliance and crack depth showed that initial notch compliances conformed with theory. Once crack extension commenced, the experimental relationships differed from conventional theory due to the influences of strain-softening and closing stresses in the microcracked zone. Beam depth affected the experimental relationships, and larger beams conformed more closely to theory than smaller beams. This was thought to be due to the greater restraint operating in the fracture zones of larger beams; on the other hand, smaller beams experienced greater relative beam deflections leading to greater crack-surface rotation and aggregate pull-out in the fracture zone.

Crack growth during testing was studied using compliance relationships. The results showed that slow crack growth prior to maximum load was appreciable even in large beams where it amounted to between 10 to 25 per cent of initial notch depth. Slow crack growth measurement in 100mm beams was made difficult by the small size, and values based on conventional compliance relationships may be

overestimated by as much as 30 per cent. This can cause serious overestimation of calculated fracture parameters.

10.2.3 FRACTURE ZONE MEASUREMENT AND CHARACTERISATION

The presence, extent, and nature of microcracked fracture zones in notched beams were investigated using strain and ultrasonic pulse velocity measurements. Four distinct stress zones occur in a fracture beam:- they are the destressed zone surrounding the main crack, the microcracked tension zone, the intact tension zone, and the compression zone. Strain measurements were used to plot strain profiles which showed two distinct linear regions during fracture:- one region in the intact portion of the beam, and the other in the cracked and microcracked portion of the beam. The two linear regions were separated by a point of discontinuity, giving rise to distortion of the strain profile. This distortional effect was most severe in the deeper beams, while the 100mm beams suffered very little distortion, thus showing that the notch effect was limited for these beams. During early load cycles, the development of the microcracked zone was graphically shown by the rapid rise in the neutral axis position to a point roughly one-third of the depth of the beam below the upper face. Thereafter during fracture, the depth of tension zone remained roughly twice that of the compression zone. Crack opening displacements at tips of visible cracks during crack extension varied from 37μm to 64μm on average, the larger beams obtaining the higher values.

The strain measurements were used to deduce, firstly, limits to the size of the microcracked zone. It was concluded that theoretically the depth of this zone could vary from approximately 37 per cent to 68 per cent of residual ligament depth. Strain and ultrasonic measurements were then used to physically measure microcracked zone depths:- for the 100mm beams this depth was found to be about 40 per cent of residual ligament depth; for the larger beams the values

were significantly higher at about 45 to 47 per cent. The important implication of this was that average fracture zone stresses in the 100mm beams would be significantly lower than in larger beams, since results for the 100mm beams fell close to the lower limit which was based on a condition of zero stress transfer. Finally it was found that the ultrasonic technique was useful for assessing crack growth during the fracture test, since crack growth influenced pulse path length.

10.2.4 FRACTURE PARAMETERS AND CRITERIA

The final section of the thesis dealt with the application of fracture mechanics principles to notched concrete beams of varying depth . The linear-elastic approach was first considered and a relationship between minimum beam depth as a function of material parameters (i.e. fracture toughness and modulus of rupture) and beam/notch geometry was developed. This showed that for the present beams a critical value for some suitable stress-intensity factor K'_c would be approximately 1,0MPa$\sqrt{m}$. Such a value would satisfy the notch-sensitivity results, which previously had showed that 100mm beams were notch-insensitive. Beams having K'_c values less than this critical value would therefore not fulfil the requirements for application of LEFM. The importance was stressed of creating valid instability conditions, and of correct estimation of slow crack growth for proper study of fracture parameters. Failure to give attention to these aspects has been the disadvantage of many other investigations.

Emphasis was placed on evaluating the linear-elastic stress-intensity factor K at the points of fracture initiation (K_0) and maximum load instability (K_c). The compressive strength variations had no real effect on K_0 or K_c. This was thought to be due to the compressive strength variations being caused primarily by bleeding. Initial notch depth ratio in the range 0,2 to 0,4 had a minor effect on K_0 and K_c. However, K_c values were about 40 per

cent higher in unnotched beams (using results from previous tests), and about 40 per cent lower in deeply notched beams ($c_0/d = 0,5$), when compared with results from shallow to medium-notched beams. This was ascribed to the different fracture processes induced by the various notch depths. Beam depth was found to have a very marked effect on K_0, values for 800mm beams being roughly 60 per cent greater than those for 100mm beams. The reason for this was not clear, except that possibly plane stress/plane strain effects were present. K_0 was thus deemed unsuitable as a fracture criterion for the beams. The effect of beam depth on K_c was significant, with about a 15 per cent difference between 200mm and 800mm beams. The 800mm beams had a mean K_c of 1,72MPa$\sqrt{m}$. However, this value would reduce by about 10 per cent if experimental rather than theoretical compliance-based crack depths had been used. The 100mm beams were found to have a mean K_c of about 0,96MPa$\sqrt{m}$, thus substantiating the earlier remark concerning the unsuitability of these beams for fracture analysis. Despite the fact that K_c as an LEFM criterion looked promising, it was concluded that the similarity in K_c values for the different beam sizes was due to the uniform influence of the approximately constant relative size of the microcracked zone. Thus in a fundamental sense, K_c was not valid as a fracture criterion.

As far as non-linear fracture parameters were concerned, a stress model confirmed earlier intuitive conclusions that fracture zone stresses were higher in larger beams compared with 100mm beams. The stress model used the concept of an effective crack which comprised the stress-free crack and the microcracked zone. A moment of resistance relationship was used to show that average stresses and relative microcracked zone size tend to increase during crack growth, thus increasing fracture resistance. Two types of R-curves were drawn:- one using a stress-intensity parameter K_R, and the other an energy parameter γ_R. Both parameters incorporate the effects of the non-linear zone, and promising results for use of these parameters as possible fracture criteria were obtained. In particular, the R-curves confirmed the tendency for average microcracked zone stresses to increase during crack growth. Finally, the effective fracture surface energy γ' was also evaluated, and

found to be about 15 to 20 per cent lower for 100mm beams when compared with larger beams. It was also substantially lower (40 per cent) for deeper notched beams ($c_0/d = 0,5$). For beams of depth 200mm and greater, and for shallow to intermediate notching, a mean $\mathcal{G}'$ value of 104N/m was obtained. The $\mathcal{G}_R$-curves showed, however, that $\mathcal{G}'$ evaluated from the total work of fracture is overestimated, by possibly as much as 20 per cent, due to extraneous energy mechanisms occurring near ultimate failure.

10.3 MAJOR CONCLUSIONS

1. Results from fracture tests on a total of 69 notched concrete beams of width 100mm and depth ranging from 100mm to 800mm have been reported. The 100mm deep beams were found to be notch-insensitive. For the larger beams, notch-sensitivity increased with beam depth.

2. Accurate fracture calculations require that careful attention be given to experimental procedures. In particular, neglect of the effects of support roller friction and inaccurate estimation of crack growth was found to influence the calculations adversely.

3. Compliance relationships based on LEFM theory were not entirely valid for concrete beams, due to the influence of microcracking and irrecoverable deformations. Experimental compliance-crack depth relations must therefore be derived. The use of compliance relationships to study slow crack growth showed that even in large beams this amounted to between 10 to 25 per cent of initial notch depth prior to maximum load. Therefore, slow crack growth cannot be ignored in fracture calculations.

4. Both strain and ultrasonic pulse velocity measurements were found to be useful techniques for detecting and studying the development and propagation of macro-and microcracking in con-

crete beams. Strain measurements showed that relationships between tension and compression zone sizes exist which are characteristic of material fracture behaviour. Concrete was shown to depart considerably from the ideal elastic-brittle condition. The tension zone was roughly twice the depth of the compression zone during fracture, which allowed theoretical upper and lower limits to be derived for the size of the microcracked zone. Strain and ultrasonic measurements of the depth of this zone showed that for larger beams the depth was approximately 47 per cent of the residual ligament depth during the early stages of crack growth. For small 100mm beams, the corresponding figure was about 40 per cent, which was close to the theoretical lower limit of 37 per cent. The lower limit was obtained from a condition of zero stress transfer. This implied that significantly lower closing stresses existed in the fracture zones of 100mm beams when compared with larger beams.

5. LEFM parameters were calculated for the beam tests. K_0, the stress-intensity factor calculated at the point of fracture initiation, appeared to be unsuitable as a fracture criterion due to its excessive dependence on beam depth. K_c, calculated at the point of maximum load, appeared to be more promising, being not greatly affected by notch depth (for shallow to medium notching) or beam depth. However, R-curves using K values showed that K_c did not represent a unique point in the fracture process; furthermore it was considered that the uniform influence of the microcracked zone had allowed similar K_c values to be calculated for different beam depths. The very presence of an extensive non-linear zone violated the LEFM assumptions. Thus, K_c was not valid as a fracture criterion in the fundamental sense.

6. The results of non-linear fracture parameters were preliminary and firm conclusions could not be based upon them. However, R-curves appeared promising insofar as they have the ability to reveal important fracture aspects such as the stress-intensity factor required to develop the microcracked

zone. The effective fracture surface energy γ' may be useful as a "global" parameter describing the entire fracture process. Unfortunately it was found to suffer from effects of excessive damage near ultimate fracture in the beam test. There was also a fundamental difference in γ' values for deeply notched beams when compared with shallow notched beams.

10.4 FRACTURE OF PLAIN CONCRETE - A PHILOSOPHICAL DISCUSSION

In this section, the implications of the test results for the fracture of concrete as a material, and for the progress of concrete fracture testing, will be broadly examined. The content will therefore be philosophic rather than specific, interpretive rather than definitive.

Firstly concrete fracture is not simple. This is due to the nature of the material itself. Irrespective of the level of scale being considered, the structure of concrete is highly heterogeneous, complex, and multi-phase. The presence and influence of numerous interfaces between constituent materials lends to concrete a fairly unique response to stress. Therefore, any fracture theory will have limitations in trying to describe the complex response of the material to stress, and must generalise by deciding on the level of scale at which the material is to be characterised. In this work, the approach has been to look at the level of macro-scale, and attempt to characterise fracture of the composite material as a whole. Processes at a micro-scale level have not been neglected, however; in particular the presence of microcracking has been studied in some detail. The important point is that different fracture processes and phenomena occur in concrete depending on factors such as notching, strain rate, and specimen size, and fracture parameters or characterisations must be linked with these processes. The various processes should be identified, and then studied and

characterised, before suitable descriptive or predictive parameters are developed and tested.

Secondly, it cannot be overemphasized that testing and interpretation of tests results require the utmost care. For testing of concrete in general, the material's heterogeneity results in a scatter of results at the best of times; in fracture testing this scatter can render test results almost useless. It is also not an understatement to say that test data interpretation is the greatest challenge facing the the fracture investigator, and it is possible to use results to deduce the very opposite of what they actually demonstrate. For instance, failure to recognise the effects of inaccurate crack growth monitoring, or support roller friction, can give a false picture of the fracture behaviour of small specimens in particular.

On the other hand, the use of fairly simple techniques such as careful measurement of load and associated deformation in the form of deflection and strain can give a great deal of information about basic fracture mechanisms and processes. More refined techniques such as use of ultrasonics can be coupled to the simpler techniques, but very often provide only confirmatory information.

Regarding beam tests on concrete, various stress zones exist; measurements of neutral axis position and size of the microcracked zone can lead to simple but informative relationships which are characteristic of the material's fracture behaviour. For example, the relationship between tension and compression zone depths can be interpreted in terms of how closely the material approaches the ideal elastic-brittle state. The plotting of these relationships for a range of different materials will therefore categorise them relative to their fracture characteristics. Other relationships can be used in a similar way; for instance the relationship between non-linear zone size and stress in the zone is also characteristic of the fracture behaviour of the material. These characteristic relationships appear to hold great promise for furthering the understanding of fracture in cemented materials.

By far the most important single insight concerning fracture of concrete beams is a recognition of the presence, the extent, and the considerable influence of the non-linear microcracked zone. This leads naturally to the understanding that the fracture behaviour of concrete is basically determined by this zone. Stated another way, the microcracked zone should be seen as the dominant factor in concrete fracture. For example, the existence in this zone of varying levels of average stress depending on beam depth imparts varying fracture resistances to concrete:- in larger specimens average stresses tend to be higher, and fracture toughness is greater; the opposite occur in smaller specimens, which therefore tend not to be governed by fracture mechanics principles. The increase in average stresses during crack growth leads to increased fracture toughness, and the mobilising of additional energy-absorbing mechanisms. It is important that this zone be extensively studied. Much is still unknown about it:- cracking mechanisms and the development of microcracking remote from the main crack tip require study; various experimental techniques (eg. ultrasonics and acoustic emission) to detect and measure the extent of the microcracked zone require further development; a great deal of work can still be done on stress states in this zone; better models are required to study the contribution of the zone to the effective crack depth, and the variations in size and average stresses during crack growth require further study.

Other aspects showing the importance of this zone are (a) the damage-energy which it absorbs and which affects the fracture surface energy term; (b) its influence on compliance, whereby the initial development of this zone induces greater compliance; thereafter larger beams with greater zone stresses are markedly less compliant than small beams with smaller zone stresses; and (c) the effect of this zone on strain profiles, whereby it imparts a lower effective stiffness for the material, causing an abrupt discontinuity in the profile. There is no doubt that the presence of an extensive microcracked zone is what differentiates heterogeneous cemented materials from other materials. The stress transfer that occurs in this zone, but in the absence of true yielding, is essentially what governs fracture. Therefore *the behaviour of the*

microcracked zone is the key to an understanding of concrete fracture.

Finally it is true to say that no really suitable fracture mechanics parameter has yet been found to fully describe concrete fracture. The simple reason is that fracture is complex in the sense that different mechanisms and processes exist, governed inter alia, by specimen size and type, presence or absence of notching, and basic structure of the material. Therefore, it seems that eventually a number of parameters may be required to cover the different practical situations. There would be considerable advantages in adopting the LEFM approach if it were obvious that it was applicable in the majority of situations. Its main advantage lies in its simplicity and the numerous formulations available for solving practical problems. Despite the fact that K_c measured in the present tests was reasonably independent of notch depth (for shallow to medium notch depths) and of beam depth (excluding the 100mm beams which did not conform to LEFM principles), there are a number of reasons why LEFM formulations must be treated with great caution for concrete fracture beams.

Firstly, concrete is simply not a linear elastic, homogeneous, isotropic material; the slow crack growth which occurs due to its heterogeneity prevents all but very large specimens being viewed as reasonably approaching LEFM assumptions. Secondly, the presence of an extensive non-linear fracture zone cannot be ignored, since, as described above, it is really this zone that governs fracture. Hence, in the present tests the apparently encouraging LEFM results must be interpreted in the light of the more or less consistent and similar influence that the microcracked zone had on the fracture beams. This was fortuitous since the relative size of this zone was the same for beams of depth 75mm or greater. The presence of this non-linear zone in concrete precludes the ready adoption of LEFM in strict fundamental terms. This is not to say that LEFM may not be of some practical use, particularly for mortars, microconcretes, and relatively large concrete specimens; however, the limitations of specimen type and size will have to be considered.

The development of non-linear fracture mechanics (NLFM) parameters for cemented materials is still very much in its infancy. However, the advantage of NLFM for concrete is that it helps to clarify important aspects of the fracture process. For example, using stress-intensity factors evaluated at the tip of an effective crack (i.e. K_R values) gives a measure of the K value required to develop the microcracked zone. At present, the major problem with K_R is that it is not clear how much of the microcracked zone ought to be included in the effective crack depth.

Hence, the complexity of concrete fracture means that the subject will be studied for as long as the material is used. However, fracture parameters must be linked with processes, and this is a distinguishing feature for cemented materials. Overcomplicated non-linear formulations should preferably be avoided, and practical parameters must still be sought.

10.5 FURTHER WORK REQUIRED

A host of possible avenues for further work has been suggested by the work done to date. However, I consider the four most important avenues to be as follows:-

1. Further studies of the microcracked zone, using notched fracture beams:- in particular, confirmation of existing relationships for (a) the size of the zone in beams of different depth, (b) zone stresses relative to zone sizes, and (c) variation of zone size and zone stresses during crack growth; the extension of these relationships to cover other types of cemented materials, both plain and fibre-reinforced; the use of microcracking zone relationships to characterise fracture behaviour of a full range of cemented materials.

2. Studies of the microcracked zone in different specimen types; an investigation of the differences between microcracked zone

relationships, and an assessment of the relative importance of the microcracked zone, for different specimen types.

3. In conjunction with 1. and 2. above, the measurement of LEFM and NLFM parameters on different specimen types, to confirm the relative influence of the microcracked zone, and the intuitive conclusion that very different parameters will be measured if microcracked zone relationships are different; further testing of size and notch depth effects.

4. Regarding NLFM parameters in particular, further experimental and analytical work in order to confirm and develop the present preliminary relationships; particular emphasis to be placed on analysis of stresses in fracture zones of different specimens; a concerted attempt to identify the major causes of experimental scatter; further testing of size effects.

10.6 A PERSONAL NOTE

Speaking personally, the work undertaken for this thesis has increased and broadened my understanding of the fracture behaviour of notched concrete beams, and hence of the processes of damage and microcracking that occur. The ability of the material to actually develop fracture toughness through the microcracking mechanism is fascinating. The characterisation of fracture behaviour by studies of fracture zones seems to be a rewarding avenue to pursue since it sheds light on the basic fracture-resisting mechanisms developed by the material. The question of finding suitable and valid fracture parameters should not be allowed to predominate over the need to further study and understand how concrete or cemented materials resist the stresses imposed upon them and how they respond to the presence and propagation of cracks.

A A Wells[53] has said that the study of fracture in materials is both challenging and rewarding, and is commended to those who relish a

difficult intellectual problem. His remarks were made generally with reference to metallic materials, which macroscopically at least are immensely more homogeneous, isotropic, and uniform than concrete. If the fracture problem for metals has at times been intractable especially regarding elasto-plastic fracture, we should not expect it to be any less intractable when approaching a material such as concrete with its complex, and at times perverse, nature! Having said that, it is precisely this complex nature of cemented materials that makes them so rewarding from a researcher's point of view. The fact is that, in concrete, we have such a highly successful, extremely versatile, and seemingly simple material; yet our knowledge about its nature and behaviour is still so limited. Two consequences arise from this:- firstly, we ought to respect the material for behaving so acceptably in most situations, and especially for being so tolerant when we abuse or misuse it; secondly we ought not to be surprised when occasionally it becomes obstinate and decides to pursue its own course, simply because we have not understood the inevitability of such a course being followed. This alone should act as the incentive to pursue our knowledge of the material, so that it might be better used, and better respected. And that, I think, is enough said!

APPENDIX A

DETAILS OF CONCRETE MIXES AND PRODUCTION PROCEDURES FOR FRACTURE TESTS

A.1 MATERIALS

A.1.1 CEMENT

SERIES F1 AND F2

Ordinary Portland Cement, obtained during June 1982 in a single batch of approximately 700kg from the Anglo-Alpha cement factory in Roodepoort, Transvaal.

SERIES F3

As for series F1 and F2, except that the cement was obtained during March 1985.

The cement was obtained fresh from the grinding mill, and on arrival at the laboratory was immediately stored in sealed steel drums until used. The cement complied with SABS 471-1971: Portland Cement and Rapid Hardening Portland Cement[103].

A.1.2 AGGREGATES

STONE

1. Crushed Reef Quartzite stone of nominal 19mm single-size. The average properties of this stone, according to Davis[99], are:-

   Relative Density (R.D.) = 2,71

   Loose Bulk Density (L.B.D.) = 1330-1350kg/m^3

   The stone derives from the waste rock produced by mining of the auriferous conglomerate bands on the Witwatersrand, and geologically falls into rocks of the Witwatersrand Supergroup. The stone used for series F1 and F2 came from the Scoops plant of Hippo Quarries, near Brakpan, Transvaal. This stone was used in all the batches of Series F1, and in the first three batches of Series F2. The final two batches of Series F2 (representing fracture specimens F2/4, 11-15, 22-26 used crushed granite stone as detailed below. The stone used for series F3, while also being derived from the Witwatersrand quartzites, was obtained from a commercial supplier (M. Fihrer) in Industria, Johannesburg, and its original source was unknown. Nevertheless, it was similar to the stone for series F1 and F2, except that it appeared to have a slightly larger nominal size.

2. Crushed Halfway House Granite stone of nominal 19mm single size. The average properties of this rock are[99]:-

   R.D. = 2,64

   L.B.D. = 1300kg/m^3

   Geologically, the rock derives from the Halfway-House Granite Dome (Basement Rocks). The elastic modulus of this rock may be somewhat lower than that of the Reef quartzites, and consequently concretes made with this stone as aggregate may be expected to have slightly lower elastic moduli than concretes made with Reef quartzite. In the present series of tests, it appeared that there was no practical difference between elastic moduli of concretes using the two different coarse aggregates.

SAND

Reef Quartzite Crusher Sand was used in all the concretes. Davis[11] quotes the following average properties:-

R.D. = 2,70
Fineness Modulus (F.M.) = 2,94

Sand from the Scoops plant near Brakpan used for the present tests generally had a higher F.M. of about 3,1 for series F1 and F2, and 3,25 for series F3.

A.2 BATCHING AND MIXING

All solid materials were weigh-batched using a laboratory scale. The water was measured in measuring cylinders. Aggregates were air-dried in the laboratory (average temperature = 20°C, average relative humidity (R.H.) = 55 per cent) before use, and then stored dry. The dry solids were placed in a horizontal pan mixer (40 litres capacity) and given one or two stirs prior to introducing the water over a period of about 30 seconds with the mixer in operation. The concrete was then mixed for a further 90 seconds. The resulting consistency of the concrete rendered it suitable for placing with moderate mechanical vibration, or by hand. Slumps varied from 30mm to 60mm for series F1 and F2, but were higher for series F3, varying from 80mm to 130mm, presumably due to the differences in grading of cement and sand compared with the earlier batches.

A.3 CASTING AND CURING

A.3.1 MOULDS

The small fracture beams (100x100x450mm), Young's modulus beams and prisms, modulus of rupture (MR) beams, and four inch cubes were all cast in steel moulds made from structural channel sections bolted together, or standard cube moulds. The rectangular notch-formers for the small fracture beams of series F1 and F2, and for all the fracture beams of series F3, were made from 3mm plate with the notch edge machined to produce a 30° apex angle. These notch-formers were clamped onto the upper flanges of moulds during casting.

The larger fracture beams (i.e. greater than 100mm deep) were cast on shutterboard on the floor, the sides being of 100mm deep shutterboard supported on double-angle steel frames. Spacer boards were used to form the ends of the beams. The side shutters were clamped together with threaded rods at the end of the moulds and if necessary with carpenter's clamps near the centre of the mould. The notch-formers for the larger fracture beams of series F1 and F2 were made of 1mm thick annealed galvanised sheet metal, also clamped to the sides of the moulds. While it was possible to remove the steel formers from the small fracture beams before testing, this was not true for the sheet-metal formers, even although they had been oiled. Consequently, they were left in the concrete during the test, but had no effect on the load-deflection output. The variable section fracture beams were cast horizontally in the same type of wooden mould as detailed above, except that profiled polystyrene sheets 100mm thick were included in the moulds to form the specimen shape. Small perspex sheets were glued onto the polystyrene sheets to form a smooth face for the vertical "steps" used for ultrasonic measurements in series F3.

The beams of span 1200mm, 2000mm, and 3200mm had lengths of threaded steel rod cast into the upper faces, one rod on each side of beam

mid-span, for the purpose of attaching lifting hooks and shackles. These beams were lifted off the floor before testing, and manoeuvred onto the test bed with the aid of a wheeled crane. The lifting rods were positioned such that a net compressive stress existed at the root of the notch during handling.

Photographs of the various moulds are shown in figures A1 to A4. Figure A5 shows a number of demoulded specimens on the laboratory floor prior to commencement of curing.

A.3.2 PROCEDURE

All the fracture beams with a depth greater than 100mm, but including the 100x100x450mm beams and the 100x100x850mm beams of series F2, were cast horizontally on the floor, and compacted with the use of a small poker vibrator. Special care was taken to obtain uniform compaction throughout the beam. Where more than one batch of concrete was required to fill a mould, the mould was progressively filled from one side. The time taken to fill a large 800mm deep beam mould was about two hours. For series F3, bleeding could be detected on the concrete surfaces.

Referring to the 100x100x450mm beams of Series F1 and F3, these were filled with concrete and then compacted by clamping them onto a laboratory vibrating table and vibrating them for between one-half to one minute, depending on the consistency of the concrete. Excessive vibration times were avoided.

The fracture beams for series F3 were also used to visually monitor crack growth during testing, and for this reason the beam face above the notch was made smooth by placing a 100mm wide perspex sheet on the upper surface of the plastic concrete and pressing it lightly into the surface. The opposite lower face was cast on a horizontal shutter board and therefore was already smooth when stripped.

Control compressive strength cubes, elastic modulus beams and prisms, and modulus of rupture beams for series F1 and F3, were compacted on the vibrating table in the same way as described above. The control cubes for series F2 were compacted with the small poker vibrator. The reason for this was that series F1 and F3 specimens were cast and tested in an upper laboratory where the mixer and vibrating table were situated, while series F2 specimens were cast and tested in a ground-floor laboratory where a machine large enough for testing the large fracture beams was situated. Moulds were stripped at variable times, from one to several days after casting, with the smaller specimens being stripped earlier than the larger ones. Specimens larger than 100x100mm cross-section were left undisturbed on the floor until the time of testing. Notch-formers were removed generally one day after casting.

A.3.3 CURING

Immediately after casting, the specimens were covered with plastic sheeting for about 24 hours. Thereafter, the small specimens including cubes were stripped and placed on the surface of the larger specimens. The specimens were then covered with damp hessian cloth and plastic sheeting, and the hessian was kept damp until the time of testing. There was one exception to this method for the final batch of small fracture beams of series F2 (specimen numbers F2/13-15, 24-26) for which the curing was achieved by placing the specimens and associated cubes in a water-filled curing tank and maintaining the temperature at 20°C. The specimens were all tested in a saturated condition. Ambient temperatures in the laboratories where the specimens were cast varied on a daily cycle between about 10°C and 20°C for series F1, and between about 15°C and 25°C for series F2. The specimens for series F3 were cast and cured in a curing room which had not been available when series F1 and F2 were cast. It was possible to better control the temperature in the curing room, and over the seven week period of casting and storage, the temperature varied between 19 and 23°C.



Figure A1 Wooden mould with two 100x100x850mm beams (series F2)

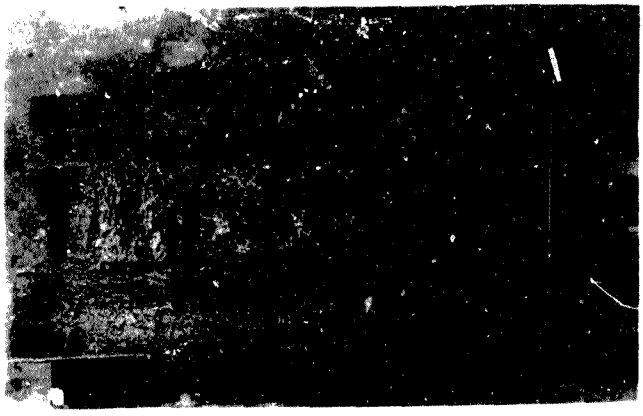


Figure A2 Steel mould with 100x100x450mm beam (series F2)

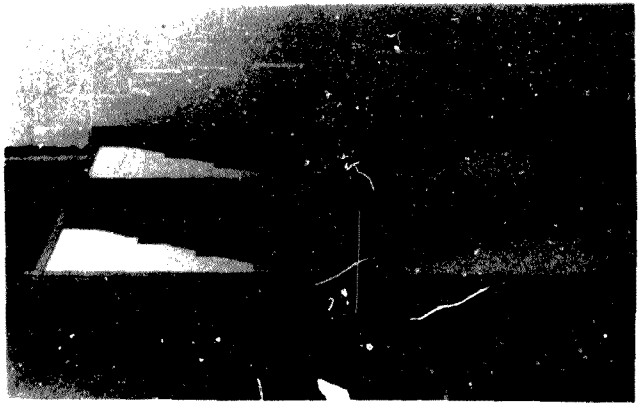


Figure A3 Wooden moulds for 100x300x1275mm variable section beams (series F3) (Note polystyrene inserts to form variable section, and "steps")

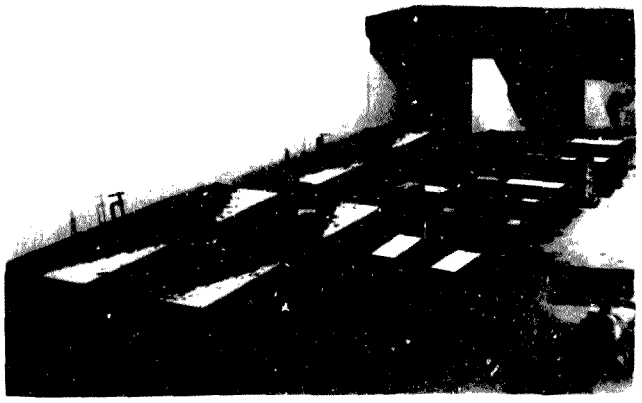


Figure A4 Filled moulds of various types (series F3)

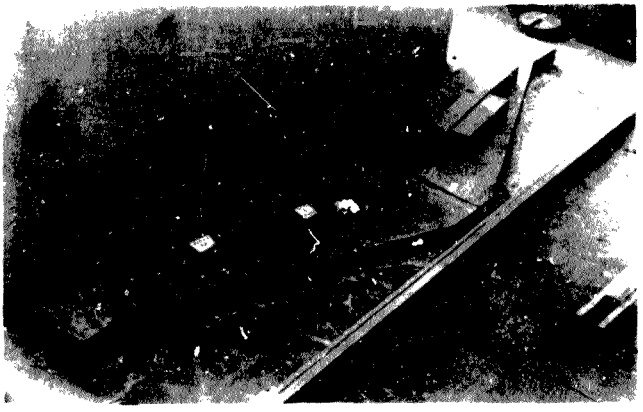


Figure A5 Demoulded beams on laboratory floor, prior to commencement of curing (series F2)

APPENDIX B

DETAILS OF EXPERIMENTAL APPARATUS

B.1 DEFLECTION RIG

The deflection rig to support the LVDTs was fabricated primarily from 25x3mm steel angle and 20x3mm steel flat strip. Other components included threaded rods to act as spacers or as support pins, and flat plates to act as extension legs. The entire assembly was bolted together. The essential feature of the design was that it allowed the rig to be adjusted for use on all the fracture beams. This was achieved by having movable end supports, and by additional members which could be bolted onto the basic rig to allow for the variable section beams. Views of the rig have been shown in chapter 4; other views are given in figures B2(a) to (d) hereunder.

The other essential element for deflection measurement was a device which could clamp onto the specimen below the loading roller and upon which the moving cores of the LVDTs could be supported. This clamp is shown photographically together with the loading roller in figure B1. The diameter of the loading roller was 50mm. The clamp was positioned at the required distance (10mm or 20mm) below the upper face of the beam by means of polystyrene inserts under the horizontal arms of the clamp. The horizontal threaded screws supported the LVDT cores. (See figure 4.3(d) in main test). Further pictures of the basic deflection rig in position on a 100x100x850mm beam and a 500mm deep constant section beam are shown in figures B2(a),(b). The rig with one of its modifications in position on one side of an 800mm deep variable section beam is shown

in figure B 2(c). The other modification to the rig in position on a 300mm deep variable section beam is shown in figure B2(d).

The possibility of extraneous deflections being introduced due to localised strain distortions under the loading roller was investigated. A 100mm deep plain beam was placed on the flat base of a testing machine, and the deflection rig, LVDTs, and specimen clamp attached in the standard manner. The specimen clamp was attached first at 10mm below the loading roller, and then at 20mm, while the maximum loads applied through the loading roller were 10kN and 20kN respectively. The load-deflection relationships for the two arrangements are given in figure B3, which shows that the loading curves are reasonably linear and the residual deformations after unloading are fairly small. Much of this extraneous deflection is therefore elastic in nature. Also, the curve for the x=10mm position is not too far displaced from the x=20mm curve, showing that the magnitude of the effect is similar in both cases. In particular it can be seen that the maximum localised deflections for the two arrangements were 0,0083mm and 0,0135mm respectively.These deflections are a maximum of about 10 per cent of the total deflection measured at maximum load in the fracture tests. Chapter 4 (4.4.1) contains details of an analysis of the effect of these deflections on compliance and fracture parameters.

B.2 ELECTRONIC TRANSDUCERS AND POWER SUPPLY MODULES

B.2.1 ELECTRONIC LOAD CELL

Made by Kyowa Electronic Instruments Co. Ltd, Tokyo, Japan.
Type : Kyowa Strain Gauge Based Load Cell, Compression/Tension.
Series No: LU-2TE.
Capacity : 20kN



Figure B1 Detail of deflection clamp and loading roller



Figure B2(a) Basic deflection rig in position on a 100x100x850mm beam (series F2)

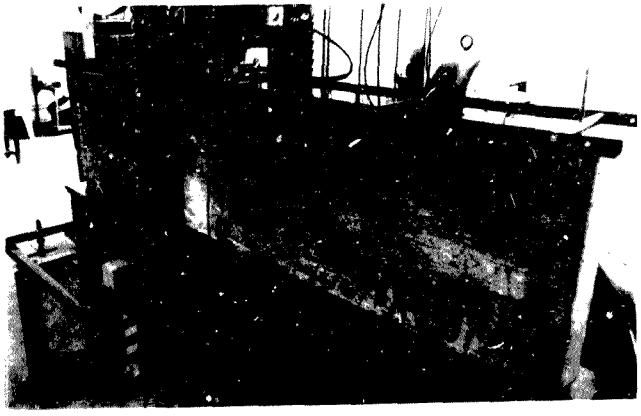


Figure B2(b) Basic deflection rig in position on a 500mm deep constant section beam (series F1)

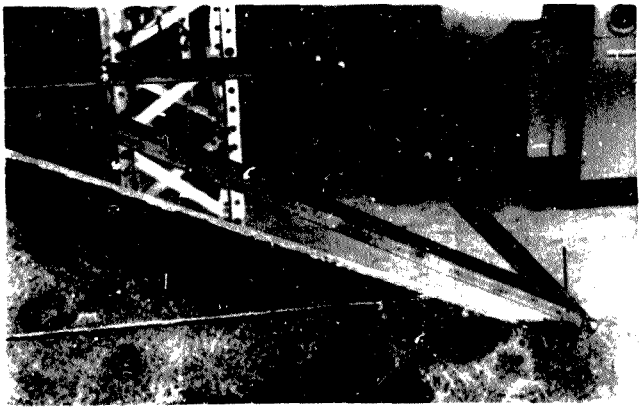


Figure B2(c) One side of modified deflection rig in position on a 800mm deep variable section beam (series F2)

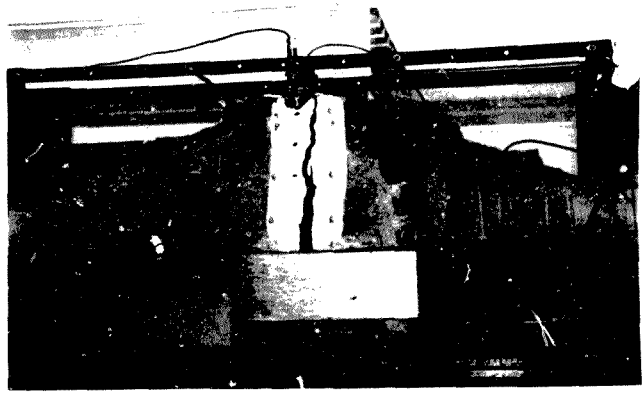


Figure B2(d) Modified deflection rig in position on a 300mm deep variable section beam (series F3) (Note different modification to that of figure B2(c))

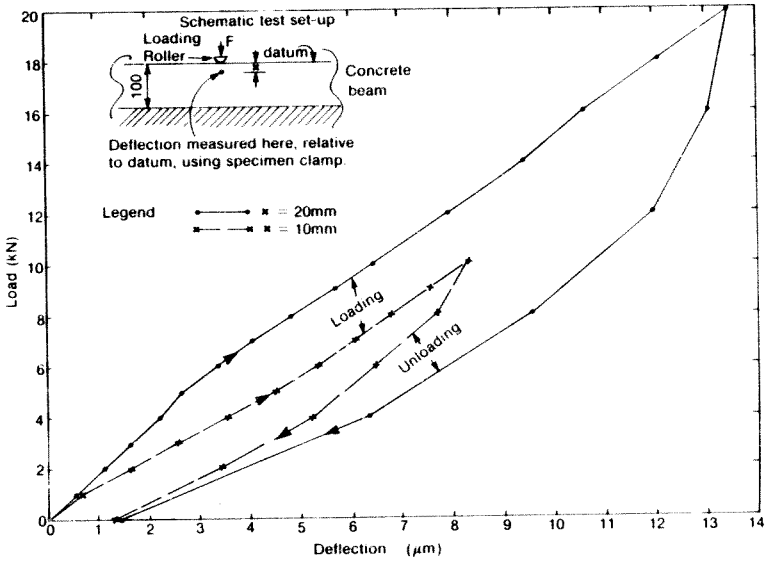


Figure B3 Load-deflection curves showing effect of loading roller on measured deflections



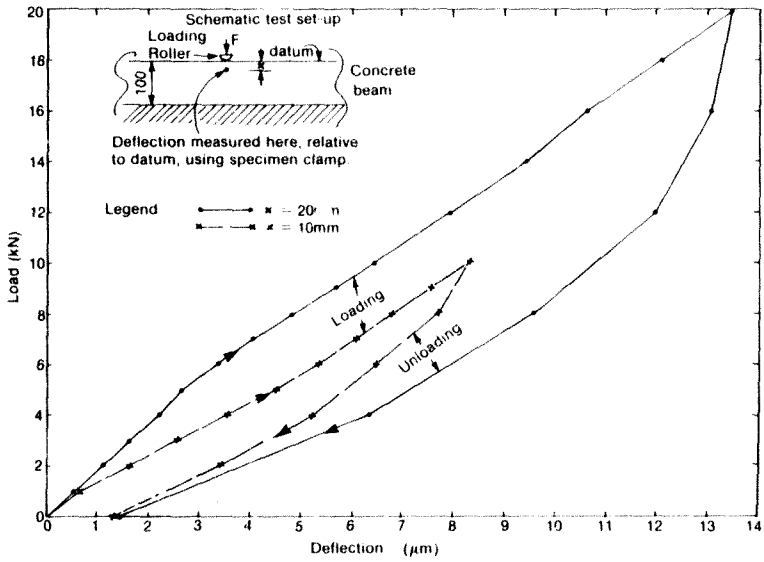


Figure B3 Load-deflection curves showing effect of loading roller on measured deflections

Bridge Voltage : 10,0 V D.C.
Output Voltage Sensitivity : 2mV/V ± 0,2 per cent.

B.2.2 LINEAR VARIABLE DIFFERENTIAL TRANSFORMERS (LVDTs)

SET 1

Made by G.L. Collins Corp., Long Beach, California.
Transducer Length : 20mm.
Transducer Diameter : 10mm.
Linear Range : ± 1,0mm.
Linearity : approx. 0,80 per cent full scale.
Excitation : 5,53 V D.C.
This set of LVDTs was used mainly for initial exploratory tests.

SET 2

Made by RDP Electronics Ltd, Wolverhampton, UK.
Transducer length : 53mm) Type D2/200A
Transducer diameter : 21mm) Serial Numbers 651 and 665
Linear Range : ±5,0mm)
Linearity : Approx. 0,25 per cent full scale
Excitation : 6,0 V D.C.
This set of LVDTs was used for the majority of the tests.

B.2.3 POWER SUPPLY MODULES

A separate power supply module was used to power the load cell and the LVDTs.

SERIES F1 AND F2

Load Cell Module : Operational Amplifier (OA2) Module.
LVDT Module : Type IC 100/6.
Made by Coutant Electronics Ltd, Reading, England.
Powered by 220 V A.C. mains voltage.

SERIES F3

Load cell and LVDT modules : Regulated DC Power Supply Modules.
0-20V; 0-1A.
Made by Metronix Corporation, Tokyo, Japan.
Powered by 220V A.C. mains voltage.

B.3 RECORDING EQUIPMENT

B.3.1 XY RECORDER

Made by J J Lloyd Instruments Ltd, Warsash, Southampton, UK.
Type PL 2500, Serial No. 775.
Effective writing area : 240mm (Y scale).
: 360mm (X scale).
Recorder also had a chart drive motor with variable speed drive.
Linearity > 0,1 per cent f.s.d.
See figure B4 for view of XY recorder.

B.3.2 STRIP CHART RECORDERS

TWO PEN RECORDER

Electronic Polyrecorder, made by TOA Electronics Ltd, Tokyo, Japan.
Model EPR - 200A.
Effective recording area : 150mm x 15m.
Accuracy : ± 0,5 per cent of span.
Chart speed : 6 Stepped settings between 5 to 160mm/h.
and : 7 Stepped settings between 5 to 320mm/min.
Two cartridge type electronic pens.
See figure B4 for view of two-pen recorder.

MULTI-CHANNEL RECORDER

Linearcorder Mark VII WR3101, made by Graphtec Corp., Tokyo, Japan.
Six channels of varying paper width, electronic heat pens.
Accuracy : within ±0,5 per cent over full scale.
Sensitivity : ±2,5V/40mm
Chart speed : 14 Speeds: 5,10,25.100,250 and 500mm/min or mm/s.
See figure B5 for view of multi-channel recorder.

B.3.3 ULTRASONIC PULSE EQUIPMENT

Type : Dr Steinkamp Ultrasonic Tester, BP IV.
Natural frequency of standard transducers : 40-50kHz.
Frequency response : 20-200Hz.
Transducers (pulse transmitter and receiver) : electro-acoustical type.
Liquid crystal display of transit time, directly in µs.
See figure B6 for view of ultrasonic pulse equipment.

B.3.4 STRAIN GAUGE EQUIPMENT

"Demec" mechanical strain gauges locating in drilled stainless steel targets glued to beam.

Made by W.H. Mayes and Son, Windsor, England.

Calibrated by Cement and Concrete Association, Slough, England.

100mm gauge (No. 1847) : Gauge Factor :- 1 div. = $1{,}64.10^{-5}$

200mm gauge (No. 3738) : Gauge Factor :- 1 div. = $0{,}80.10^{-5}$

See figure B7 for view of strain gauge instruments.

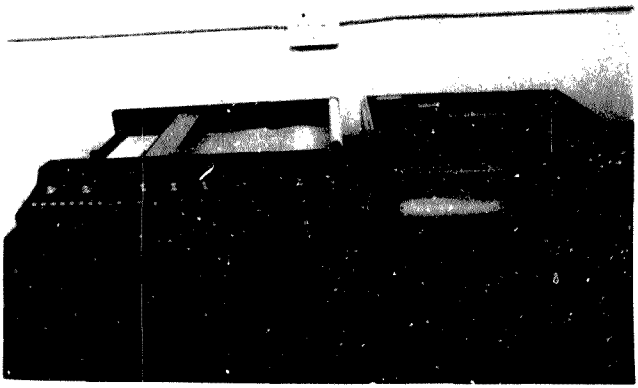


Figure B4 View of XY recorder and two-pen strip chart recorder

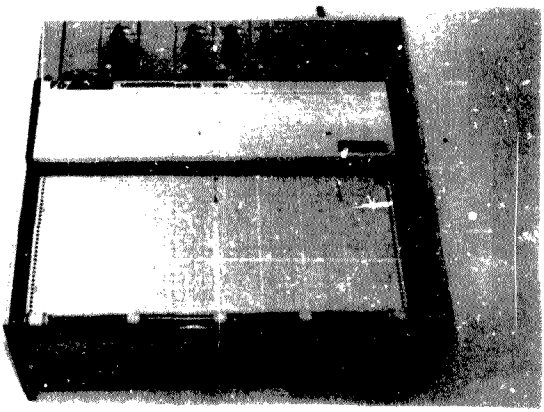


Figure B5 View of multi-channel recorder

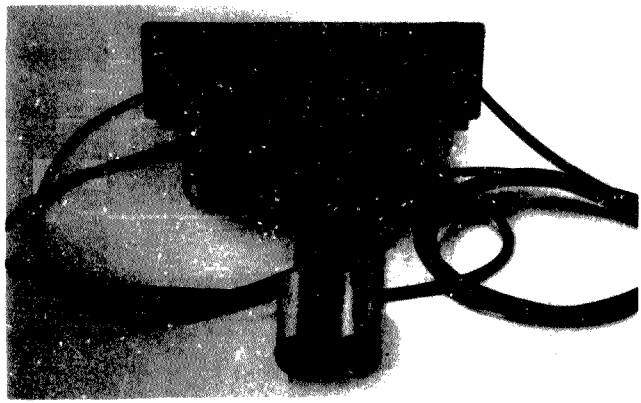


Figure B6 View of ultrasonic equipment

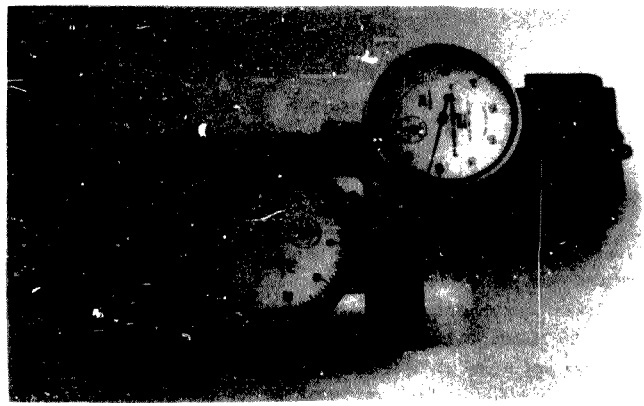


Figure B7 View of "Demec" strain gauge instruments

APPENDIX C

SELECTED DETAILS AND DISCUSSION FOR MATERIALS CONTROL TESTS

C.1 SEEWALD EFFECT AND BEAM TEST FOR ELASTIC MODULUS

Details of the Seewald effect and beam test for elastic modulus are provided by means of an addendum to this appendix containing a reprint of a paper published by the author[83], and written discussion thereon[84]. See the addendum.

C.2 EXPLANATION OF HIGH COMPRESSIVE STRENGTHS FOR CUBES ASSOCIATED WITH BEAMS F1/12-14

The results for cubes associated with beams F1/12-14 are obviously an anomaly. The mean cube strength for this batch was 69,9MPa. Two batches of concrete were mixed to produce the three small fracture beams, the three cubes, and one beam for moduli of rupture and elasticity. The first batch was used to mould the cubes and MR/E beam, while the second batch was used to mould the fracture beams. During mixing, it was noticed that the first batch was very stiff, while the second batch had a normal consistency. The quantities of cement and water required for each batch were 5,06kg and 2,77 litres respectively (c/w = 1.83). It was afterwards realised

that the water had been incorrectly measured at 1,77 litres for the first batch, giving a c/w = 2,86. The theoretical target strength for this c/w ratio is between 60 to 65 MPa[83]. This should be compared with the measured value of 69,9MPa, which while slightly higher than the theoretical value, seems consistent with the probable error in batching. The MR and E values for this batch are also consistent with the high cube strength (see later). The second batch of concrete was correctly batched and mixed. Thus, the concrete for the fracture beams should have achieved the correct design strengths in line with the other beams of this series.

C.3 DISCUSSION OF EFFECT ON ELASTIC MODULUS OF USE OF GRANITE COARSE AGGREGATE, AND ELASTIC MODULUS OF HIGH STRENGTH CONCRETE ASSOCIATED WITH BEAMS F1/12-14

C.3.1 EFFECT ON ELASTIC MODULUS OF USE OF GRANITE COARSE AGGREGATE

While the mean $E/\sqrt{f_{cu}}$ value for series F2 was slightly lower than for series F1 (see table 5.3), it is difficult in view of the small number of results to ascribe this directly to the use of granite coarse aggregate in the last two batches of series F2. It would appear from the results in table 5.3 that the use of the granite aggregate has not had a marked effect on the measured E values. This can be seen by comparing the mean E values from column 4 of table 5.3 for the quartzite and granite aggregate specimens. There is virtually no difference between these values.

C.3.2 ELASTIC MODULUS OF HIGH STRENGTH CONCRETE ASSOCIATED WITH BEAMS F1/12-14

The measured E value for the high strength concrete ($\bar{f}_{cu}$ = 69,9MPa) of series F1 is interesting when compared with values suggested by Carrasquillo et al[194] for high strength concretes. They state that care must be taken when extrapolating results for low or medium strength concretes to high strength concretes. In general, over-prediction will occur since stiffness is controlled by both mortar and aggregate whereas strength is controlled mainly by quality of the mortar. They suggest a relationship for concretes of compressive strength 21MPa to 83MPa as follows:-

$$E_c \text{ (MPa)} = 3320\sqrt{f'_c} + 6900 \text{ (MPa)} \qquad \text{(C.1)}$$

where E_c is a compressive elastic modulus and
f'_c refers to 6 inch x 12 inch cylinder strengths(MPa)

Converting $\bar{f}_{cu}$ = 69,9 MPa to an equivalent cylinder strength using Evans's values given in Neville[87] we get:-

$$E_c = 3320\ \sqrt{0,96.69,9} + 6900$$
$$= 34\ 090 \text{ MPa. (Cylinder modulus)} \qquad \text{(C.2)}$$

Using the relationship between cylinder modulus and beam modulus given in ref. 86, we obtain an equivalent beam modulus as

$$E_{beam} = 1,1244\ (34,09)$$
$$= 38,3\text{GPa} \qquad \text{(C.3)}$$

This value compares very favourably with the measured beam E-value of 38,8GPa.

C.4 DISCUSSION ON EFFECT OF BLEEDING ON ELASTIC MODULUS AND COMPRESSIVE STRENGTH, SERIES F3

The high slump values (80-130mm) for concretes of series F3 resulted in significant bleeding. In the case of the 200mm deep prisms which were cast vertically, the tendency for the bleed water to rise to the surface would be substantially lower than for the 100mm deep beams which were cast on their sides. Consequently, it could be expected that water would be trapped in the prisms, and particularly under the coarse aggregate particles, leading to zones of weakness representing appreciable flaws. These flaws might be thought of as ellipsoids with the major axes aligned at right angles to the direction of load in the prisms. Their effect would be to reduce the stiffness of the prisms since the prisms would effectively contain numerous insertions of very low stiffness. The shallow beams as cast could be expected to contain significantly fewer such flaws which would generally be of smaller size. Those flaws which did exist in the beams would be orientated during testing with major ellipsoid axes in the direction of the major principal stresses. Clearly such orientation would have very little effect on the stiffness of the beam, since stresses could easily "flow" around the flat ellipsoids, and since the stress concentration effect of the flaws would be minimal. This would not be true of the prisms where the major principal stress would induce high stress concentrations at the tips of the flaws.

The comments on bleed voids given above can also be extended to the question of compressive strength. Considering firstly the cubes, the presence of flaws due to bleeding could significantly lower the strength, and this is consistent with the somewhat puzzling lower cube strengths recorded for series F3 when compared with the earlier series. Quoted results[83] for the effect of voids on compressive strength (i.e. roughly 5 per cent loss in strength for 1 per cent voids) would indicate that a void content of about 2,5 per cent could have led to the strength reduction for series F3, and this figure does not seem unrealistic. Secondly seven 100x100x200mm prisms were crushed during the tests, and the mean value for the compressive strength was 23,9MPa (range = 21,8 MPa to 28,0MPa), i.e. 77,3 per cent of the mean cube value of 30,9MPa. According to Neville[87], an expected ratio of prism to cube strength for the dimensions of the present specimens would be about 86 per

cent. This reinforces again the argument that the effect of bleeding will be more severe on the deeper prisms than on the shallower cubes. (Note that the large variation in prism E and strength values would also be accounted for by the bleed effect).

Hence, both strength and stiffness of the cubes and prisms of series F3 have been adversely affected by the high slump and associated bleeding, but the effect on the fracture beams has been far less due to the aspects of depth of section and orientation of bleed flaws relative to direction of stress. In this case, the material parameters for the fracture beams will be very much closer to those of series F1/F2 than the standard materials tests would suggest.

ADDENDUM

See reprints on following pages.

A simple bending test for elastic and rupture moduli for plain concrete and mortar



by
MG Alexander
Lecturer in Construction Materials
Department of Civil Engineering
University of the Witwatersrand

A simple test for elastic and rupture moduli of plain concrete or mortar beams is outlined, and compared with existing standard test methods. The test is based on the standard modulus of rupture test, but incorporates measurement of the load-deflection relationship for the beam. A load-cycling technique is used which effectively eliminates non-linear behaviour of the beam during the initial loading stages. While the measurement of beam deflections is relatively simple, it is important to ensure that extraneous deflections are excluded from the test results, and that a shear correction factor is included in the calculations.

With sufficient attention to detail, the simple beam test provides reliable material parameters and has the advantages of better repeatability and linearity than the cylinder test. Comparative tests showed that the proposed beam test gave slightly greater elastic moduli and slightly lower rupture moduli when compared with the standard tests.

'n Eenvoudige toets vir elastisiteits- en breukmodulusse van ongewapende beton- of daghabalke word beskryf en met die bestaande standaard toetsmetodes vergelyk. Die toets is op die standaard breukmodulustoets gebaseer, maar sluit ook die meet van die balk se las-defleksie-verband in. 'n Lassiklusseringstegniek word gebruik wat nie-lineêre gedrag van die balk tydens die aanvanklike belastingstadiums effektief uitskakel. Hoewel die meet van balkdefleksies betreklik eenvoudig is, is dit tog belangrik om te verseker dat vreemdsoortige defleksies nie by die toetsresultate ingesluit is nie en dat die berekeninge wel 'n skuifkorreksiefaktor insluit.

As daar genoeg aandag aan detail geskenk word, lewer die eenvoudige balktoets betroubare materiaalparameters terwyl dit ook die voordeel inhou dat die herhaalbaarheid en lineariteit daarvan beter is as dié van die silindertoets. Vergelykende toetse het getoon dat die voorgestelde balktoets effens hoër elastisiteitsmodulusse en effens laer breukmodulusse as die standaard toetse lewer.

Introduction

IN the construction of major highways in South Africa, considerable use is being made at the present time of rigid concrete pavements on suitable subbase and subgrade layers which are usually made of stabilised materials. The load-carrying capacity of the pavement-base-subgrade structure is achieved largely by 'beam action' of the pavement. The concrete slab itself is normally the major component of the structure, and the stresses induced in this element have been given detailed consideration by many investigators.[1-3] In particular, the allowable stress in the pavement is related to the flexural strength of the concrete, determined by the modulus of rupture (MOR) test. A further material parameter that influences the magnitude of stresses and deformations in a pavement is the elastic modulus, normally evaluated in separate tests on concrete cylinders loaded in compression. Frequently considerable time and effort is expended in the laboratory and on site to evaluate material parameters as a control on quality of construction, or as a check on design assumptions.[2] This paper describes a simple test which will yield elastic and rupture moduli for pavement materials, thus eliminating the need for a separate cylinder test, which is generally not a standard test in South Africa. A comparison between the measured moduli in the present test, and those obtained in the normal standard tests, is also included for completeness.

Review of existing tests

Flexural strength

Procedures for measuring the flexural strength of concrete by means of beam bending tests are well established.[3,4,5] Third-point loading has now generally replaced centre-point loading, and standard test methods call for careful control of specimen dimensions, batching, mixing and moulding of the concrete, curing, rate of load application, and interpretation of test results. The calculated modulus of rupture over-estimates the tensile strength of the concrete relative to direct tension tests due to a number of reasons:

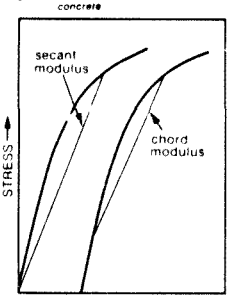
(i) the actual shape of the stress block at failure is approximately parabolic[6] and not triangular as assumed;

(ii) the volume of material subjected to maximum stress, and hence the probability of a weak element occurring in a highly stressed zone is lower in the flexure test than in the direct tension test;

(iii) the maximum fibre stress in flexure is higher than in direct tension because propagation of the crack is blocked by lower-stressed material near the neutral axis.

Nevertheless, the flexure test has found wide acceptance due to its simplicity and adaptability for site or laboratory. For the testing of road materials, Otte[7] has argued that the test adequately simulates the flexural behaviour of a pavement and yields strength values directly applicable in design.

Figure 1. Typical stress-strain curve for concrete



Elasticity

Concrete is not an elastic material nor does it possess a linear stress-strain relationship. For practical purposes, however, different moduli can be defined and measured.[8] The two moduli most often evaluated are the static secant modulus or the chord modulus, illustrated in Figure 1, and generally obtained from a short-term compression test on a concrete cylinder. Alternatively, a dynamic test involving the monitoring of vibrations in a concrete specimen under a suitable mode of resonant vibration can be used.[9] The elasticity of concrete has normally been measured using static compression cylinders, but attempts have been made to evaluate elastic moduli in tension and flexure.[10,11,12] For the flexure tests, moduli can be determined from load-deflection measurements, or alternatively from strain measurements on the tension and compression faces of the beam.

The test outlined in BS 1881 : Part 5 : 1970[2] for the static modulus of elasticity uses a 150 mm diameter, 300 mm long cylinder, load cycled to one-third of the ultimate compressive strength based on cube tests. The test is regarded as valid when the recorded strains on two successive cycles agree to within 5%, and three cycles are usually sufficient. The load cycling technique reduces creep and curvature of the lower portion of the stress-strain curve. A stress of 1 MPa is maintained on the specimen at the start of the second and subsequent cycles. The static modulus is taken as the slope of the best-fit straight line drawn through the plotted stress-strain points, and is thus not a true chord modulus.

In ASTM C 469[3], a similar procedure is adopted to the British test, except that the modulus is a chord modulus from an initial load at a strain of 10.10^{-6} to a maximum load at 40% of the ultimate cylinder strength, which is roughly equivalent to one-third of the ultimate cube strength. Strain is measured on two or more gauge lines uniformly spaced around the cylinder perimeter. The easiest way of measuring strain is by means of a suitable compressometer which clamps onto the cylinder. A further addition to the rig allows transverse strains to be measured, which gives Poisson's ratio for the concrete.

Comparatively little work has been directed at assessing elastic modulus of concrete in flexure, the test suggested in this paper is a useful alternative to the traditional compression test for checking on moduli used in design or research, and can be combined with a rupture modulus test which is frequently required in practice.

Proposed test method

The beam test outlined below is based on SABS Method 864 "Flexural Strength of Concrete"[3]; modifications to the standard test in order to determine the elastic modulus by load-deflection measurements are outlined, and the reader is assumed to be acquainted with the test method. The requirement that the beams shall be tested in the moist condition is important, since Hsu and Slate[4] have found that partially air-dry specimens, in their case tested in direct tension, had strengths as low as 81% of the strength of moist specimens.

Specimen preparation and dimensions

The SABS method calls for preferred beam dimensions of 150x150x750 mm tested in third-point loading, although 100x100x500 mm beams are acceptable, in either case, the ratio of support span to depth of the beam (i.e. ℓ/d) is four. The ASTM C 78-64 test specifies $\ell/d = 3$. A considerable improvement in sensitivity for the deflection readings of the beam is obtained by increasing the ℓ/d ratio to a value greater than four. Otte[5] used $\ell/d = 5$, and the tests reported herein used 102x102x700 mm beams with $\ell/d = 6$. A comparison between the rupture moduli obtained in the standard test and on the longer beams is made in a later section of the paper.

Procedure

(i) The dimensions of the specimen should be accurately determined, preferably to the nearest 0,5 mm, to minimise inaccuracies in the calculation of the moduli.

(ii) Immediately before the test, an estimate of the modulus of rupture should be obtained by one of the following means:

(a) by testing a companion beam or beams, moulded and cured in the same way, or,

(b) by crushing at least three cubes in a standard fashion, and calculating the average compressive strength of the material.

An estimate of the modulus of rupture for normal concrete specimens can be obtained by dividing the average compressive strength by 10, and rounding off to the nearest 0,1 MPa. Calculate the value C as one-third of the estimated or measured modulus of rupture, to the nearest 0,1 MPa.

(iii) Before placing the specimen in the machine, the deflection-measuring equipment should be attached to the specimen in such a way that extraneous deflections are eliminated from the readings.

(iv) The preliminary loading consists of applying two cycles of load continuously and without shock, the first cycle up to an extreme fibre stress of C MPa, maintaining the load for 1 minute and then unloading to an extreme fibre stress of 0,1 C, and the second cycle up to a stress of 0,9 C and then unloading to a stress of 0,1 C. On the second cycle, deflection readings are taken at the start and finish as well as at the peak stress. The load cycling technique allows the repeatability of the test to be noted, and provides for checking of the deflection apparatus and effective elimination of initial non-linearity in the load-deflection relationship. Loading and unloading are all at the standard rate of about 1,5 MPa/min.

(v) A third cycle of load is then applied and deflection readings taken at ten approximately equal increments of stress up to a stress of 0,9 C. Thereafter, the load is increased to failure, and if the full load-deflection curve is required, deflection readings at a further approximately ten equal increments of stress are taken up to failure. The maximum load, and if possible, the deflection at maximum load is recorded.

Further specimens are tested in the same way. Results for any specimen are disregarded if the repeatability of the deflection readings is not within 5%, or the specimen fractures outside the middle-third of the support span.

Calculations

Modulus of Rupture: This is calculated in the standard way to the nearest 0,05 MPa as:

$$f(\text{MPa}) = \frac{P\ell}{bd^2} \qquad (1)$$

where P = breaking load, N
ℓ = support span, mm
b,d = width and depth respectively, mm.

Modulus of Elasticity: This is calculated, for third-point loading and measurement of central deflections, to the nearest 100 MPa, as:

$$E(\text{MPa}) = \frac{23}{1296}\,\frac{F}{\delta}\,\frac{\ell^3}{I}\left[1 + \frac{216}{115}\left(\frac{d}{\ell}\right)^2 (1+\nu)\right] \qquad (2)$$

where $\frac{F}{\delta}$ = the slope of the best-fit straight line drawn through the plotted points of the initial portion of the load-deflection curve, N/mm
ℓ = support span, mm
I = second moment of area of the section, mm^4
d = depth of the section, mm
ν = Poisson's ratio. For concrete, it is usually acceptable to take ν as 0,15 to 0,2 and such a variation has a minimal effect on the calculated value of E.

Equation (2) above, and equation (3) which follows, are derived from simple beam bending theory.

The expression in square brackets is a shear correction factor, suggested by Otte [1].

A third material parameter, frequently used in material characterisations, namely the strain at failure, ε_u, can be calculated knowing the deflection at maximum load:

$$\varepsilon_u = \frac{108}{23}\,\delta_{max}\,\frac{d}{\ell^2}\left[1 + \frac{216}{115}\left(\frac{d}{\ell}\right)^2(1+\nu)\right]^{-1} \quad (3)$$

where δ_{max} = central deflection at maximum load P, mm.

The method outlined above was used to test a number of concrete beams for rupture and elastic moduli. Comparative tests were done on standard moduli of rupture beams and compression cylinders in order to compare strength and elasticity parameters obtained in the different tests.

Experimental details

Testing techniques

Beam bending tests for elastic and rupture moduli

These tests were performed according to the method outlined above, using nominal 102 x 102 x 700 mm beams tested on a 610 mm support span. Shorter 450 mm long beams were used for obtaining standard modulus of rupture values according to SABS Method 864. The tests were performed in a 60 ton Tinius Olsen compression testing machine. The loads and deflections were recorded manually. The mid-span deflections of the longer beams were measured by two linear variable differential transformers mounted in a deflection rig and having plungers attached to the upper surface of the beam. Deflections could be recorded within an accuracy of 0.0015 mm. A photograph of the test set-up is shown in Figure 2.

Figure 2. Arrangement for beam tests

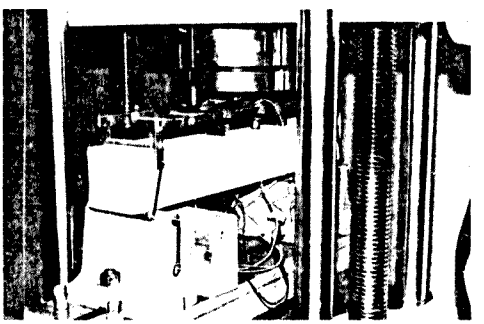
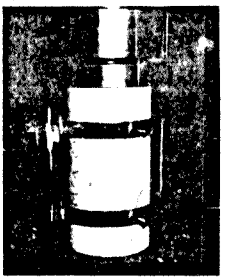


Figure 3. Arrangement for cylinder tests



Cylinder compression tests for elastic modulus

These tests were done according to BS 1881: Part 5: 1970, using either the Tinius Olsen machine mentioned above or a 200 ton Amsler compression testing machine. Longitudinal strains were manually recorded within an accuracy of $3.3 \cdot 10^{-6}$ using a compressometer. A photograph of the test set-up is shown in Figure 3.

Specimen preparation

Two series of concrete specimens, C1 and C2, and one series of mortar specimens, M1 were prepared. Materials were ordinary Portland cement obtained in a single batch, crushed Reef quartzite sand (F.M. = 3.08), and 19 mm single-sized crushed Reef quartzite stone. Mix proportions for the concrete by mass were: c:w ratio = 1.82; A:c ratio = 4.87; sand:stone ratio = 0.74. Mortar mix proportions were c:w ratio = 1.82; sand:cement ratio = 3.94. Series C1 for rupture and elastic modulus tests consisted of 12 cylinders, nominal dimensions 150 mm diameter by 300 mm, and 12 beams, nominal dimensions 102 mm square tested on a 610 mm span. Series C2 for the standard modulus of rupture tests used 12 beams of 102 mm square cross-section, tested on a 400 mm span. Series M1 consisted of 3 cylinders, and 3 beams tested on a 610 mm span. Specimens were cured in water at 20°C for 28 days before being tested in the wet condition.

Results and discussion

Experimental technique

The test procedure outlined above calls for a load-cycling technique to be applied to the specimen before measurement of a representative load-deflection relationship over the range of load required. The load-cycling technique is well established in elasticity testing, and serves to decrease non-linearity of the initial portion of the load-deflection curve. A typical percentage plot of the load-cycling technique for a concrete beam is shown in Figure 4. The second and third load cycles have been displaced horizontally for clarity. The hysteresis loop is small, and linear behaviour is rapidly established. The slopes of the loading portions of the curve are virtually identical, and the second and subsequent cycles follow the same path. A slight degree of non-linearity does exist, however, at the start of the initial loading cycle. The cycling

Author Alexander Mark Gavin
Name of thesis Fracture Of Plain Concrete: A Comparative Study Of Notched Beams Of Varying Depth. 1985

PUBLISHER:
University of the Witwatersrand, Johannesburg
©2013

LEGAL NOTICES:

Copyright Notice: All materials on the University of the Witwatersrand, Johannesburg Library website are protected by South African copyright law and may not be distributed, transmitted, displayed, or otherwise published in any format, without the prior written permission of the copyright owner.

Disclaimer and Terms of Use: Provided that you maintain all copyright and other notices contained therein, you may download material (one machine readable copy and one print copy per page) for your personal and/or educational non-commercial use only.

The University of the Witwatersrand, Johannesburg, is not responsible for any errors or omissions and excludes any and all liability for any errors in or omissions from the information on the Library website.